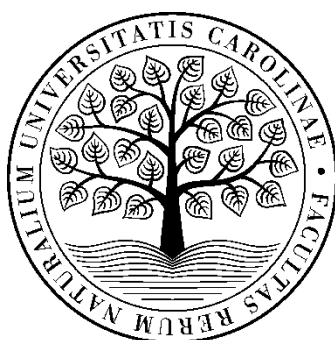# Charles University
Faculty of Science

Study program: Physical Chemistry

Mgr. Milan Boublík

Ionic effects and online preconcentration techniques in separation systems

Dissertation thesis

Supervisor: doc. RNDr. Iva Zusková, CSc.

Prague, 2020

This thesis summarizes my results obtained during my Ph.D. studies at Faculty of Science, Charles University.

Supervisor: doc. RNDr. Iva Zusková, CSc.

Department of Physical and Macromolecular Chemistry

Faculty of Science, Charles University

PROHLÁŠENÍ

Prohlašuji, že jsem tuto dizertační práci vypracoval samostatně a všechny informační zdroje a literaturu jsem řádně citoval. Tato práce ani její podstatná část nebyla předložena k získání jiného nebo stejného akademického titulu.

V Praze, dne

....

Milan Boublík

Acknowledgements

Table of contents

List of abbreviations

ACN	acetonitrile
APAA	4-aminophenyl acetic acid
APBA	4-aminophenyl butyric acid
BGE	background electrolyte
CD	cyclodextrin
CE	capillary electrophoresis
cIEF	capillary isoelectric focusing
CZE	capillary zone electrophoresis
EDTA	ethylenediaminetetraacetic acid
EKC	electrokinetic chromatography
EOF	electroosmotic flow
GMP	guanosine monophosphate
HILIC	hydrophilic liquid interaction chromatography
HPLC	high performance liquid chromatography
IEF	isoelectric focusing
IEC	ion exchange chromatography
m.u.	electrophoretic mobility unit $10^{-9}\,m^2V^{-1}s^{-1}$
MS	mass spectrometry
MIC	micelles
R-Flu	R-flurbiprofen
TAPS	3-{[1,3-dihydroxy-2-(hydroxymethyl) propan-2-yl]amino}propane-1-sulfonic acid
t-BOC	terc-butyloxycarbonyl protecting group
TEA	triethylamine
Tris	2-Amino-2-(hydroxymethyl) propane-1,3-diol

List of symbols

a_i activity of i-th form

c_i concentration of i-th form

γ_i activity coefficient of i-th form

I ionic strength

z_i relative charge

N_{AV} Avogadro constant

δ_i Kronecker delta

$\mu^\infty{}_i$ limiting electrophoretic mobility of i-th form

μ_i ionic electrophoretic mobility of i-th form

ε permittivity

e elementary charge

η dynamic viscosity

k Boltzmann constant

T absolute temperature

s overall number of ionic species

μ_A electrophoretic mobility of free analyte

$\mu_{CD,eff}$ effective electrophoretic mobility of cyclodextrin in presence of analyte

$\mu_{A,eff}$ effective electrophoretic mobility of analyte in presence of cyclodextrin

EF_{tot} total enhancement factor of conductivity detection

EF_κ enhancement factor of conductivity detection

F preconcentration factor

K equilibrium constant

K_a acid dissociation constant

K_{as} analyte – selector complex stability constant

K' apparent equilibrium constant

Abstract

Online preconcentration techniques in capillary electrophoresis (CE) improving sensitivity of electrophoretic separations and are in the scope of interest of many research groups. Therefore, proposal of new techniques for preconcentration and their theoretical description is desirable for their wider application. In this thesis, new preconcentration techniques are proposed and models of ionic strength effects in separation systems of CE and hydrophilic liquid interaction chromatography (HILIC) are presented and new set of pI markers for isoelectric focusing (IEF) was showed with their utilization for characterization of IEF pH gradient.

Part of this thesis is keen on proposal of new preconcentration techniques and their theoretical description. We presented two preconcentration techniques, while first is based on sweeping with neutral complexing agent, the second one utilizes pH boundaries that are induced by disturbing phenomena of system zones. Both techniques are described theoretically by means of numerical simulations and by experiments. Both techniques are even utilized for real drug sample or for mixture of similar analytes. For system peak preconcentration technique, flow chart of how to design such method is presented.

Second part of this thesis have rather more fundamental subject and that is ionic effects in separation systems of CE and HILIC mode of HPLC. In CE, topic of ionic effects is focused on ionic strength corrections in determination of dissociation constants and limiting mobilities. We presented new software AnglerFish, that implements theory of ionic strength for easy utilizable and precise correction of these parameters on zero ionic strength of solutions, while also having other advantages compared to standard approaches. For HILIC separation system, we showed how retention of various amino acids, dipeptides and their N-blocked analogues changed with type and concentration of present cation in the buffer for two different stationary phases. Surprisingly, increasing concentration of some buffer cations decrease retention of analytes, due to the competition on stationary phases.

Finally, we predicted, found and characterized set of 14 pI markers for IEF. pK_a values and limiting mobilities of these markers were determined experimentally. These

markers were utilized for characterization of IEF pH gradient by simulations and experiments.

Abstrakt

Online prekoncentrační techniky v kapilární elektroféze (CE) zvyšují citlivost detekce elektroforetických separací a jsou tak předmětem zájmu mnohých výzkumných skupin. Z tohoto důvodu je návrh nových prekoncentračních technik a jejich teoretický popis žádoucí pro jejich širší využití. Jedním z faktorů ovlivňujících separační podmínky je iontová síla separačních systémů. V rámci této disertační práce byly navrženy nové prekoncentrační techniky a popsány efekty iontové síly v separačních systémech CE a hydrofilní kapalinové interakční chromatografie (HILIC). Současně zde bylo představeno a popsáno 14 nových pI markerů pro isoelektrickou fokusaci (IEF).

První část této disertační práce se zabývá návrhem nových prekoncentračních technik a jejich teoretickým popisem. Jsou zde prezentovány dvě prekoncentrační techniky. První z nich je založena na mechanismu sweepingu pomocí neutrálního komplexačního činidla, zatímco druhá využívá pH rozhraní, která jsou vytvořena systémovými zónami. Obě techniky jsou popsány jak teoreticky pomocí numerických simulací, tak experimentálně. Tyto techniky byly také aplikovány pro prekoncentraci účinné látky v komerčně dostupném léčivu a pro směs strukturně podobných analytů. Pro metodu využívající prekoncentraci pomocí systémových zón byl vytvořen diagram umožňující snadnou optimalizaci této techniky.

Druhá část této práce je věnována základnímu fyzikálně chemickému popisu separačních systémů – iontovým efektům v separačních systémech CE a HILIC módu HPLC. V rámci CE byl popis iontových efektů zaměřen na korekce na iontovou sílu při stanovení disociačních konstant a limitních elektroforetických mobilit. Pro správnost a usnadnění těchto korekcí byl vytvořen program AnglerFish, který implementuje teorie vlivu iontové síly na aktivitní koeficienty a elektroforetické mobility. Tímto přístupem byla získána přesněji korigovaná data stanovovaných parametrů. Současně tento přístup nabízí další výhody v porovnání s již dříve známými postupy pro korekce daných parametrů. Při popisu iontových efektů v separačním módu HILIC byla sledována retence různých aminokyselin, dipeptidů a jejich N-blokovaných variant v závislosti na struktuře a koncentraci různých kationtů obsažených v pufru pro dvě stacionární fáze. Ve většině případů zvyšující se koncentrace kationtů způsobovala zvýšení nebo nulovou změnu retence. V ostatních případech však zvýšení koncentrace kationtu mělo za následek snížení retence analytu v důsledku kompetice na stacionární fázi.

V poslední části této práce zabývající se IEF bylo navrženo a popsáno 14 pI markerů. Experimentálně byly stanoveny jejich pohyblivosti a disociační konstanty, které byly následně zkorigovány na limitní pohyblivosti a termodynamické disociační konstanty. Navržené markery byly použity pro charakterizaci pH gradientu v IEF. Experimentálně získaný tvar pH gradientu vykazoval dobrou shodu s tvarem získaným numerickými simulacemi.

List of publications

I.   Enhancement of the conductivity detection signal in capillary electrophoresis systems using neutral cyclodextrins as sweeping agents

M. Boublík, M. Riesová, P. Dubský, B. Gaš

Electrophoresis, 2018, 39, 1390-1398

II.   Online preconcentration of weak electrolytes at the pH boundary induced by system a zone in capillary zone electrophoresis

M. Boublík, M. Riesová, J. Šteflová, V. Hruška

Analytica Chimica Acta, 2019, 1085, 126-135

III.   Determination of thermodynamic acidity constants and limiting ionic mobilities of weak electrolytes by capillary electrophoresis using a new free software AnglerFish

M. Malý, **M. Boublík**, M. Pocrnić, M. Ansorge, K. Lorinčíková, J. Svobodová, V. Hruška, P. Dubský, B. Gaš

Electrophoresis, 2019, https://doi.org/10.1002/elps.201900283

IV.   The effect of buffer concentration and cation type in the mobile phase on retention of amino acids and dipeptides in hydrophilic interaction liquid chromatography

K. Kalíková, **M. Boublík**, G. Kučerová, P. Kozlík

Chemical Papers, 2018, 72, 139-147

V.   CE determination of the thermodynamic pKa values and limiting ionic mobilities of 14 low molecular mass UV absorbing ampholytes for accurate characterization of the pH gradient in carrier ampholytes-based IEF and its numeric simulation

M. Ansorge, B. Gaš, **M. Boublík**, M. Malý, J. Šteflová, V. Hruška, G. Vigh

Electrophoresis, 2019, https://doi.org/10.1002/elps.201900381

1.   Introduction

Capillary electrophoresis (CE) and high-performance liquid chromatography (HPLC) are well established and highly efficient separation techniques. Both of mentioned methods are widely used for routine analysis of chemical and biological samples and have stable spot among other analytical methods. Their general separation mechanisms are already well known, however some phenomena influencing them are not yet fully understood and described. For example, concentration of charged species and their structure present in the background electrolyte (BGE) or in the mobile phase has an impact on electromigration in CE and on retention in HPLC.

There are several HPLC modes, where pH and ionic strength of aqueous part of mobile phase play crucial role as they influence substantially the strength of adsorption of analyte onto stationary phase or even modify retention mechanism. Ion-exchange chromatography (IEC) utilizes gradient of ionic strength or pH (or both) for separation of charged analytes interacting electrostatically with oppositely charged stationary phase. Hydrophilic liquid interaction chromatography (HILIC) employs additional separation mechanism – partitioning of analyte between organic part of mobile phase and water layer (aqueous part of mobile phase) partially immobilized on the polar stationary phase. This partitioning is naturally strongly affected by presence and concentrations of charged species in mobile phase utilized. The impact of ionic strength and pH of mobile phase on HILIC results are difficult to predict as the whole retention mechanism is such complicated. Characterization of HILIC stationary phases together with various mobile phases used is ongoing topic nowadays.

Considering CE, electromigration is influenced by ionic strength via the dependency of all the activity coefficients (that further propagates into dissociation constants) and electrophoretic mobilities on ionic strength. Where additional equilibria (complexation, partitioning with micelles etc.) are taking place, ionic strength influences their equilibria constants thru the activity coefficients as well. The main advantage of CE prior HPLC is that, it is well mathematically described and there are prediction and simulation software that enables various electromigration phenomena investigation and result prediction *in silico*. Obviously, the software needs to work with reliable input parameters (all equilibria constants and electrophoretic mobilities mentioned above) and the way how they are changing with ionic strength must be

known and well described. Once the effect of ionic strength is known, we can predict reliably electromigration velocities of analytes in various electrophoretic systems or on the other hand, we can utilize CE as a method for determination of correct, thermodynamic equilibrium constants or limiting electrophoretic mobilities.

While CE separation process can be predicted and investigated by simulation software, it suffers from lower detection sensitivity compared to HPLC due to its shorter optical path of detection window. However, this issue can be compensated by online preconcentration techniques in CE, to increase concentrations of measured analytes and thus increase sensitivity of detection. The importance of improving lower detection sensitivity of CE by online preconcentration techniques makes these techniques an ongoing issue in the field of CE method development.

1.1. Ionic effects in capillary electrophoresis

CE serves most often as a powerful separation technique, but can also be utilized for determination of physicochemical parameters such as acid-base dissociation constants[1, 2], limiting electrophoretic mobilities (μ^∞_i) [1, 2] or complex stability constants [3, 4]. Methods for determination of above mentioned constants by CE are already well established and have been described in numerous publications [5-7]. The constants obtained are measured at certain ionic strength and have to be recalculated to zero ionic strength to get correct thermodynamic parameters. Thermodynamic equilibrium (dissociation, stability…) constant is defined as:

$$K = \prod_i a_i^{v_i} \qquad (1)$$

where a_i is activity of i-th compound in the equilibrium to power of stoichiometric coefficient. Thermodynamic activity of i-th ion can be calculated as:

$$a_i = c_{i,\text{rel}}\gamma_i \qquad (2)$$

$c_{i,\text{rel}}$ is relative concentration of i-th ion (where $c_{i,\text{rel}} = c_i/c^0$, $c^0 = 1$ mol·dm^{-3}) and γ_i is its activity coefficient. Combining equations (1) and (2) equilibrium constant can be calculated as

$$K = \prod_i c_{i,\text{rel}}^{v_i} \cdot \prod_i \gamma_i^{v_i} \tag{3}$$

where the first product is often called apparent equilibrium constant K'. This constant is often determined by experimental measurements however, to obtain true thermodynamic equilibrium constant, apparent equilibrium constant needs to be corrected on zero ionic strength of the surrounding solution.

The ionic strength I is a quantity that includes concentration of all charged species in the solution (counting H_3O^+ and OH^-) and thus assessing intensity of coulombic interactions in the solution. The ionic strength is defined as:

$$I = \frac{1}{2}\sum_{i=1}^{n} c_i z_i^2 \tag{4}$$

where c_i and z_i are the concentration and the charge number of the i-th ionic species, n is the number of the ionic constituents.

To demonstrate the impact of ionic strength on physicochemical parameters we calculated the dependences of consecutive $pK'a$ constants and electrophoretic mobilities of citric acid univalent and trivalent anion on ionic strength by means of PeakMaster 5.3 software [8, 9].
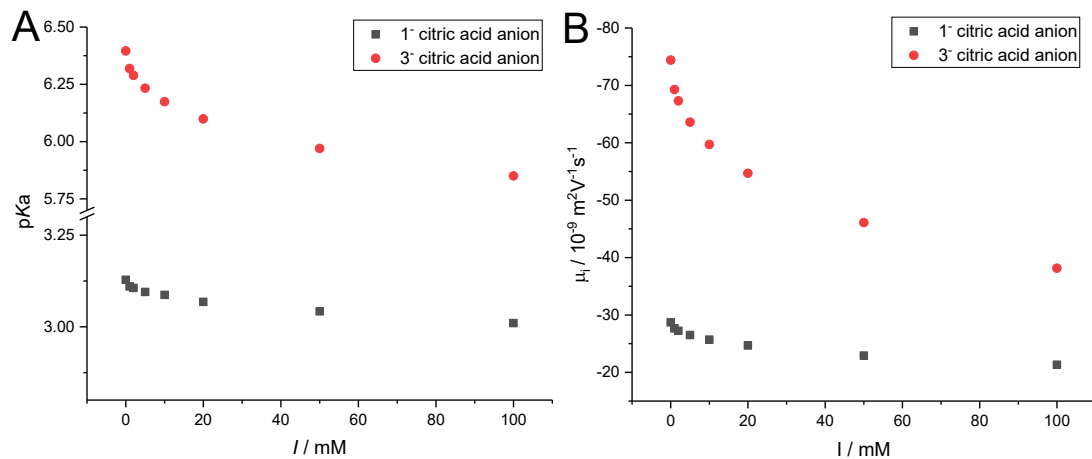

Figure 1. Calculated dependences of $pK'a$ constants (**A**) and ionic electrophoretic mobilities (**B**) for citric acid as univalent and trivalent ion on ionic strength of the solution. Black squares are values for univalent anion of citric acid and red circles values stand for trivalent anion of citric aci.

Figure 1A shows shifts of pK'a constants of citric anions in two different charge states. For citric acid in 1⁻ charge state the shift of pK'a is around 0.1 unit of pK'a with increase of ionic strength from 1 to 100 mM and for 3⁻ state the shift is even more significant, being up to 0.5 unit. Figure 1B depicts the same shift of ionic electrophoretic mobilities on ionic strength of surrounding solution. This dependency is showing shift for 1⁻ citric acid of 7 mobility units (mobility unit is defined as $m.u. = 10^{-9}\,m^2V^{-1}s^{-1}$) and for citric acid 3⁻ shift of 37 $m.u.$ for the increase of ionic strength from 1 mM to 100 mM. Both dependences demonstrate necessity of proper ionic strength corrections that must be made for obtaining correct values of measured parameters.

To obtain thermodynamic equilibrium (dissociation or complex stability) constants or limiting electrophoretic mobilities, apparent equilibrium constants and ionic mobilities needs to be measured at constant ionic strength and then corrected by some of the theoretical model to zero ionic strength [10-13].

The theory of activity coefficients was first proposed by Debye and Hückel [14, 15].

$$\log \gamma_i = -\frac{A z_i^2 \sqrt{I}}{1 + Ba\sqrt{I}} + 0.1 z_i^2 I \qquad (5)$$

Equation (5) is modified version of extended Debye-Hückel law with linear term, where z_i is charge number of i-th ion. A and B are constants describing surrounding solvent and a describes effective radius of the ion. However, Debye-Hückel was derived with assumption of spherical point charges and low concentration of other ions. This equation should be applicable up to $I = 100$ mM.

Based on the Debye-Hückel theory, Onsager-Fuoss theory was derived, describing influence of ionic strength on molar conductivities and thus on electrophoretic mobilities [16]. This theory is rather more complex than the Debye-Hückel theory, which solves static influence of ionic atmosphere on the ion. The theory by Onsager and Fuoss considers two phenomena connected with the electromigration of the ionic constituents – the electrophoretic and relaxation effects. It even considers so called "mixture effect" that is propagated not only thru ionic strength of solution itself, but by mobility ratios of all the compounds present in the solution. The Onsager- Fuoss relationship adopted for ionic mobilities can be expressed as:

$$\mu_j = \mu_j^\infty - \left(B_1 z_j \mu_j^\infty \sum_{n=0}^{5} C_n R_j^{(n)} + B_2 |z_j| \right) \frac{\sqrt{\Gamma}}{1 + Ba\sqrt{\frac{\Gamma}{2}}} \tag{6}$$

$$B_1 = \frac{e^3}{12\pi} \sqrt{\frac{N_{Av}}{(\varepsilon kT)^3}}, \quad B_2 = \frac{e^2}{6\pi\eta} \sqrt{\frac{N_{Av}}{\varepsilon kT}}, \quad \Gamma = \sum_{i=1}^{s} \Gamma_i, \quad \Gamma_i = c_i z_i^2$$

where μ_j^∞ and z_j are the limiting ionic mobility and charge number of the *j*-th ionic species, respectively, c_i is the concentration of the *i*-th ionic species, e is the elementary charge, N_{Av} is the Avogadro constant, ε and η is the permittivity and dynamic viscosity of solvent, respectively, k is the Boltzmann constant, T is the absolute temperature, s is the overall number of all ionic species in the solution. C_n are the coefficients of the series

$$C_0 = \frac{1}{2}\left(2 - \sqrt{2}\right) \text{ and } C_n = -\frac{\sqrt{2}}{2}\binom{1/2}{n} \text{ for } n \geq 1 \tag{7}$$

Column vectors $R^{(n)}$ are defined by means of the recursion formula

$$R_j^{(n)} = \sum_{\sigma=1}^{s} (2\mathbf{H} - \mathbf{I})_{j\sigma} R_\sigma^{(n-1)} \quad R_j^{(0)} = z_j - \frac{\sum_{i=1}^{s} z_i \mu_i}{\sum_{i=1}^{s} \left|\frac{z_i}{\mu_i^\infty}\right| \mu_i} \left|\frac{z_j}{\mu_j^\infty}\right| \tag{8}$$

where $\mu_i = \frac{\Gamma_i}{\Gamma}$ and $\mathbf{I}$ is the unit matrix. $\mathbf{H}$ is the matrix with the elements h_{ji}

$$h_{ji} = \delta_{ji}\left(\sum_i \mu_i \frac{\omega_i}{\omega_i + \omega_j}\right) + \mu_i \frac{\omega_i}{\omega_i + \omega_j} \tag{9}$$

where δ_{ji} is Kronecker delta $\delta_{ji} = \begin{cases} 0 & (j \neq i) \\ 1 & (j = i) \end{cases}$ and ω are the limiting molar conductivities.

The limitations of this model are the same as for Debye-Hückel theory, small symmetrical point charge and ionic strength maximum of 100 mM. This theory was later expanded by Murphy *et al.*[17] for asymmetric binary electrolytes. Another extension of the Onsager-Fuoss theory was done by Pitts who introduced the concept of finite ion diameter instead of treating the ions as dimensionless point charges [18]. Šlampová *et al.*[19, 20] showed approach to correct both limiting mobilities and p*K*as to zero ionic strength. Nonetheless, their approach was limited to single charged weak electrolytes with requirement of measuring all data at constant ionic strength. For the ionic strength corrections, simplified version of both theories were utilized. Various modifications and specializations of the basic Onsager-Fuoss theory are widely used to calculate properties of non-ideal electrolytes [21]. However, due to the complexity of

this theory and CE systems, proper corrections of limiting mobilities is rather complicated task. Utilizing proper corrections of mobilities by Onsager-Fuoss theory would require specialized software tool for nonlinear fitting as each measurement is performed in different BGE.

1.2. Ionic effects in hydrophilic interaction liquid chromatography

The same theory of electrolytes (Debye-Hückel) would be applicable for aqueous solutions in hydrophilic interaction liquid chromatography (HILIC), but in such systems it is less significant compared to other effects (for neutral analytes it is even more negligible). This is due to the utilization of other types of solvents next to the aqueous buffers in HILIC mode, mostly acetonitrile, where this theory would have to be significantly modified. It should be kept in mind that pKa values are defined for aqueous solutions conditions, however, in organic media, they may shift considerably to different values [22]. Also, ionic strength of aqueous phase itself is one of the parameters that have significant impact on HILIC retention mechanism, especially due to its complexity.

HILIC is one of the separation modes of liquid chromatography, composed of hydrophilic stationary phase, while mobile phase consists of less polar constituent with addition of water as a strong eluent. Mechanism of HILIC separation was proposed by Alpert [23], in which polar groups attached to stationary phase attract water molecules from mobile phase, forming an aqueous diffusion layer over the surface. Thus, a polar analyte in the mobile phase undergoes partitioning between the semi-immobilized aqueous layer and the mobile phase with lower content of water. The more polar analytes have higher affinity towards water layer near the stationary phase than the less polar mobile phase. This preference leads to increased interaction of the analyte with aqueous layer, thus increased retention of analyte [24]. However, in HILIC not only partitioning, but also adsorption mechanism is significantly depending on the separation system (*i.e.* stationary and mobile phase) and more types of interaction (hydrogen bonding, Van der Waals interaction) contribute to overall retention mechanism [25-27]. Even ionic interactions can be compelling, when stationary phases and analytes have permanent charge present [28, 29].

Due to its complexity retention mechanism in HILIC has not been fully described yet. However various studies have been published to clarify some of its parts. Hemström *et al.*[30, 31] showed that retention of saccharides on amino modified silica stationary phase decreased with increasing water content in the mobile phase. While increasing content of water in the mobile phase, mobile phase surrounding stationary phase becomes like the retained aqueous phase. Thus, partitioning of analyte between those phases becomes less significant. This also implies that retention is directly proportional to the polarity of the solute and inversely proportional to the polarity of mobile phase.

Composition of mobile phase is important for retention mechanism in HILIC and magnitude of some interaction can be influenced by pH, ionic strength and composition of used buffer. pH of buffers is utilized in HILIC to influence stabilization of charge of stationary phase as well as of the analytes and can enhance or even suppress some types of interactions, depending on the system [32]. As expected, the retention of neutral compounds is much less affected by pH change. Nevertheless, in the work of McCalley *et al.* it was shown that for different types of stationary phases (unmodified silica, zwitterionic and amide) changes in the ionization of bonded groups of underlying silanols can affect the thickness of the water layer on the column surface and thus solute retention [33]. McCalley *et al.* also investigated the effect of increasing ammonium formate concentration at pH 3 on the retention of various compounds. While the retention of strongly basic analytes decreased, for the acidic analytes the effect was the opposite, suggesting suppression of ionic interaction of underlying negatively charged silanol groups. West and Auroux [34] performed similar retention mechanism study for 76 probe analytes on zwitterionic columns, applying linear solvation energy model to quantify significance of each type of interactions for zwitterionic stationary phases. Only a few works focus on the effect of type of buffer cation and its concentration on retention mechanism in HILIC [25, 35]. Douša *et al.* studied retention of amino acids on different stationary phases using two buffers varying in cation type and concentration. It was shown that retention of amino acids increases with concentration of potassium formate/citrate and not changing with concentration of triethylammonium buffer. Nevertheless, the effect of the concentration of a greater variety of salts, buffers and additives on analyte retention and possible connections with

changes produced in the water layer is a complex task and would be to some extend specific for each stationary phase and type of analytes and thus it requires further study.

1.3. Online preconcentration and focusing techniques in capillary electrophoresis

One of the limitations of every analytical method is sensitivity of its detection, which leads to effort to increase the concentration of target analytes in sample prior to analysis or prior detection itself. Besides so-called offline preconcentration techniques like solid phase extraction, liquid-liquid extraction etc. performed as a sample pretreatment step prior analysis, online preconcentration taking place during separation process helps overcome this issue, especially in CE.

Online preconcentration techniques need proper experimental design. General mechanism of online preconcentration and focusing techniques in CE is to change migration velocity of targeted analytes and make their injected zone thinner, thus more concentrated. These online preconcentration techniques are often utilized as part of electrophoretic analysis in practice and thus, they are still under development and investigation. Recent progress in the field of online preconcentration techniques is summarized by Breadmore *et al.*[36-42] in the series of periodic reviews.

Online preconcentration and focusing techniques in CE can be divided into several groups based on their mechanism. *Stacking* mechanism is based on change electrophoretic velocity of analyte due to the change of conductivity of BGE (in most cases due by the dilution of BGE itself). *pH junction* techniques have pH boundaries introduced into capillary, that alters ionization state of analytes. *Sweeping* methods utilizes pseudostationary phases that affect migration velocities of analytes based on their affinity to them. Another one of the techniques utilizes *membranes* for analytes preconcentration. *Isoelectric focusing (IEF)* method utilizes hundreds of ampholytes to form stable smooth pH gradient after switching the voltage on. After that, weak analytes are focused at pH where their effective electrophoretic mobilities are zero. In practice, the combination of techniques is often used to achieve the highest preconcentration potential possible.

1.3.1. Sweeping preconcentration techniques

As was mentioned above, sweeping is online preconcentration technique based on interaction of analyte with pseudostationary phase present in the BGE, similar to electrokinetic chromatography (EKC). Sweeping was first introduced by Quirino and Terabe [43, 44] with sodium dodecyl sulfate as a pseudostationary phase. Most frequently used pseudostationary phases for sweeping are charged micelles [45, 46], but other complex forming agents such as borates [47], EDTA [48] or charged cyclodextrins (CDs) [49, 50] were also utilized. Other complexing agents besides micelles, such as cyclodextrins, are mostly utilized as additional chiral selector [51, 52] or to enhance sweeping potential of micelles [53, 54]. Neutral pseudostationary phases such as neutral cyclodextrins are utilized quite rarely [55, 56].

General mechanism of sweeping utilizes different migration velocity of analytes (those with affinity to pseudostationary phase) between BGE with and without pseudostationary phase. Mechanism of sweeping is depicted in Figure 2, modified from paper of Quirino and Terabe [43]. In the first step, model analytes A_1 and A_2 bearing the same charge are injected in the capillary with length of their injection zone l_{inj} and the capillary is filled with BGE without micelles. Micelles are present in the BGE in the inlet vial. When turning on the voltage in step 2, charged micelles start to migrate into the capillary. The analyte A_1, which have affinity to micelles, is swept in front of the micelle zone, due to change of its electroforetic mobility in presence of micelles. The analyte A_2 zone is affected in lower extend than the analyte A_1, due to its lower affinity to micelles. This results in A_2 zone being swept only partially. Micelles then migrate further into capillary (steps 3 and 4), sweeping A_1 in its forehead thus preconcentrating it, leaving A_2 and separating both analytes.
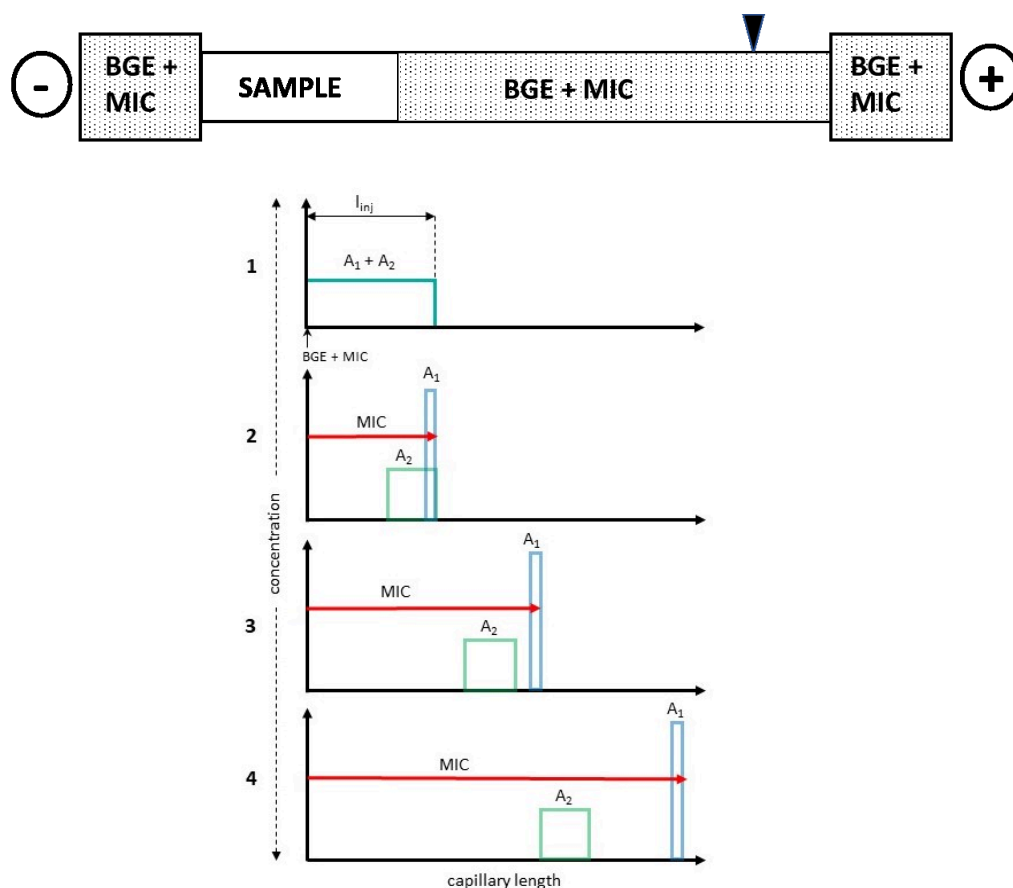
Figure 2. Evolution of analyte zones in EKC under sweeping conditions. Upper part of picture shows capillary setup after analyte injection.(**1**) Injection of sample into capillary without micelles (MIC) present (BGE with micelles is present in both vials).(**2**) Micelles from the inlet vial penetrating analyte zones and sweeping analyte A_1 due to its affinity, slightly affecting A_2.(**3,4**) Micelles completely penetrate both analyte zones, A_1 migrating on its forehead preconcentrated, separated from A_2. Adopted from [43]

The theoretical calculations and predictions of sweeping were investigated in several papers. Quirino and Terabe [43, 44] predicted narrowing factor of analyte zone in considerable homogenous electric field as $1/(1+k)$, where k is partition coefficient of analyte in presence of micelles. When sweeping preconcentration is combined with stacking (analyte zone does not containing any charged micelles thus its conductivity is lower), theoretical description becomes even more complicated, because both analytes as well as micelles are preconcentrated on the stacking boundary [57, 58]. Quirino [59] also showed possibility of calculating preconcentration factor for sweeping when utilizing complexation agent such as borate instead of micelles, when knowing complex

stability constant and electrophoretic mobility of complex. In some works, insight to sweeping process was brought by numerical simulations. Breadmore *et al.*[60] used software GENTRANS for numerical simulations of EKC with sweeping process. GENTRANS was later utilized for simulations of enantioseparations in EKC with neutral CD by Thormann *et al.*[61] and revealed that stacking phenomena occur in CD containing electrolyte.

Although sweeping is efficient and specific online preconcentration technique, it is mostly coupled only with UV detection. Coupling sweeping with conductivity detection is sort of difficult task, because when employing multiply charged compounds as micelles and cyclodextrins in different zones in BGE, it can make interpretation of conductivity detection signal quite difficult. Signal response of conductivity detection is not only proportional to the concentration of analyte itself, but also to concentrations and mobilities of all compounds in the analyte zone [62]. Thus, only few works, utilizing other preconcentration techniques such as stacking [63-65] or pH junction [66] featuring conductivity detection have been reported so far.

1.3.2. Dynamic pH junction

Dynamic pH junction utilizes changes of ionization state of analytes due to the pH differences in the capillary. This online preconcentration technique was first introduced in CE by Aebersold and Morrison [67] and its theoretical description was later expanded by Britz-McKibbin *et al.*[68-70]. Cao's group published numerous theoretical and practical studies on moving reaction boundary, which are summarized in published review [71]. Development and applications of pH junction preconcentration technique over last years is compiled in the review of Kazarian [72] and also in the series of Breadmore reviews [36-42].

While conceptually very simple, the precise mechanism of dynamic pH junction is quite complicated. The general mechanism involved in this type of preconcentration is based on a difference in the pH between the sample and electrolyte (or two different electrolytes with different pH). It is also necessary, that mobility of analytes targeted for preconcentration must change when analyte moves from one pH to another. Figure 3 shows the mechanism of dynamic pH junction of peptides and proteins with different

isoelectric points (pI) using sample with low pH and BGE with high pH, with electroosmotic flow (EOF) present as well, similar to works of Monton *et al.*[73] and Imami *et al.*[74]. Large plug of sample in the BGE of low pH is introduced into capillary as depicted at step 1. At low pH proteins bear positive charge and upon application of voltage (step 2), they migrate towards cathode. Once they encounter the high pH BGE, the positively charged proteins become negatively charged in it and migration is reversed towards anode. At this boundary, peptides become focused into sharp thus more concentrated zones. After some time (that depends on length of injected zone and BGE components), low sample pH is titrated with surrounding high BGE and proteins are separated in the normal capillary zone electrophoresis (CZE) and brought to detector by EOF (step 3). The same approach is applicable also for weak electrolyte analyte. In such cases, the direction of electromigration is not reversed on pH boundary as in ampholyte cases, but the velocity of target analyte is reduced and it can be focused and preconcentrated [75].
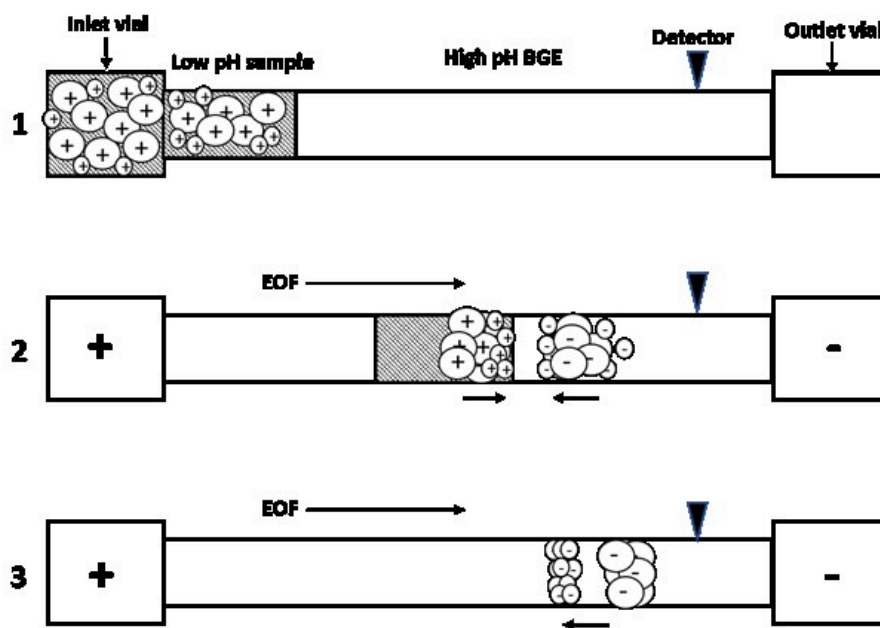
Figure 3. Model of pH junction mechanism for proteins. (1) Sample of proteins is injected into capillary in low pH BGE, rest of the capillary is filled with high pH BGE. (2) Voltage is turned on, peptides are preconcentrated on the pH boundary between two buffers. (3) pH boundary dissipates thus peptides migrate freely to anode, EOF drags everything to cathode and detector. Adopted from [73].

While the difference of pH on the boundary is one of the main parameters of the pH junction, there are other parameters important for successful preconcentration, such

as duration, speed and migration direction of the boundary [75-77]. All these parameters depend on composition of both sample and BGE. The concentration of the ions in the sample, its pH and the pKa of compounds in the sample matrix determine its buffering capacity and the amount of sample matrix that must be titrated by the BGE for the boundary to dissipate. Determining migration direction of boundary is also quite complicated, because it relies on movement of all compounds, their mobilities and pKa values as has been shown by Cao *et al.* [78-81].

As was mentioned above, pH discontinuity is usually induced by injecting analyte in a sample matrix which have different constituents and different pH. These systems are usually specifically designed for targeted analyte. Most common buffers used for pH junction are borate buffer as a BGE and acetate, phosphate or formate buffer as the sample matrix solution, because of their suitable properties (like their high electrophoretic mobility, thus fast titration of their zone)[72]. In several reports, authors used same component for both sample matrix and BGE for pH junction preconcentration. These simplifications of pH junction preconcentration were utilized to simulate dynamics of such boundaries [75], describe their movement [82] or to couple CE with MS [74]. In some of these works [75, 82, 83], pH difference between BGE and sample matrix is caused by having pH of BGE around pKa of weak acid (standard buffer solution), while injecting sample with matrix containing salt of the same weak acid or over-titrated salt in favor of the base. From the simulations of preconcentration system, the relationship between velocities of analytes and pH boundary are given to achieve maximum focusing efficiency. The influence of the sample matrix pH on focusing performance was experimentally investigated when optimizing the CE-MS method for four peptides mixture [74].

1.3.3. Capillary isoelectric focusing

Another way to introduce linear smooth pH gradient along the whole capillary length, is method called isoelectric focusing (IEF). Isoelectric focusing , similarly to dynamic pH junction, also preconcentrate analytes, but its main purpose is a separation of ampholytes, especially proteins and peptides [84]. It is often used for characterization of biological samples, determination of protein samples purity or even determination of

pI values of proteins. Capillary isoelectric focusing (cIEF) combines high resolving power of gel IEF with quantitation advantage of CE instrumentation. When electric potential is applied along the capillary, hundreds of carrier ampholytes with different pI form a stable pH gradient along the whole capillary. In this pH gradient the proteins are separated according to their isoelectric points and become focused at position, where their net charge is zero *i.e.* pH = pI. When focused protein get out of the zone by diffusion, reversal of its charge returns it into focusing position, due to that cIEF gives higher resolving power than classical CE separation [85]. However, to successfully determine pI of focused proteins in cIEF, its pH gradient needs to be characterized. For characterization of gradient and determination of pI of focused proteins, concept of pI marker was introduced [86].

Compounds employed in IEF as carrier ampholytes should be amphoteric compound with both p*K*a values close to each other, thus forming stable pH gradient with sufficient buffering capacity and conductivity [87, 88]. For pI markers, the requirements are even more strict: they have to have suitable UV absorption band (ideal absorption at 280 nm, because that is wavelength used in most protein studies); having good focusing power defined by –dz/d(pH) (differential of relative charge to differential of pH) or small value of Δp*K*a; high stability and purity; they also should not have high affinity to silanols of capillary wall [89]. Various pI markers were utilized over the years differing in the pH range that they cover, in their structure; some of them have even fluorescence emission [90-95]. In this manner, it is desired to have set of commercially available pI markers covering whole pH range, which are fulfilling requirements proposed by Šťastná [89] and have their electrophoretic behavior in IEF well-described.

2.   Objectives of the thesis

The general aims of this thesis are to describe and clarify some parts of ionic effects in separation systems of CE and HILIC mode of HPLC. Further, to propose new online preconcentration techniques for CE and characterize them by numerical simulation and experiments.

The particular objectives of the thesis are:

- proposal of new preconcentration technique based on sweeping with neutral sweeping agent and utilization of conductivity detection for this technique
- utilization of disturbing phenomena of system zones as pH boundaries for pH junction type of preconcentration
- development of freeware that adopts proper theories of ionic strength for corrections of pKa constants and limiting mobilities determined by capillary electrophoresis
- investigation of influence of buffer composition on retention of analytes in HILIC
- characterization of new, well-defined, low molecular pI markers for cIEF and their utilization for characterization of cIEF gradient by simulations and experiments

3. Results and discussion

3.1. New online preconcentration techniques in CE: Papers I; II

The first part of this thesis is focused on proposal of new online preconcentration techniques in CE, their application and characterization by numerical simulations and model experiments. The first technique is based on sweeping of charged analytes by neutral complexing agent with beneficial use of conductivity detection (Paper I). The second technique belongs to pH junction family, but the pH boundaries are formed by means of system zones – the phenomena considered mostly as disturbing in CE (Paper II).

Paper I propose online technique where charged analytes are swept due to their complexation with neutral cyclodextrin. Conductivity detection is utilized for this sweeping technique and its signal enhancement factor is also fully predictable by numerical software. Model system demonstrating the method consisted of R-flurbiprofen (R-flu) as an analyte and β-cyclodextrin (β-CD) as a neutral sweeping agent, both at various concentrations. BGE consisted of TAPS/LiOH 10/5 mM with pH = 8.3, where R-flu is fully ionized (weak acid, pKa = 4.17). β-CD as a sweeping agent was diluted in the BGE (its concentration varied from 0 – 5 mM), sample solutions did not contain any β-CD. Mechanism of proposed method was based on migration of fully charged analyte in CD free BGE and then its retardation due to the complexation, when migrating into CD containing BGE thus increasing its concentration. In real experiments, also EOF had to be considered as depicted on scheme of Figure 4. R-flu is dissolved and injected from β-CD free BGE into capillary filled also by BGE without cyclodextrin. After injection of R-flu, inlet BGE vial is replaced with BGE containing β-CD. When voltage is turned on, R-flu migrates towards inlet, penetrating BGE containing β-CD and thus being swept by its interaction with CD, while all the solution is being dragged towards detector by the EOF, including swept concentrated zone of R-flu.
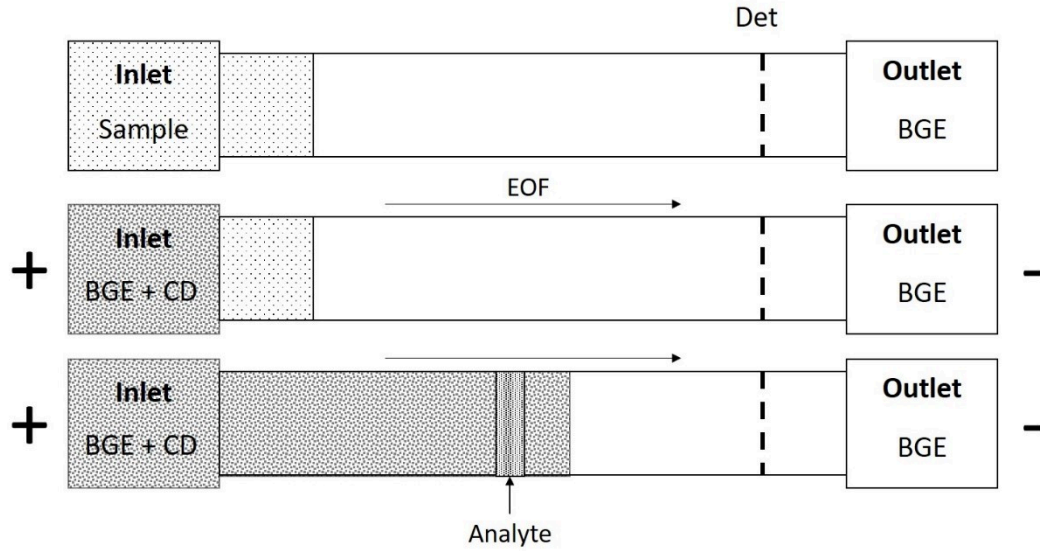
Figure 4. Experimental setup of sweeping of negatively charged analyte R-flu with neutral β-CD with positive EOF present.

From the motion equations, the equation for preconcentration factor (parameter describing increase of analyte concentration during sweeping) have been derived, see equation (10):

$$F = \frac{\mu_A - \mu_{CD,eff}}{\mu_{A,eff} - \mu_{CD,eff}} \tag{10}$$

where μ_A is electrophoretic mobility of free analyte and $\mu_{A,eff}$ is effective electrophoretic mobility of analyte in BGE containing CD. Even when CD is neutral and thus should not move in electric field, it does, due to the interaction with charged analyte that forms a charged complex. This partial mobilization of neutral CD in presence of charged analyte is represented by $\mu_{CD,eff}$. Both, mobility of analyte in presence of CD and mobility of CD in presence of charged analyte can be calculated by equation derived by Wren and Rowe [3]:

$$\mu_{A,eff} = \frac{\mu_A + \mu_{ACD} \cdot K_{as} \cdot c_{CD}}{1 + K \cdot c_{CD}} \tag{11}$$

where, μ_{ACD} is mobility of complex analyte-cyclodextrin, μ_A is mobility of free analyte, c_{CD} is a concentration of cyclodextrin and K_{as} is complex stability constant. If there is sufficient excess of CD, it leads $\mu_{CD,eff}$ to zero and equation (10) can be simplified and defined for maximum preconcentration factor of this method:

$$F = \frac{\mu_A}{\mu_{A,eff}} \tag{12}$$

For our model system, where effective electrophoretic mobility of free R-flu in the buffer was $-24.5 \cdot 10^{-9}$ $m^2V^{-1}s^{-1}$ and effective mobility of R-flu in presence of 5 mM β-CD calculated from eq. (11) was $-11.9 \cdot 10^{-9}$ $m^2V^{-1}s^{-1}$, the maximum preconcentration factor (that corresponds to exact increase of R-Flu concentration) was only 2.05. However, the sensitivity of detection could be improved further by utilizing conductivity detection. In conductivity detection, signal of analyte depends not only on concentration of analyte itself, but on the whole composition of analyte zone *i.e.* types and concentrations of all compounds of BGE in the analyte zone. When analyte passes through the β-CD boundary, concentration of all compounds of BGE in analyte zone are rearranged, adjusting to the different BGE, which contains β-CD. Total enhancement factor of conductivity detection EF_{tot} can be calculated as:

$$EF_{tot} = F \cdot EF_\kappa \tag{13}$$

where preconcentration factor *F* describes how much concentration of analyte increases and EF_κ is conductivity enhancement factor, that describes rearrangement of all compounds in analyte zone and its effect of conductivity signal of analyte zone. EF_κ is predictable by our software PeakMaster 5.3. [96, 97], when recalculating analyte zone for BGE containing cyclodextrin. Preconcentration factor *F* is also predictable, when knowing mobilities of targeted analyte and its complex with utilized sweeping agent, making total enhancement factor of conductivity predictable as well. To confirm predictability of preconcentration and enhancement factors, we calculated both preconcentration factors *F* from equations (10) and (12) and EF_κ by using PeakMaster 5.3. software. With both factors predicted, we have been able to calculate total enhancement factor of conductivity detection EF_{tot}. We have compared our predicted total conductivity enhancement factors with experimentally obtained ones and also with the ones obtained by numerical simulation in Simul 5 Complex software [98, 99].

With increasing concentration of β-CD, its effective mobility ($\mu_{CD,eff}$) limited to zero, enabling simplification of the eq. (10) to the eq. (12). To show suitability of simplified equation (12), we have compared calculated values of preconcentration factor *F*, with the values obtained from numerical simulations of Simul 5 Complex and the values that were obtained experimentally. When concentration of β-CD as a sweeping

agent was 5 mM, we obtained preconcentration factor calculated from eq. (12) with value of 2.02 and the one from numerical simulation was 2.01 [100]. Preconcentration factor for R-flu system that was obtained experimentally was slightly lower, with value of 1.66. This can be caused, by decrease of molar absorption coefficient of R-flu in presence of β-CD (this was also experimentally verified). The total enhancement fator, $EF_{tot,}$ was calculated from eq. (13), where EF_κ is obtained from calculations in PeakMaster 5.3 and preconcentration factor F was obtained from equation (12) with theoretical values. Calculated values of EF_{tot} were in a good agreement with experimentally obtained ones (experimental values were obtained from signal to noise ratio of system with and without sweeping), showing good predictability of not only preconcentration factor, but also conductivity enhancement factor of this method.

This online preconcentration method was also utilized for real drug sample, Strepfen pastille. Strepfen pastille have declared content of 8.75 mg of flurbiprofen as active pharmaceutical ingredient. Strepfen was diluted in the buffer, filtrated and injected as a sample without any further sample pre-treatment. We have compared analysis of real stepfen sample with and without preconcentration, demonstrating efficiency of conductivity enhancement. Flubiprofen signal on conductivity detection in system without sweeping was bellow limit of detection, showing significant improvement of conductivity signal when sweeping is present.

Further, it was observed that, when analyte is penetrating through the CD boundary and being swept, another set of system zones is being induced [100]. System zones are rather disturbing phenomena, because they can be misinterpreted as peaks of analytes or comigrate with them and cause their unexpected broadening. For this reason, the origin of the new set of system zones may be worrying, but we revealed that their mobilities are the same as the mobilities of the original system zones. Thus, the position of the system zone in electropherogram can be easily predicted which prevents wrong data interpretation.

In the Paper II the system zones were even utilized for selective analyte preconcentration. Because system zones are disturbances in BGE components concentration, they have different pH and conductivity then BGE itself, thus they can be utilized as pH boundaries for preconcentration of weak analytes. System zones are inherent to each electrophoretic system, and their number is always equal to the number

of BGE components. They have their own electrophoretic mobilities, system mobilities or eigenmobilities, which are given by the composition of entire BGE, including OH⁻ and H_3O^+ ions. [101].

In binary buffers of pH below 5 and above 9, one of the system zones migrates with certain electrophoretic mobility while the second one is stationary, having zero mobility. Their amplitude depends on initial disturbance of BGE *i.e.* on the composition of sample injected. Thus, when carefully designed the electrophoretic system can have system zones position (velocity or mobility) and the size (amplitude of pH change) suitable for preconcentration of target analyte. Our PeakMaster 5.4 software is a powerful tool for such designing [8, 9]. Scheme of preconcentration by moving system zone boundary is depicted on Figure 5.
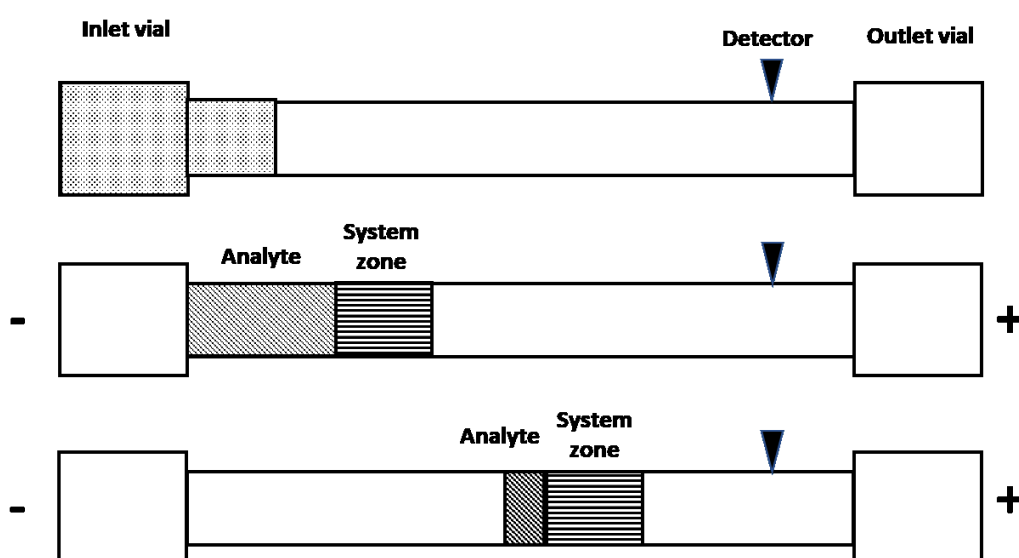
Figure 5. Model of moving system zone boundary preconcentration. In the upper part, analyte is injected into capillary from the sample matrix suitable for preconcentration. In the middle part, voltage is turned on and analyte and system comigrate towards outlet. Analyte have higher mobility than moving system zone, but due to its pH disturbance is unable to pass thru it and gets preconcentrated behind it - bottom part.

First, to show preconcentration on moving system zone boundary, we chose *p*-cresol (weak acid, p*K*a = 10.96) as model analyte. To achieve preconcentration of *p*-cresol, buffer with pH close to its p*K*a – Triethylamine (TEA)/HCl 60/40 mM, pH = 10.62 (pH of buffer close to *p*-cresol p*K*a is to have steep dependence of mobility of *p*-cresol on pH) was used. It was calculated in PeakMaster that this buffer has two

system zones with mobilities of 0 and -8.09·10⁻⁹m²V⁻¹s⁻¹ and the *p*-cresol is faster in the buffer than the moving system zone, having the mobility of –9.81·10^{-9}m^{2}V^{-1}s^{-1}. However, with proper amplitude (*i.e.* disturbance of pH in the system zone) *p*-cresol is slower in the system zone and is unable to migrate thru it, thus being stuck behind it and preconcentrated. To achieve this, sample composition necessary for *p*-cresol preconcentration was calculated by PeakMaster in "Amplitudes and shapes" window. To fulfil the rule, that amplitude of system zone must be sufficient to retardate *p*-cresol in it, within few iterations in Peakmaster we chose sample composition of TEA/HCl 60/60 mM. With this sample composition, the stationary system zone had only negligible disturbance in the pH compared to BGE (thus stationary system zone doesn't interfere in preconcentration process) and moving system zone had pH disturbance of few units of pH. This obeys the rule, that p-cresol is in buffer itself faster than system zone, but in the system zone itself p-cresol gets protonated and is unable to migrate thru zone and being preconcentrated behind it. Suitability of this system for preconcentration of *p*-cresol was confirmed by numerical simulations in Simul 5 Complex and also experimentally (Figures 2 and 5 in paper II) [102].

Not only moving system zones were utilized for analyte preconcentration, but also the stationary ones were utilized as well. Because the mobile system zones are present only in acidic or basic pH in binary buffers, in pH range 5-9 we employed stationary system zones for analyte preconcentration. The idea behind stationary system zone preconcentration is slightly different compared to moving system zone preconcentration. To achieve preconcentration of analyte on stationary system zone, selected buffer should have pH, where targeted analyte has zero or almost zero electrophoretic mobility. While pH disturbance of stationary system zone should have pH where analyte is ionized as much as possible. Thus, when analyte migrates out of the stationary system zone *i.e.* its injection zone, it slows down and is preconcentrated.

As a model analyte for preconcentration on stationary system zone, we chose *p*-nitrophenol (weak acid, p*K*a = 7.15). BGE consisted of MES/LiOH 50/20 mM, pH = 5.86 with two stationary system zones present. In this buffer, *p*-nitrophenol has mobility of -1.60·10^{-9}m^{2}V^{-1}s^{-1}. We utilized two sample matrix concentrations, MES/LiOH 5/5 mM and 50/50 mM, where pH disturbance of one of the stationary system zones was around +5.8 units of pH. Two sample matrixes were utilized, because

in sample matrix with concentrations of 5/5 mM there is also stacking phenomena present, that contributes synergistically to overall *p*-nitrophenol preconcentration (Figures 4 and 7 in paper II) [103]. In the sample matrix with concentrations of 50/50 mM destacking phenomena is present, which causes the opposite effect – broadening of the analyte peak. Systems with two different sample matrixes were simulated by Simul 5 Complex software and measured by means of experiment to show their preconcentration potential. From all the results it was noticeable that when analyte was injected from sample matrix of MES/LiOH 5/5 mM the synergy of system zone preconcentration and the stacking gives the highest preconcentration factor of 9. When sample matrix of MES/LiOH 50/50 mM was used, preconcentration factor only about 4 was observed due to destacking effect.

This newly proposed preconcentration method was also utilized for the selective preconcetration of two structurally similar ampholytes with p*K*a values close to each other: 4-aminophenylacetic acid (APAA, pI = 4.24) and 4-aminophenylbutyric acid (APBA, pI = 4.73). This selective preconcentration was achieved on moving system zones as pI values of both ampholytes are between 4-5, while around pH 4 one of the system zones in binary buffers starts to migrate. We designed system for selective preconcentration of each one of the ampholytes next to each other. Buffers consisting of formic acid/LiOH were utilized, varying only in their concentrations. Mechanism of APAA or APBA preconcentration was very similar to the one for *p*-cresol. However, both are ampholytes and when utilizing moving system zone preconcentration, they bear opposite charge in the system zone itself, changing its migration direction.

However, sometimes finding right buffer and sample composition for system zone preconcentration is not straightforward and all the rules are not that easy to follow. From the authors knowledge of designing such systems, flow chart have been constructed. It is presented in the paper and it helps user to design such preconcentration systems for routine analysis in the analytical practice.

3.2. Ionic strength corrections in determinations of pKa and limiting mobilities by capillary zone electrophoresis: Paper III

The second part of this thesis focuses mainly on description and characterization of ionic effects in separation systems, mainly CE and HILIC. CE mechanism is easier to describe mathematically compared to HILIC, where such description is not possible. In CE, the theories of ionic strength influence on activity coefficients and molar conductivities (thus limiting mobilities) have already been developed and improved over the years, see chapter 1.1. We utilized those theories and implemented them into software we called AnglerFish. We have demonstrated its advantages compared to standard approaches by correcting of measured pKa and limiting mobilities for ionic strength.

The theoretical equations of Debye-Hückel and Onsager-Fuoss laws (in chapter 1.1.) were implemented in computer program AnglerFish, that performs proper physico-chemical corrections of pKa and limiting mobilities evaluated by CE measurements with these equations. Measured ionic mobilities of compound for evaluation of pKa and limiting mobilities in exact buffers of know pH are an input into AnglerFish program. However, for proper correction by Onsager-Fuoss theory, exact buffer composition (pKa and limiting mobilities of buffering compounds) needs to be considered as well as they are part of the theory. This rather complicated input is simplified by the fact that Hirokawa's [104] database is also part of AnglerFish program, having values of pKa and limiting mobilities of most of the buffering compounds in it. The last piece of input, that AnglerFish needs for fitting of data, are initial estimates of fitted pKa values and limiting mobilities, so the algorithm of AnglerFish knows around what values of fitted parameters to expect. Estimates of corrected values should be always higher than the measured ionic mobilities, since ionic strength effect lowers (in absolute) values of electrophoretic mobilities. With all above, AnglerFish can perform nonlinear regression of experimental parameters by Debye-Hückel and Onsager-Fuoss laws, see input window of Anglerfish on Figure 6. As results are obtained thermodynamic parameters corrected for zero ionic strength, providing also residuals and another effective mobilities calculated from resulting pKa and limiting mobilities for each value.
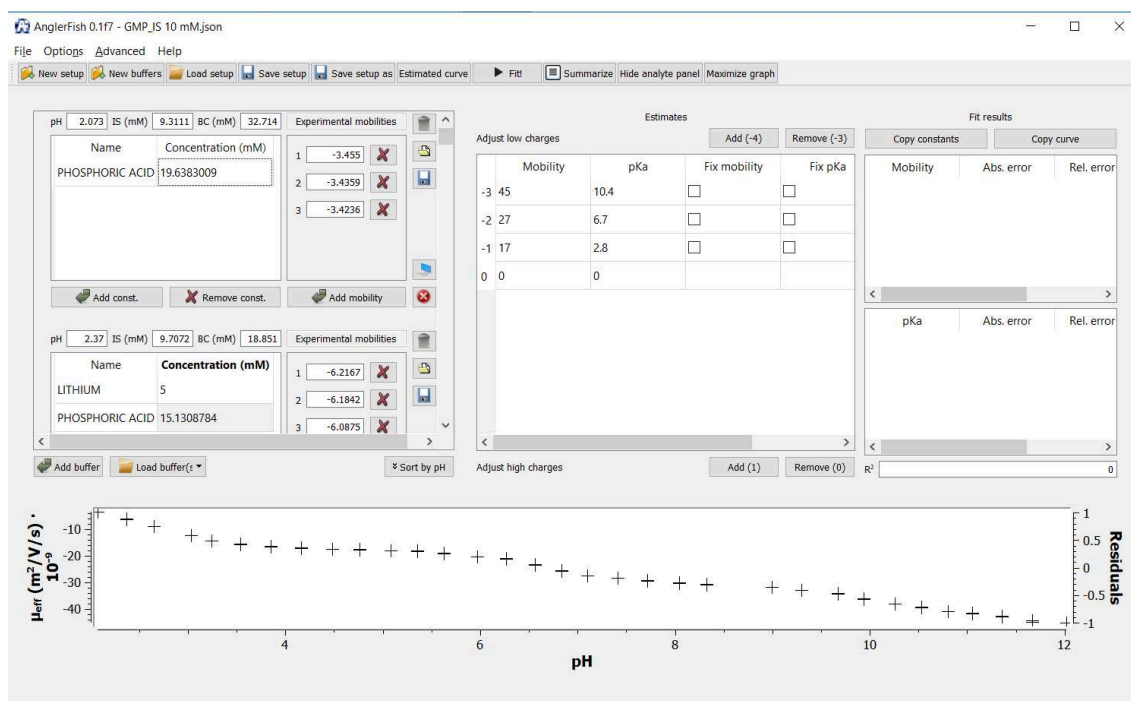
Figure 6. Input window of AnglerFish. In left corner are input of utilized buffer and measured mobilities. Upper middle window contains initial estimates of limiting mobilities and p*K*as (based on measured values). Bottom window shows dependence of experimentally measured mobilities of measured compounds (GMP) on pH.

Having whole buffer composition as an input parameter offers another advantage besides proper Onsager-Fuoss correction and that is possibility of having different ionic strength in each buffer for the measured dependence for the compound of interest. In standard approach for evaluating p*K*a constants and limiting mobilities, it is obligatory to keep ionic strength constant, because dependence of effective mobilities on pH have to be fitted by proper curve (where ionic strength is constant) and then values of p*K*a and ionic mobilities obtained by the fit are corrected by some simplified version of above mentioned laws [11-13]. In case of AnglerFish fitting this is no longer obligatory, because in Onsager-Fuoss theory (equation (6)), whole buffer setup is in input thus dependency of effective mobilities on buffer composition is fitted.

In Paper III we have compared obtained values of p*K*a values and limiting mobilities for multiply charged compound such as guanosine monophosphate (GMP) showing another advantage of this approach and that is the fact it considers so called "mixture effect". Mixture effect influences effective mobilities of compounds based on the actual measured buffer composition (mobilities and p*K*a of the compounds in the

buffer), even when pH and ionic strength are constant. This effect is more significant for multiply charged compounds such as GMP. In pH around 12, where effective mobility of GMP is already almost constant (when ionic strength is kept constant), its absolute value can still change due to this mixture effect (for exaple changing buffering ions in the buffer *i.e.* swapping lithium for potassium or changing buffer composition). The mixture effect of fast hydroxide ions speeds up the negative GMP^{3-} ions, so their mobility is increases due to it. This is well recognized by AnglerFish and the fitted points lie close to experimental points at high pH around 12, while classical approach could not precisely fit such values. Another advantage of AnglerFish approach is, that in more acidic or alkaline pH, ionic strength could not be kept constant anymore due to the higher concentration of H_3O^+ or OH^- ions. This is also considered in AnglerFish fitting, demonstrating lower standard deviances (and having fitted points close to experimental points as well) on AnglerFish fitting approach compared to classical approach. The only limitation observed was the value of ionic strength itself as it is also the limitation of both theories as well. However, when measuring pKa and limiting mobilities, the ionic strength is kept rather low to prevent joule heating.

3.3. Effect of cation type on retention mechanism in hydrophilic liquid interaction chromatography: Paper IV

Ionic effects in HILIC are more complex compared to CE due to the overall complexity of HILIC separation mechanism. Variety of different stationary phases, buffers and their concentrations used in mobile phase and difference in structure of separated analytes prevents from creation of general mathematical model, describing HILIC separation mechanism and the ionic effects that are influencing it. As was mentioned in chapter 1.2., the influence of buffer composition on HILIC separation mechanism is usually described experimentally.

We have performed study to clarify ionic effects on two selected stationary phases in HILIC. For this study we chose TSK gel Amide-80 (amide column) and Kromasil 60-5Sil (silica column) both same size (250 × 4.6 mm) and the same size of the particles (5 μm), to have results fully comparable. Two volume ratios of mobile phases were utilized for this study, having ACN/buffer 90/10 and 80/20. Various types

of buffers and concentrations were utilized. Buffers were always composed of acetic acid as a buffering anion and the buffer cation was variable (Li^+, NH_4^+, triethylamine (TEA), 2-Amino-2-(hydroxymethyl)propane-1,3-diol (Tris)), also concentration of both compounds was varying (as a variation of ionic strength of buffer). pH of buffer was kept always at 4, the only parameters that were changing were ionic strength of buffer and type of its cation. Different types of analytes were measured *i.e.* native amino acids (tyrosine, tryptophan, phenylalanine), their N-blocked versions (tert-butyloxycarbonyl, t-BOC), and various dipeptides. Retention of all analytes was studied with correspondence to utilized mobile and stationary phase.

First, the retention of native and N-blocked amino acids was studied. Most retained compound on both stationary phases was tyrosine as it is also the most polar one, while all N-blocked amino acid were much less retained compared to nonblocked ones. Correlation between polarity and retention was observed for amino acids on silica stationary phase. However, on the amide column tryptophan eluted before phenylalanine and this stationary phase showed higher retention of all N-blocked amino acids showing more complex retention mechanism on this stationary phase. From the obtained data it was shown that with increasing ionic strength of utilized buffer, retention of all N-blocked amino acids on both stationary phases in all type of mobile phases also increases. In this case, higher ionic strength of buffer enabled better transition of these analytes into water layer near the stationary phase by increase in solvation of those analytes. For both stationary phases, buffers containing Tris cation gave the highest retention. This is related to the structure of Tris, which contains three hydroxyl groups and one amino group, while the other cations have only one hydroxyl or amino group. For the native amino acids, influence of ionic strength of buffer on their retention was not that straight forward. Their retention increased, decreased or even did not change with increasing buffer concentration. In addition, we also tested buffers containing Ba^{2+} as a cation, having the same pH and ionic strength as other buffers. Previously it was shown that barium cations in the mobile phase caused increase in retention of some binaphthyl atropisomers. [105] Much higher retention for native and N-blocked amino acids was observed for both stationary phases, compared to other buffers. This is probably due to the sorption of barium cations on stationary phase, enabling ion-exchange mechanism to take a place as well.

Nonblocked dipeptides showed significantly lower retention compared to native amino acids. This is probably due to their lower polarity and bigger molecule size. Blocked analogues of dipeptides had similar retention to the blocked amino acids. Similar trend as for the amino acids was observed for the dipeptides, where buffers containing Tris gave highest retention on both columns. The retention behaviour of dipeptides differed for each of the columns. On the amide stationary phase, increasing buffer concentration resulted in increased retention for all utilized buffers except TEA, where it did not change with increasing concentration. While TEA buffers on silica columns showed opposite trend, decreasing retention with buffer concentration. This can be due to the fact, that TEA cation is able to compete for negatively charged sites on stationary phase and silica stationary phase have more of these than amide derivatized stationary phase. Opposite trend was observed for all other buffers with dipeptides. Also, barium as a cation was utilized for dipeptide retention measurements, showing again increase in retention for all dipeptides compared to other buffers. Moreover, retention of nonblocked dipeptides was for barium buffers higher than the native amino acids under these conditions, what is reversed in comparison with other tested buffers.

The results suggest that using different types and concentration of buffers in the mobile phase could be utilized to tune the retention of complex mixtures of analytes in HILIC separation mode.

3.4. Characterization and utilization of new set of pI markers for isoelectric focusing: Paper V

Paper V proposes new set of 14 commercially available or easily prepared pI markers with well-defined structure and adequate purity for IEF. These markers cover range of pH gradient in the 3 < pH < 10 range and contain no more than two acidic and two basic functional groups. pKa and pI values of these markers were first predicted by SPARC [106] and Chemsketch [107] software to have some initial estimates for pI of each marker to cover whole pH gradient. Electrophoretic mobilities in dependence on pH were measured experimentally to obtain precise values of pKa constants and electrophoretic mobilities for each of selected pI markers. However, to obtain

thermodynamically correct values of pKa and limiting electrophoretic mobilities, these values needed to be corrected to zero ionic strength. For this purpose, we utilized our new software AnglerFish, that is subject of Paper III (see chapter 3.2) and adopts proper correction of these values by Debye-Hückel and Onsager-Fuoss theories.

The characterized markers were used in a cIEF experiment to trace the shape of the pH gradient obtained with the SH AES carrier ampholyte mixture in a CEInfinite instrument (Advanced Electrophoresis Solutions, Cambridge, ON, Canada). However, from all of the 14 characterized markers in total, only 12 of them were detected as the CEInfinite instrument utilizes UV scanning at wavelength of 280 nm, where glycyl-histidine and 3-methylhistidine do not absorb. From obtained position of each marker with known value of pI the shape of pH gradient created of SH AES carrier ampholyte mixture was shown (Figure 3 in paper V) [108].

Since we have obtained not only pKas of each marker, but also limiting electrophoretic mobilities of each marker, we have studied their focusing behavior by numerical simulations of whole IEF gradient in Simul 5 Complex. IEF gradient for simulations consisted of phosphoric acid and LiOH as anolyte and catholyte respectively. Middle part of gradient contained 181 uni-univalent hypothetical carrier ampholytes with increasing values of pKa, starting from an anionic pKa of 3.5 to an anionic pKa of 10.8 with ΔpKa = 1 between the anionic and cationic forms, and a pKa step of 0.0406 for each following ampholyte. Their cationic and anionic mobilities were set to 20 m.u. and their concentrations were 0.01 mM. The applied voltage for formation of gradient was 100 V for 3000 s. Results from the simulations showed that two of the markers (3-methylhistidine and labetalol) had wider peaks after their focusing compared to the other markers. This was since their ΔpKa was higher compared to the other markers, showing importance of this value as a parameter for pI marker selection.

Shape of pH gradient obtained from measurements with pI markers was compared with simulations, showing very good agreement in its middle linear part with slight deviations on its edges. These nonlinearities observed in experimentally obtained shape of pH gradient were caused by bidirectional isotachophoretic process[109] that always accompanies IEF measurements.

4. Conclusion

First part of this thesis was focused on theoretical description and proposal of new online preconcentration techniques in CE. We proposed two new online preconcentration techniques in this thesis. First one was based on sweeping of charged analytes with neutral complexing agent and the second one was based on focusing on pH boundaries induced by system zones. For the sweeping with neutral complexing agent technique, we derived theoretical equations, predicting its preconcentration factor and compared calculated values with experimental and simulated ones. We have utilized conductivity detection for the sweeping for the first time and shown, that conductivity detection signal is also enhanced for this technique and it is also fully predictable by means of theoretical calculations. This method was then utilized for preconcentration of active pharmaceutical ingredient in real drug sample. The second proposed method showed that system zones in CE, which are considered mostly as disturbing phenomena, can be utilized for selective analyte preconcentration. It was shown, that both types of system zones, stationary and moving, can be utilized for analyte preconcentration. Mechanism of these preconcentrations was described by means of numerical simulations and experiments on various types of analytes. The method developed was then utilized for selective preconcentration of two structurally similar ampholytes. Flow chart guiding on how design such preconcentration systems was constructed.

Second part of this thesis was keen on ionic effects in CE and HILIC mode of HPLC. For CE, already developed theory of Onsanger-Fuoss and Debye-Hückel were implemented into new software AnglerFish. This software enables fitting of dependence of effective electrophoretic mobilities on pH for all type of compounds with proper correction of fitted values on zero ionic strength of solution. It was shown that another advantage of this approach is that ionic strength does not need to be constant parameter anymore, enabling measurement in highly acidic or alkaline solutions. The limitation that is absolute value of ionic strength of solutions of this approach is discussed, showing applicability of this approach to ionic strength of 20 mM. The study of ionic effects in HILIC separation mode proved the influence of cation type and its concentration in the mobile phase buffers on the retention of amino acids, dipeptides and their N-blocked analogues. From all the buffering cation tested, it was showed that

NH$_4^+$ cation gave lowest shift of retention with its increasing concentration. On the other hand, triethylamine gave the lowest retention for all tested analytes on both stationary phases, due to its possible competitive interaction with stationary phase, while the other buffering cations gave opposite results. In this work, it was demonstrated how utilization of different types and concentration of buffers forming the mobile phase could be exploited to tune the retention of analytes in HILIC mode, especially when more complex mixtures are analyzed.

Last paper of this thesis was devoted to development of new set of pI markers for isoelectric focusing. We have found 14 easily obtainable small molecules with well-defined structure, fulfilling all the requirements for pI marker. These compounds were then characterized by means of determination of their pKa and limiting mobility values. Determined pKas and limiting mobilities were corrected via AnglerFish software, obtained true thermodynamic constants. Set of obtained pI markers was utilized in experiments and numerical simulations for characterization of pH gradient within isoelectric focusing, showing good agreement, except highly acidic and alkaline pH part of the gradient due to bidirectional isotachophoretic process.

5.   References

[1] I. Zuskova, A. Novotna, K. Vcelakova, B. Gas, Determination of limiting mobilities and dissociation constants of 21 amino acids by capillary zone electrophoresis at very low pH, Journal of Chromatography B-Analytical Technologies in the Biomedical and Life Sciences, 841 (2006) 129-134.

[2] S.K. Poole, S. Patel, K. Dehring, H. Workman, C.F. Poole, Determination of acid dissociation constants by capillary electrophoresis, Journal of Chromatography A, 1037 (2004) 445-454.

[3] S.A.C. Wren, R.C. Rowe, THEORETICAL ASPECTS OF CHIRAL SEPARATION IN CAPILLARY ELECTROPHORESIS .1. INITIAL EVALUATION OF A MODEL, Journal of Chromatography, 603 (1992) 235-241.

[4] S.A.C. Wren, R.C. Rowe, THEORETICAL ASPECTS OF CHIRAL SEPARATION IN CAPILLARY ELECTROPHORESIS .3. APPLICATION TO BETA-BLOCKERS, Journal of Chromatography, 635 (1993) 113-118.

[5] P. Nowak, M. Wozniakiewicz, P. Koscielniak, Application of capillary electrophoresis in determination of acid dissociation constant values, Journal of Chromatography A, 1377 (2015) 1-12.

[6] M. Shalaeva, J. Kenseth, F. Lombardo, A. Bastinz, Measurement of dissociation constants (pK(a) values) of organic compounds by multiplexed capillary electrophoresis using aqueous and cosolvent buffers, Journal of Pharmaceutical Sciences, 97 (2008) 2581-2606.

[7] C.X. Jiang, D.W. Armstrong, Use of CE for the determination of binding constants, Electrophoresis, 31 (2010) 17-27.

[8] V. Hruska, M. Riesova, B. Gas, A nonlinear electrophoretic model for PeakMaster: I. Mathematical model, Electrophoresis, 33 (2012) 923-930.

[9] M. Riesova, V. Hruska, B. Gas, A nonlinear electrophoretic model for PeakMaster: II. Experimental verification, Electrophoresis, 33 (2012) 931-937.

[10] V. Solinova, V. Kasicka, D. Koval, M. Cesnek, A. Holy, Determination of acid-base dissociation constants of amino- and guanidinopurine nucleotide analogs and related compounds by capillary zone electrophoresis, Electrophoresis, 27 (2006) 1006-1019.

[11] V. Solinova, V. Kasicka, Determination of acidity constants and ionic mobilities of polyprotic peptide hormones by CZE, Electrophoresis, 34 (2013) 2655-2665.

[12] R. Konasova, J.J. Dytrtova, V. Kasicka, Determination of acid dissociation constants of triazole fungicides by pressure assisted capillary electrophoresis, Journal of Chromatography A, 1408 (2015) 243-249.

[13] T. Tumova, L. Monincova, V. Cerovsky, V. Kasicka, Estimation of acidity constants, ionic mobilities and charges of antimicrobial peptides by capillary electrophoresis, Electrophoresis, 37 (2016) 3186-3195.

[14] P. Debye, E. Hückel, 24 (1923) 185 - 206.

[15] P. Debye, E. Hückel, 24 (1923) 305 - 325.

[16] L. Onsager, R.M. Fuoss, J. Phys. Chem., 36 (1932) 2689-2778.

[17] T.J. Murphy, E.G.D. Cohen, CORRECTIONS TO FUOSS-ONSAGER THEORY OF ELECTROLYTES, Journal of Chemical Physics, 53 (1970) 2173-&.

[18] E. Pitts, AN EXTENSION OF THE THEORY OF THE CONDUCTIVITY AND VISCOSITY OF ELECTROLYTE SOLUTIONS, Proceedings of the Royal Society of London Series a-Mathematical and Physical Sciences, 217 (1953) 43-70.

[19] A. Slampova, P. Bocek, Statistical data processing of mobility curves of univalent weak bases, Electrophoresis, 29 (2008) 538-541.

[20] A. Slampova, L. Krivankova, P. Gebauer, P. Bocek, Standard systems for measurement of pK values and ionic mobilities 2. Univalent weak bases, Journal of Chromatography A, 1216 (2009) 3637-3641.

[21] R.M. Fuoss, REVIEW OF THE THEORY OF ELECTROLYTIC CONDUCTANCE, Journal of Solution Chemistry, 7 (1978) 771-782.

[22] M. Roses, E. Bosch, Influence of mobile phase acid-base equilibria on the chromatographic behaviour of protolytic compounds, Journal of Chromatography A, 982 (2002) 1-30.

[23] A.J. Alpert, HYDROPHILIC-INTERACTION CHROMATOGRAPHY FOR THE SEPARATION OF PEPTIDES, NUCLEIC-ACIDS AND OTHER POLAR COMPOUNDS, Journal of Chromatography, 499 (1990) 177-196.

[24] M.R. Gama, R.G.D. Silva, C.H. Collins, C.B.G. Bottoli, Hydrophilic interaction chromatography, Trac-Trends in Analytical Chemistry, 37 (2012) 48-60.

[25] D.V. McCalley, Study of the selectivity, retention mechanisms and performance of alternative silica-based stationary phases for separation of ionised solutes in hydrophilic interaction chromatography, Journal of Chromatography A, 1217 (2010) 3408-3417.

[26] T. Yoshida, Peptide separation by Hydrophilic-Interaction Chromatography: a review, Journal of Biochemical and Biophysical Methods, 60 (2004) 265-280.

[27] A. Berthod, S.S.C. Chang, J.P.S. Kullman, D.W. Armstrong, Practice and mechanism of HPLC oligosaccharide separation with a cyclodextrin bonded phase, Talanta, 47 (1998) 1001-1012.

[28] D.V. McCalley, Understanding and manipulating the separation in hydrophilic interaction liquid chromatography, Journal of Chromatography A, 1523 (2017) 49-71.

[29] A.E. Karatapanis, Y.C. Fiamegos, C.D. Stalikas, A revisit to the retention mechanism of hydrophilic interaction liquid chromatography using model organic compounds, Journal of Chromatography A, 1218 (2011) 2871-2879.

[30] P. Hemstrom, K. Irgum, Hydrophilic interaction chromatography, Journal of Separation Science, 29 (2006) 1784-1821.

[31] P. Orth, H. Engelhardt, SEPARATION OF SUGARS ON CHEMICALLY MODIFIED SILICA-GEL, Chromatographia, 15 (1982) 91-96.

[32] D.V. McCalley, Study of retention and peak shape in hydrophilic interaction chromatography over a wide pH range, Journal of Chromatography A, 1411 (2015) 41-49.

[33] A. Kumar, J.C. Heaton, D.V. McCalley, Practical investigation of the factors that affect the selectivity in hydrophilic interaction chromatography, Journal of Chromatography A, 1276 (2013) 33-46.

[34] C. West, E. Auroux, Deconvoluting the effects of buffer salt concentration in hydrophilic interaction chromatography on a zwitterionic stationary phase, Journal of Chromatography A, 1461 (2016) 92-97.

[35] M. Dousa, J. Srbek, Z. Stransky, P. Gibala, L. Novakova, Retention behavior of a homologous series and positional isomers of aliphatic amino acids in hydrophilic interaction chromatography, Journal of Separation Science, 37 (2014) 739-747.

[36] M.C. Breadmore, Recent advances in enhancing the sensitivity of electrophoresis and electrochromatography in capillaries and microchips, Electrophoresis, 28 (2007) 254-281.

[37] M.C. Breadmore, J.R.E. Thabano, M. Dawod, A.A. Kazarian, J.P. Quirino, R.M. Guijt, Recent advances in enhancing the sensitivity of electrophoresis and electrochromatography in capillaries and microchips (2006-2008), Electrophoresis, 30 (2009) 230-248.

[38] M.C. Breadmore, M. Dawod, J.P. Quirino, Recent advances in enhancing the sensitivity of electrophoresis and electrochromatography in capillaries and microchips (2008-2010), Electrophoresis, 32 (2011) 127-148.

[39] M.C. Breadmore, A.I. Shallan, H.R. Rabanes, D. Gstoettenmayr, A.S.A. Keyon, A. Gaspar, M. Dawod, J.P. Quirino, Recent advances in enhancing the sensitivity of electrophoresis and electrochromatography in capillaries and microchips (2010-2012), Electrophoresis, 34 (2013) 29-54.

[40] M.C. Breadmore, R.M. Tubaon, A.I. Shallan, S.C. Phung, A.S.A. Keyon, D. Gstoettenmayr, P. Prapatpong, A.A. Alhusban, L. Ranjbar, H.H. See, M. Dawod, J.P. Quirino, Recent advances in enhancing the sensitivity of electrophoresis and electrochromatography in capillaries and microchips (2012-2014), Electrophoresis, 36 (2015) 36-61.

[41] M.C. Breadmore, A. Wuethrich, F. Li, S.C. Phung, U. Kalsoom, J.M. Cabot, M. Tehranirokh, A.I. Shallan, A.S.A. Keyon, H.H. See, M. Dawod, J.P. Quirino, Recent advances in enhancing the sensitivity of electrophoresis and electrochromatography in capillaries and microchips (2014-2016), Electrophoresis, 38 (2017) 33-59.

[42] M.C. Breadmore, W. Grochocki, U. Kalsoom, M.N. Alves, S.C. Phung, M.T. Rokh, J.M. Cabot, A. Ghiasvand, F. Li, A.I. Shallan, A.S.A. Keyon, A.A. Alhusban, H.H. See, A. Wuethrich, M. Dawod, J.P. Quirino, Recent advances in enhancing the sensitivity of electrophoresis and electrochromatography in capillaries and microchips (2016-2018), Electrophoresis, 40 (2019) 17-39.

[43] J.P. Quirino, S. Terabe, Exceeding 5000-fold concentration of dilute analytes in micellar electrokinetic chromatography, Science, 282 (1998) 465-468.

[44] J.P. Quirino, S. Terabe, Sweeping of analyte zones in electrokinetic chromatography, Analytical Chemistry, 71 (1999) 1638-1644.

[45] M.J. Gong, K.R. Wehmeyer, P.A. Limbach, W.R. Heineman, On-line sample preconcentration by sweeping with dodecyltrimethylammonium bromide in capillary zone electrophoresis, Journal of Chromatography A, 1125 (2006) 263-269.

[46] A. Gavenda, J. Sevcik, J. Psotova, P. Bednar, P. Bartak, P. Adamovsky, V. Simanek, Determination of anthracycline antibiotics doxorubicin and daunorubicin by capillary electrophoresis with UV absorption detection, Electrophoresis, 22 (2001) 2782-2785.

[47] M.J. Markuszewski, P. Britz-McKibbin, S. Terabe, K. Matsuda, T. Nishioka, Determination of pyridine and adenine nucleotide metabolites in Bacillus subtilis cell extract by sweeping borate complexation capillary electrophoresis, Journal of Chromatography A, 989 (2003) 293-301.

[48] L.Y. Fan, C.J. Li, W. Zhang, C.X. Cao, P. Zhou, Z.X. Deng, Quantitative investigations on moving chelation boundary within a continuous EDTA-based sample sweeping system in capillary electrophoresis, Electrophoresis, 29 (2008) 3989-3998.

[49] D.L. Kirschner, M. Jaramillo, T.K. Green, Enantioseparation and stacking of cyanobenz f isoindole-amino acids by reverse polarity capillary electrophoresis and sulfated beta-cyclodextrin, Analytical Chemistry, 79 (2007) 736-743.

[50] L.P. Quirino, S. Terabe, K. Otsuka, J.B. Vincent, G. Vigh, Sample concentration by sample stacking and sweeping using a microemulsion and a single-isomer sulfated beta-cyclodextrin as pseudostationary phases in electrokinetic chromatography, Journal of Chromatography A, 838 (1999) 3-10.

[51] E.P. Lin, K.C. Lin, C.W. Chang, M.M. Hsieh, On-line sample preconcentration by sweeping and poly(ethylene oxide)-mediated stacking for simultaneous analysis of nine pairs of amino acid enantiomers in capillary electrophoresis, Talanta, 114 (2013) 297-303.

[52] K. Otsuka, M. Matsumura, J.B. Kim, S. Terabe, On-line preconcentration and enantio selective separation of triadimenol by electrokinetic chromatography using cyclodextrins as chiral selectors, Journal of Pharmaceutical and Biomedical Analysis, 30 (2003) 1861-1867.

[53] C.C. Wang, J.L. Chen, Y.L. Chen, H.L. Cheng, S.M. Wu, A novel stacking method of repetitive large volume sample injection and sweeping MEKC for determination of androgenic steroids in urine, Analytica Chimica Acta, 744 (2012) 99-104.

[54] P. Britz-McKibbin, T. Ichihashi, K. Tsubota, D.D.Y. Chen, S. Terabe, Complementary on-line preconcentration strategies for steroids by capillary electrophoresis, Journal of Chromatography A, 1013 (2003) 65-76.

[55] X.Y. Xu, Z.M. Jia, Y. Shu, L.H. Liu, Dynamic pH junction-sweeping technique for on-line concentration of acidic amino acids in human serum by capillary electrophoresis with indirect UV detection, Journal of Chromatography B-Analytical Technologies in the Biomedical and Life Sciences, 980 (2015) 20-27.

[56] L.Y. Fan, W. Yan, C.X. Cao, W. Zhang, Q. Chen, Experiments on moving interaction boundaries and their characteristics of focusing and probing of both guest and host target molecules, Analytica Chimica Acta, 650 (2009) 111-117.

[57] J.P. Quirino, S. Terabe, P. Bocek, Sweeping of neutral analytes in electrokinetic chromatography with high-salt-containing matrixes, Analytical Chemistry, 72 (2000) 1934-1940.

[58] J.P. Quirino, S. Terabe, Sweeping with an enhanced electric field of neutral analyte zones in electrokinetic chromatography, Hrc-Journal of High Resolution Chromatography, 22 (1999) 367-372.

[59] J.P. Quirino, S. Terabe, Sweeping of neutral analytes via complexation with borate in capillary zone electrophoresis, Chromatographia, 53 (2001) 285-289.

[60] M.C. Breadmore, J.P. Quirino, W. Thormann, High-resolution computer simulations of EKC, Electrophoresis, 30 (2009) 570-578.

[61] W. Thormann, J. Caslavska, R.A. Mosher, Computer simulation of electrophoretic aspects of enantiomer migration and separation in capillary electrochromatography with a neutral selector, Electrophoresis, 36 (2015) 773-783.

[62] M. Jaros, T. Soga, T. van de Goor, B. Gas, Conductivity detection in capillary zone electrophoresis: Inspection by PeakMaster, Electrophoresis, 26 (2005) 1948-1953.

[63] R.X. Wei, W.H. Li, L.R. Yang, Y.X. Jiang, T.Y. Xie, Online preconcentration in capillary electrophoresis with contactless conductivity detection for sensitive determination of sorbic and benzoic acids in soy sauce, Talanta, 83 (2011) 1487-1490.

[64] L. Xu, P.C. Hauser, H.K. Lee, Determination of nerve agent degradation products by capillary electrophoresis using field-amplified sample stacking injection with the electroosmotic flow pump and contactless conductivity detection, Journal of Chromatography A, 1216 (2009) 5911-5916.

[65] Y. Xu, W.L. Wang, S.F.Y. Li, Simultaneous determination of low-molecular-weight organic acids and chlorinated acid herbicides in environmental water by a portable CE system with contactless conductivity detection, Electrophoresis, 28 (2007) 1530-1539.

[66] S. Anouti, O. Vandenabeele-Trambouze, H. Cottet, Heart-cutting 2D-CE with on-line preconcentration for the chiral analysis of native amino acids, Electrophoresis, 31 (2010) 1029-1035.

[67] R. Aebersold, H.D. Morrison, ANALYSIS OF DILUTE PEPTIDE SAMPLES BY CAPILLARY ZONE ELECTROPHORESIS, Journal of Chromatography, 516 (1990) 79-88.

[68] P. Britz-Mckibbin, A.R. Kranack, A. Paprica, D.D.Y. Chen, Quantitative assay fdr epinephrine in dental anesthetic solutions by capillary electrophoresis, Analyst, 123 (1998) 1461-1463.

[69] P. Britz-Mckibbin, J. Wong, D.D.Y. Chen, Analysis of epinephrine from fifteen different dental anesthetic formulations by capillary electrophoresis, Journal of Chromatography A, 853 (1999) 535-540.

[70] P. Britz-McKibbin, G.M. Bebault, D.D.Y. Chen, Velocity-difference induced focusing of nucleotides in capillary electrophoresis with a dynamic pH junction, Analytical Chemistry, 72 (2000) 1729-1735.

[71] C.X. Cao, L.Y. Fan, W. Zhang, Review on the theory of moving reaction boundary, electromigration reaction methods and applications in isoelectric focusing and sample pre-concentration, Analyst, 133 (2008) 1139-1157.

[72] A.A. Kazarian, E.F. Hilder, M.C. Breadmore, Online sample pre-concentration via dynamic pH junction in capillary and microchip electrophoresis, Journal of Separation Science, 34 (2011) 2800-2821.

[73] M.R.N. Monton, K. Imami, M. Nakanishi, J.B. Kim, S. Terabe, Dynamic pH junction technique for on-line preconcentration of peptides in capillary electrophoresis, Journal of Chromatography A, 1079 (2005) 266-273.

[74] K. Imami, M.R.N. Monton, Y. Ishihama, S. Terabe, Simple on-line sample preconcentration technique for peptides based on dynamic pH junction in capillary electrophoresis-mass spectrometry, Journal of Chromatography A, 1148 (2007) 250-255.

[75] M.C. Breadmore, R.A. Mosher, W. Thormann, High-resolution computer simulations of stacking of weak bases using a transient pH boundary in capillary electrophoresis. 1. Concept and impact of sample ionic strength, Analytical Chemistry, 78 (2006) 538-546.

[76] K. Vitkova, J. Petr, V. Maier, J. Znaleziona, J. Sevcik, Study of electromigration effects on a pH boundary during the on-line electrokinetic preconcentration by capillary electrophoresis, Electrophoresis, 31 (2010) 2771-2777.

[77] J.B. Kim, P. Britz-McKibbin, T. Hirokawa, S. Terabe, Mechanistic study on analyte focusing by dynamic pH junction in capillary electrophoresis using computer simulation, Analytical Chemistry, 75 (2003) 3986-3993.

[78] C.X. Cao, Moving chemical reaction boundary and isoelectric focusing - I. Conditional equations for Svensson-Tiselius' differential equation of solute concentration distribution in idealized isoelectric focusing at steady state, Journal of Chromatography A, 813 (1998) 153-171.

[79] C.X. Cao, Moving chemical reaction boundary and isoelectric focusing - II. Existence of quasi/equal fluxes (or transference numbers) of hydrogen and hydroxyl ions in stationary electrolysis and Svensson's isoelectric focusing, Journal of Chromatography A, 813 (1998) 173-177.

[80] C.X. Cao, S.L. Zhou, Y.T. Qian, Y.Z. He, C.R. Wang, X.Y. Zheng, W.K. Chen, Investigations on factors that influence the moving neutralization reaction boundary method for capillary electrophoresis and isoelectric focusing, Journal of Chromatography A, 952 (2002) 29-38.

[81] C.X. Cao, S.L. Zhou, Y.Z. He, X.Y. Zheng, W.K. Chen, Y.T. Qian, Experimental study on moving neutralization reaction boundary created with the strong reactive electrolytes of HCl and NaOH in agarose gel, Journal of Chromatography A, 891 (2000) 337-347.

[82] W. Zhu, W. Zhang, L.Y. Fan, J. Shao, S. Li, J.L. Chen, C.X. Cao, Study on mechanism of stacking of zwitterion in highly saline biologic sample by transient moving reaction boundary created by formic buffer and conjugate base in capillary electrophoresis, Talanta, 78 (2009) 1194-1200.

[83] C.X. Cao, W. Zhang, W.H. Qin, S. Li, W. Zhu, W. Liu, Quantitative predictions to conditions of zwitterionic stacking by transient moving chemical reaction boundary created with weak electrolyte buffers in capillary electrophoresis, Analytical Chemistry, 77 (2005) 955-963.

[84] B. Bjellqvist, K. Ek, P.G. Righetti, E. Gianazza, A. Gorg, R. Westermeier, W. Postel, ISOELECTRIC-FOCUSING IN IMMOBILIZED PH GRADIENTS - PRINCIPLE, METHODOLOGY AND SOME APPLICATIONS, Journal of Biochemical and Biophysical Methods, 6 (1982) 317-339.

[85] R. Rodriguez-Diaz, T. Wehr, M.D. Zhu, Capillary isoelectric focusing, Electrophoresis, 18 (1997) 2134-2144.

[86] K. Shimura, W. Zhi, H. Matsumoto, K. Kasai, Accuracy in the determination of isoelectric points of some proteins and a peptide by capillary isoelectric focusing: Utility of synthetic peptides as isoelectric point markers, Analytical Chemistry, 72 (2000) 4747-4757.

[87] O. Vesterberg, SYNTHESIS AND ISOELECTRIC FRACTIONATION OF CARRIER AMPHOLYTES, Acta Chemica Scandinavica, 23 (1969) 2653-+.

[88] H. Rilbe, HISTORICAL AND THEORETICAL ASPECTS OF ISOELECTRIC FOCUSING, Annals of the New York Academy of Sciences, 209 (1973) 11-22.

[89] M. Stastna, M. Travnicek, K. Slais, New azo dyes as colored isoelectric point markers for isoelectric focusing in acidic pH region, Electrophoresis, 26 (2005) 53-59.

[90] D. Mohan, C.S. Lee, Extension of separation range in capillary isoelectric focusing for resolving highly basic biomolecules, Journal of Chromatography A, 979 (2002) 271-276.

[91] K. Slais, Z. Friedl, LOW-MOLECULAR-MASS PI MARKERS FOR ISOELECTRIC-FOCUSING, Journal of Chromatography A, 661 (1994) 249-256.

[92] K. Slais, M. Horka, J. Novackova, Z. Friedl, Fluorescein-based pl markers for capillary isoelectric focusing with laser-induced fluorescence detection, Electrophoresis, 23 (2002) 1682-1688.

[93] K. Shimura, Z. Wang, H. Matsumoto, K. Kasai, Synthetic oligopeptides as isoelectric point markers for capillary isoelectric focusing with ultraviolet absorption detection, Electrophoresis, 21 (2000) 603-610.

[94] K. Shimura, K. Kamiya, H. Matsumoto, K. Kasai, Fluorescence-labeled peptide p1 markers for capillary isoelectric focusing, Analytical Chemistry, 74 (2002) 1046-1053.

[95] V. Gyula, M.-C. Li, Fluorescent pI Markers for Isoelectric Focusing Separations and Fluorescent Labeling, in: J. Patents (Ed.), USA, 2017.

[96] V. Hruska, J. Svobodova, M. Benes, B. Gas, A nonlinear electrophoretic model for PeakMaster: Part III. Electromigration dispersion in systems that contain a neutral complex-forming agent and a fully charged analyte. Theory, Journal of Chromatography A, 1267 (2012) 102-108.

[97] M. Benes, J. Svobodova, V. Hruska, M. Dvorak, I. Zuskova, B. Gas, A nonlinear electrophoretic model for PeakMaster: Part IV. Electromigration dispersion in systems that

contain a neutral complex-forming agent and a fully charged analyte. Experimental verification, Journal of Chromatography A, 1267 (2012) 109-115.

[98] V. Hruska, M. Benes, J. Svobodova, I. Zuskova, B. Gas, Simulation of the effects of complex- formation equilibria in electrophoresis: I. Mathematical model, Electrophoresis, 33 (2012) 938-947.

[99] J. Svobodova, M. Benes, V. Hruska, K. Uselova, B. Gas, Simulation of the effects of complex- formation equilibria in electrophoresis: II. Experimental verification, Electrophoresis, 33 (2012) 948-957.

[100] M. Boublik, M. Riesova, P. Dubsky, B. Gas, Enhancement of the conductivity detection signal in capillary electrophoresis systems using neutral cyclodextrins as sweeping agents, Electrophoresis, 39 (2018) 1390-1398.

[101] B. Gas, V. Hruska, M. Dittmann, F. Bek, K. Witt, Prediction and understanding system peaks in capillary zone electrophoresis, Journal of Separation Science, 30 (2007) 1435-1445.

[102] M. Boublik, M. Riesova, V. Hruska, J. Steflova, Online preconcentration of weak electrolytes at the pH boundary induced by a system zone in capillary zone electrophoresis, Analytica Chimica Acta, 1085 (2019) 126-135.

[103] D.S. Burgi, R.L. Chien, OPTIMIZATION IN SAMPLE STACKING FOR HIGH-PERFORMANCE CAPILLARY ELECTROPHORESIS, Analytical Chemistry, 63 (1991) 2042-2047.

[104] T. Hirokawa, M. Nishino, N. Aoki, Y. Kiso, Y. Sawamoto, T. Yagi, J. Akiyama, TABLE OF ISOTACHOPHORETIC INDEXES .1. SIMULATED QUALITATIVE AND QUANTITATIVE INDEXES OF 287 ANIONIC SUBSTANCES IN THE RANGE PH 3-10, Journal of Chromatography, 271 (1983) D1-D106.

[105] V. Maier, K. Kalikova, A. Pribylka, J. Vozka, J. Smuts, M. Svidrnoch, J. Sevcik, D.W. Armstrong, E. Tesarova, Isopropyl derivative of cyclofructan 6 as chiral selector in liquid chromatography and capillary electrophoresis, Journal of Chromatography A, 1338 (2014) 197-200.

[106] SPARC 2018, in, ARChem, Danielsville, USA, 2019, pp. www.archemcalc.com.

[107] ACD/Labs, in, Advanced Chemistry Development, Inc., Toronto, ON, Canada, 2019, pp. www.acdlabs.com.

[108] M. Ansorge, B. Gas, M. Boublik, M. Maly, J. Steflova, V. Hruska, G. Vigh, CE determination of the thermodynamic pK(a) values and limiting ionic mobilities of 14 low molecular mass UV absorbing ampholytes for accurate characterization of the pH gradient in carrier ampholytes-based IEF and its numeric simulation, Electrophoresis, 9.

[109] T. Hirokawa, K. Watanabe, Y. Yokota, Y. Kiso, BIDIRECTIONAL ISOTACHOPHORESIS .1. VERIFICATION OF BIDIRECTIONAL ISOTACHOPHORESIS AND SIMULTANEOUS DETERMINATION OF ANIONIC AND CATIONIC COMPONENTS, Journal of Chromatography, 633 (1993) 251-259

6. Appendix

I

Enhancement of the conductivity detection signal in capillary electrophoresis systems using neutral cyclodextrins as sweeping agents

M. Boublík, M. Riesová, P. Dubský, B. Gaš

Milan Boublík
Martina Riesová
Pavel Dubský
Bohuslav Gaš

Faculty of Science, Department
of Physical and Macromolecular
Chemistry, Charles University in
Prague, Prague, Czech Republic

Research Article

Enhancement of the conductivity detection signal in capillary electrophoresis systems using neutral cyclodextrins as sweeping agents

Conductivity detection is a universal detection technique often encountered in electrophoretic separation systems, especially in modern chip-electrophoresis based devices. On the other hand, it is sparsely combined with another contemporary trend of enhancing limits of detection by means of various preconcentration strategies. This can be attributed to the fact that a preconcentration experimental setup usually brings about disturbances in a conductivity baseline. Sweeping with a neutral sweeping agent seems a good candidate for overcoming this problem. A neutral sweeping agent does not hinder the conductivity detection while a charged analyte may preconcentrate on its boundary due to a decrease in its effective mobility. This study investigates such sweeping systems theoretically, by means of computer simulations, and experimentally. A formula is provided for the reliable estimation of the preconcentration factor. Additionally, it is demonstrated that the conductivity signal can significantly benefit from slowing down the analyte and thus the overall signal enhancement can easily overweight amplification caused solely by the sweeping process. The overall enhancement factor can be deduced a priori from the linearized theory of electrophoresis implemented in the PeakMaster freeware. Sweeping by neutral cyclodextrin is demonstrated on an amplification of a conductivity signal of flurbiprofen in a real drug sample. Finally, a possible formation of unexpected system peaks in systems with a neutral sweeping agent is revealed by the computer simulation and confirmed experimentally.

1 Introduction

On-line preconcentration techniques in capillary electrophoresis (CE) have been improving their detection sensitivity for more than 25 years and nowadays they are an integral part of most electrophoretic analytical applications. Reviews of Breadmore and co-workers have been reporting regularly progress in this field [1–6] and they show that development and application of preconcentration procedures are still a contemporary issue.

Sweeping, a preconcentration technique employing an interaction of an analyte with a pseudostationary phase present in a background electrolyte (BGE), was first introduced by Quirino and Terabe [7,8]. Charged micelles are BGE additives most frequently used to sweep various analytes into narrower, thus more concentrated, zones [9, 10]. Complexforming agents such as EDTA [11], borates [12,13] or charged

cyclodextrins [14–16] are utilized rarely; either for particular applications, for the enhancement of the sweeping power of micelles [17–22], or as an additional chiral resolving agent in a micellar sweeping system [23–28]. In general, cyclodextrins (CDs) are widely used BGE additives as they are well-known complexation agents for many compounds of pharmaceutical and environmental interest or various food additives. They find applications in separations of structurally similar compounds, often enantiomers [29]. Nevertheless, our aim is to introduce them as a possible sweeping (or better conductivity-signal-amplifying) agents even when not needed for the actual separation. Neutral cyclodextrins as single sweeping agents have been reported, to the authors' best knowledge, only in one application [30] and one study on a moving interaction boundary [31].

Theoretical calculations of sweeping preconcentration factor have been investigated in several works. The narrowing factor of an analyte zone in micellar sweeping systems with a considerably homogenous electric field can be predicted easily and calculated as $1/(1+k)$, where k is the retention

Correspondence: Dr. Pavel Dubský, Charles University in Prague, Faculty of Science, Albertov 6, CZ-128 43 Prague 2, Czech Republic
E-mail: pavel.dubsky@natur.cuni.cz

Abbreviation: CCD, contactless conductivity detector

Color Online: See the article online to view Fig. 2 in color.

factor [7, 8]. The conjunction of sweeping with field amplified sample stacking (the sample zone has a void of micelles and its conductivity differs from the BGE) makes theoretical descriptions more complicated [32, 33] as not only analytes but also micelles are stacked on the zone boundary. A complexation constant, an electrophoretic mobility of the complex, and an effective mobility of an analyte in the presence of the pseudostationary phase can be employed to calculate the preconcentration factor when a complex-forming agent is used instead of micelles [13]. Computer simulations of sweeping were also conducted to provide insight into the process. In 2009, Breadmore and co-workers [34] modified the simulation software GENTRANS and included interactions of analytes with BGE additives. They simulated micellar electrokinetic chromatography with a sweeping stage. The software was later used for investigating the separation of enantiomers with a neutral cyclodextrin and revealed the presence of a stacking effect during the separation [35]. In the year 2009, simulation software specialized for EDTA-based preconcentrations of metal ions was also published by Jin *et al*. [36].

The ultimate goal of any preconcentration strategy is to enhance the detector response to the presence of an analyte. Among the various detection techniques, conductivity detection has several specifics. First, both direct and indirect detection principles are inseparably coupled in conductivity detection. Thus, the response of an analyte does not only depend on the analyte itself but also on the composition of the BGE [37]. Second, conductivity measurements do not involve optical paths, can be performed in the contact-less setup [38, 39] and can be easily miniaturized. This makes the conductivity detector a perfect candidate for its coupling with contemporary microchip electrophoresis devices [40]. Third, the conductivity signal is non-specific, suitable for a whole range of analytes.

Unfortunately, the sensitivity of conductivity detection is still an issue [41], while its non-specificity discriminates its utilization in combination with most on-line preconcentration techniques. These are based on a formation of various zones along the capillary, the conductivity of which varies usually significantly. Only a few works in which field-amplified sample stacking [42, 43], field-amplified sample injection [44–46] or pH junction [47] features conductivity detection, have been reported.

In this article, we show how a neutral sweeping agent can be advantageously combined with conductivity detection. A neutral cyclodextrin is employed as the sweeping agent for a charged analyte in capillary electrophoresis. The neutral agent does not deteriorate the conductivity signal, while it may provide specific interactions with an analyte leading in simultaneous peak sharpening and conductivity signal enhancement. A theoretical description of the system resulting in an equation for a preconcentration factor calculation is provided. Theoretical calculations and a mechanism of the sweeping with the neutral cyclodextrin are verified both experimentally and by means of our simulation software, Simul 5 Complex. Contactless conductivity detection is utilized in sweeping for the first time. Moreover, the conductivity signal and its enhancement after the sweeping step is shown to be fully predictable by means of our software, PeakMaster 5.3.

2 Materials and methods

All chemicals were of analytical grade purity. Lithium hydroxide monohydrate was purchased from Fluka (Steinheim, Germany). *N*-Tris(hydroxymethyl)methyl-3-aminopropanesulfonic acid (TAPS), *R*-Flurbiprofen (*R*-Flu) and β-cyclodextrin were from Sigma Aldrich (Steinheim, Germany). Strepfen pastilles (batch number CE857) containing 8.75 mg of flurbiprofen from producer Reckitt Benckiser Healthcare International Ltd. (Nottingham, United Kingdom) were purchased in pharmacy. Solution of 0.1 M sodium hydroxide for capillary flushing was obtained from Agilent Technologies (Waldbronn, Germany). Water for preparation of all solutions was deionized by Watrex Ultrapur system (Prague, Czech Republic).

All experiments were performed using Agilent 7100 capillary electrophoresis equipment operated under ChemStation software (Agilent Technologies, Waldbronn, Germany). Detection was performed with the built-in diode array detector (DAD) and the contactless conductivity detector (CCD) [48]. Fused silica capillary (50 μm i.d., 375 μm o.d.) was provided by Polymicro Technologies (Phoenix, AZ). The experiments were performed in a bare capillary with a total length and effective length to the detector DAD/CCD of 49.8 and 41.3/35.0 cm, respectively. UV spectra of *R*-Flurbiprofen were measured using Shimadzu UV-2401PC with TCC-Controller.

All CE measurements were performed in the running BGE consisting of 10 mM TAPS and 5 mM LiOH with the theoretical pH = 8.27 and an ionic strength of 5 mM. Experimental pH was 8.28. Neutral β-CD at concentration levels of 0, 0.1, 0.5, 1, 2 and 5 mM in the running BGE was used as a sweeping agent for *R*-Flu. 0 mM and 5 mM β-CD in the running BGE was used when the strepfen drug sample was analysed. The sample of 0.1 mM *R*-Flu was made by dissolving the relevant amount of *R*-Flu directly in the running buffer. Strepfen drug sample was prepared by dissolving pastille with 20 ml of running buffer and filtrated. The sample solutions did not contain β-CD. For evelution of preconcentraion and enhancement factors, an approximately 5 cm long rectangular plug of the sample zone was introduced to the capillary hydrodynamically by pressure of 20 mbar for 160 s. At the beginning of each sweeping experiment, the capillary was filled with the BGE without CD. Prior to applying voltage, a vial with the CD containing the BGE was setup as an inlet vial as Fig. 1E shows. A shorter injected zone and the same experimental setup was used for LOD determination; 1–100 μM *R*-Flu in the running buffer were injected by only 10 mbar for 15 s. The same injection conditions were used for strepfen sample preconcentraion and when system zones were investigated; 0.1 mM *R*-Flu in the running buffer was used as a sample for system zones measurements. The sample zone was pushed by 35 mbar for 120 s further to the capillary to separate positions of injection and the sweeping process. The applied
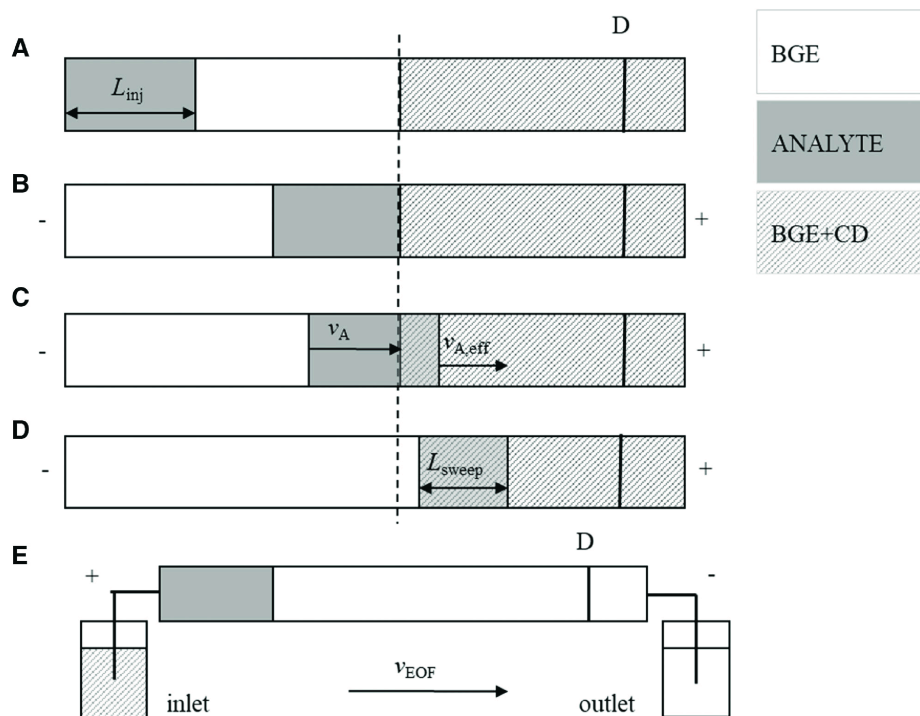
Figure 1. Mechanism of sweeping of a negatively charged analyte with a neutral sweeping agent, cyclodextrin (CD). (A) initial situation; sample zone of Linj width injected into the capillary with partial filling of CD-containing BGE; (B) voltage is applied; analyte reaches the zone containing CD; sweeping starts; (C) sweeping proceeds; (D) whole sample zone is in the CD-containing zone and it is narrowed to Lsweep width; sweeping ends; the dashed line depicts the original position of the BGE and the BGE+CD boundary. (E) real experimental arrangement with respect to the presence of EOF; D means detector position.

voltage was always $+ 10$ kV and the temperature 25°C. The new capillary was flushed with 0.1 M sodium hydroxide for 10 min, 20 min with deionized water and 20 min with the running buffer. The capillary was flushed by the running buffer without CD for 5 min prior to each run. All running buffers were filtrated with Minisart syringe filters (Sartorius Stedim Biotech, Goettingen, Germany), pore size 0.45 μm. Each run was repeated three times. DAD detection was performed at a wavelength of 247 nm. UV-Vis spectra (190-350 nm) of 0.1 mM *R*-Flu in TAPS/LiOH buffer without β-CD and with 2 mM β-CD was measured to find out the changes of the absorbance in the presence of the β-CD. The temperature was set at 25°C and a 1 cm quartz cuvette was used.

Simul 5 Complex [49, 50] with an implemented complete mathematical model of electromigration for the separation systems with complexation agents was utilized for simulations of experimental electropherograms and for the theoretical prediction of preconcentration factors. Concentrations of *R*-Flu and BGE constituents and the running parameters were set up to correspond with experimental conditions. *R*-Flu and its complexation with β-CD is characterized by following parameters which were used as input data for computer simulations and predictions: acidic dissociation constant of *R*-Flu expressed as pK_A is 4.19; limiting electrophoretic ionic mobility $\mu_A = 24.5 \times 10^{-9}$ m^{2}s^{-1}V^{-1}, complexation constants of charged and neutral form of *R*-Flu is 5310 M^{-1} and 12030 M^{-1}, respectively; limiting electrophoretic mobility of the complex $\mu_{ACD} = 11.9 \times 10^{-9}$ m^{2}s^{-1}V^{-1} [51]. All simulations were done without ionic strength correction. The PeakMaster 5.3 [52,53] was used for the prediction and calculation of conductivity

signal enhancement caused by sweeping. All predictions in PeakMaster took ionic strength into account. The Simul 5 Complex and PeakMaster 5.3 software are available as freeware at our website [54].

3   Theory

A factor of a sample zone compression within the sweeping of a charged analyte with a neutral CD was derived similarly by Quirino and Terabe [8, 13]. Figure 1 depicts the mechanism of the sweeping of a negatively charged analyte with a neutral sweeping agent. An electroosmotic flow (EOF) is not taken into account as sweeping is independent of EOF [8,13]. A factor of a sample zone compression within the sweeping of analytes with cyclodextrins can be derived in a way similar to that introduced by other authors earlier. Quirino and Terabe [8] expressed a sweeping factor in micellar electrokinetic chromatography (MEKC) by means of the analyte-micelles partitioning equilibria and the equation was later adopted to MEKC systems with neutral micelles [55], too. We show elsewhere [56] that this approach is valid only if the selector electrophoretic mobility is not affected by the complexation, an assumption generally accepted in MEKC. Later, the authors re-applied their derivation in a system with a neutral analyte and borate as a sweeping agent [13]. The derivation took a nonzero mobility of a complex into account on the one hand but was based on a zero moblity of the analyte on the other hand. Consequently, none of the former expressions is directly applicable to our system of sweeping a charged analyte with cyclodextrins.

In such a case, both an analyte and a CD are of comparable sizes so that the analyte and the analyte-CD complex have both their own nonzero mobilities. Additionally, the boundary of the CD-containing zone moves from its original position (dashed line in Fig. 1) within the sweeping process. This is due to the inevitable concurrent sweeping of the neutral or charged agent by the charged analyte as the analyte passes through the boundary. The CD zone boundary migrates with an effective velocity of the CD in the presence of the charged analyte, $v_{CD,eff}$.

Considering the velocities and the aforementioned sweeping of the CD by the analyte, the duration of the sweeping, t_{sweep}, is given as $L_{inj}/(v_A - v_{CD,eff})$. To obtain the width of the concentrated zone, L_{sweep}, t_{sweep} is multiplied by $(v_{A,eff} - v_{CD,eff})$. Thus,

$$L_{sweep} = L_{inj} \cdot \frac{v_{A,eff} - v_{CD,eff}}{v_A - v_{CD,eff}} \tag{1}$$

Obeying the mass conservation law, concentration in the swept zone is

$$c_{sweep} = c_{inj} \cdot \frac{L_{inj}}{L_{sweep}} = c_{inj} \cdot F \tag{2}$$

where F is the preconcentration factor. Noticeably, Eqs. (1) and (2) are generally valid. Nevertheless, the preconcentration factor can only be rewritten by means of corresponding electrophoretic mobilities,

$$F = \frac{\mu_A - \mu_{CD,eff}}{\mu_{A,eff} - \mu_{CD,eff}} \tag{3}$$

under a condition of a constant electric field. This condition does not apply for charged sweeping agents in general, but is naturally fulfilled for neutral sweeping agents.

If the complexation constant, K, and the electrophoretic mobility of the free analyte, μ_A, and the CD-analyte complex, μ_{ACD}, are all known, the effective electrophoretic mobility of the analyte in the presence of the CD, $\mu_{A,eff}$, at a given concentration of the CD, c_{CD}, can be estimated according to the following equation [57, 58]:

$$\mu_{A,eff} = \frac{\mu_A + \mu_{ACD} \cdot K \cdot c_{CD}}{1 + K \cdot c_{CD}} \tag{4}$$

The effective mobility of a neutral sweeping agent in a presence of a charged analyte, that is, the value of $\mu_{CD,eff}$ in our case, is given by the molar fraction of the analyte-agent complex with respect to the sweeping agent. Utilization of the sufficient excess of a sweeping agent leads to very low molar fractions and thus almost zero $\mu_{CD,eff}$ in the Eq. (3). Thus, following simple equation can be employed as the first approximation of the preconcentration factor in systems in which the charged analyte is swept with a neutral complexation agent:

$$F = \frac{\mu_A}{\mu_{A,eff}} \tag{5}$$

Furthermore, when the product of $(K \cdot c_{CD})$ in Eq. (4) is high enough, the value of $\mu_{A,eff}$ approaches the electrophoretic mobility of the complex, μ_{ACD}. Simultaneously, the product of $(K \cdot c_{CD})$ grows with increasing concentration of

the complexation agent when the approximation of $\mu_{CD,eff} = 0$ is satisfied. Consequently, the relation

$$F_{max} = \frac{\mu_A}{\mu_{ACD}} \tag{6}$$

provides the maximal preconcentration factor that can be achieved in the system at the infinite concentration of a neutral sweeping agent.

4 Results and discussion

4.1 Sweeping

We utilized Simul 5 Complex [49, 54] software to show the course of the sweeping process and to verify the preconcentration factors calculated theoretically. Our model system consisted of R-Flu at pH = 8.28 (TAPS/LiOH 10 mM/5 mM) as a fully negatively charged analyte and the neutral β-CD as a sweeping agent. The sweeping process was based on a complexation of the charged R-Flu with the β-CD, the strength of which is characterized by the complexation constant $K = 5310$ M^{-1}. The initial arrangement of each simulation was the same as shown in Fig. 1A. Figure 2 depicts three consecutive records of the concentration profiles of the R-Flu and the β-CD from the simulation. A 10 cm wide zone of 0.1 mM R-Flu (Fig. 2A) migrates through the boundary of 1 mM β-CD where its front is decelerated and the concentration of the R-Flu increases approximately twice (Fig. 2B). At the same time, the CD boundary is mobilized and migrates slowly in the direction of the movement of the zone of the R-Flu (follow the dotted line in Fig. 2). As the entire analyte zone has passed the CD interface, a narrower and concentrated zone of the R-Flu migrates to the detector site (Fig. 2C).

The simulations were provided at five concentration levels of the β-CD (0.1, 0.5, 1, 2 and 5 mM). The simulated preconcentration factors, F_{sim}, were calculated as c_{sweep}/c_{inj}, where c_{inj} and c_{sweep} is the concentration of the R-Flu before and after sweeping, respectively. The factors F_{sim} are listed in Table 1 together with the values calculated theoretically according to the Eq. (3), $F_{(eq 3)}$. Values of $\mu_{A,eff}$ and $\mu_{CD,eff}$, also listed in Table 1, were read directly from Simul 5 Complex at the position of the R-Flu zone inside the β-CD zone. We decided to read these values from Simul 5 Complex rather than utilizing Eq. (4) in order to take into account an increased concentration of the β-CD in the R-Flu zone. The simulation in Fig. 2 shows the increase in the concentration profile of β-CD, which is formed during the sweeping process and which migrates together with the analyte. This phenomenon is not generally acknowledged although it has been already observed by computer simulations in 1992 [59] and experimental evidence of it can be found in the work of Almeida and Larive [60]. The authors observed an increasing concentration of a β-CD during a preconcentration process by means of online NMR detection.
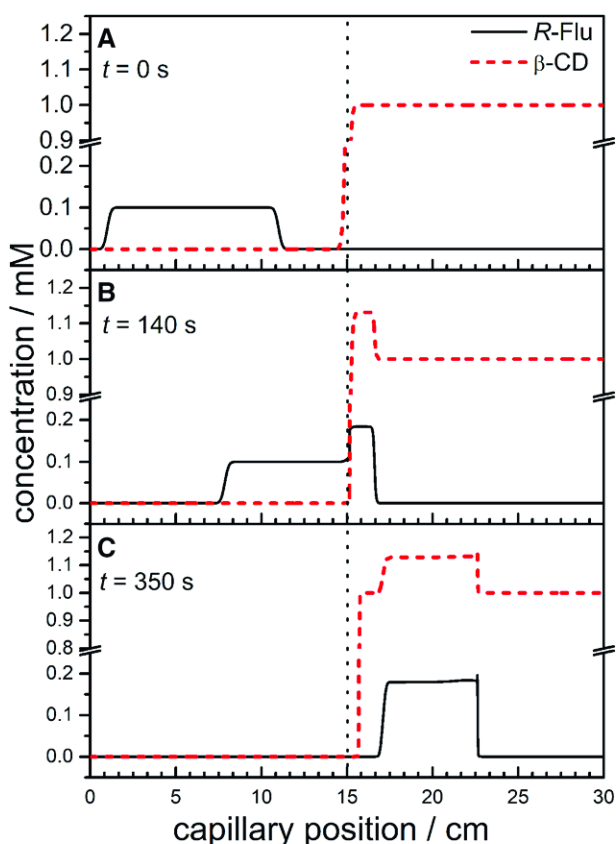
Figure 2. Records of simulation of sweeping process by Simul 5 Complex. Concentration profiles of R-Flu (analyte, black line) and β-CD sweeping agent (red dashed line) at (A) 0 s, (B) 140 s, (C) 350 s. The dotted line is at the initial position of CD boundary.

$F_{(eq 3)}$ and F_{sim} are in a very good agreement; their differences are likely just due to diffusion, which is considered in the simulations though not in the calculations. At low concentration levels of the β-CD, the sweeping potential of the system is not yet fully exploited; only 31% and 73% of the R-Flu is complexed at 0.1 and 0.5 mM β-CD, respectively. When a significant excess of the β-CD is used, the system approaches the situation with fully complexed R-Flu and thus to the preconcentration factor given by Eq. (6), $F_{max} = 24.5 \cdot 10^{-9}$ m^{2}s^{-1}V^{-1}/$11.9 \cdot 10^{-9}$ m^{2}s^{-1}V^{-1} = 2.06.

These calculations illustrate that the Eq. (3) describes the sweeping process precisely; however, it would be of no practical relevance if the input parameters could be obtained from performing the simulation only. Therefore we further calculated the preconcentration factors estimated according to the Eq. (5), and utilizing the Eq. (4) for the effective mobilities of the R-Flu, $\mu_{A,eff}$, at the various concentration levels of the β-CD. The results are listed in Table 1 as $F_{(eq 5)}$ and the values indicate that this approach serves as a good approximation of the preconcentration factor, F.

4.2 Conductivity response

The amplitude in the conductivity signal due to the presence of an analyte is composed of contributions from all ions in the system [37]. In systems with exclusively fully ionized constituents it is proportional to the difference between an analyte mobility and the mobility of a BGE co-ion. In weak electrolyte BGEs, no such simple rule of thumb can be applied. We showed that the composition of the background electrolytes can be optimized to give a good conductivity signal of analytes while still keeping electromigration dispersion near zero. The demands to achieve minimum electromigration dispersion and high sensitivity in conductivity detection can be accomplished at the same time [37].

This indicates that the amplitude of the conductivity signal can profit from changing the analyte mobility due to the complexation with a neutral complexation agent if the BGE is properly designed. The quantity responsible for the amplitude of the conductivity signal is the molar conductivity detection response b_X defined as:

$$b_X = \lim_{c_X \to 0} \frac{d\kappa}{dc_X} \tag{7}$$

where κ is the conductivity of the BGE and dκ is the change in the conductivity at the point of detection, when the analyte zone with an infinitely small concentration dc_X arrives into the detector cell. The conductivity signal can be advantageously calculated in the frame of the linear theory of electromigration [61] which is implemented in our PeakMaster freeware [54]. In this work, PeakMaster 5.3 [52,53] was employed for predicting the conductivity signal enhancement in the

Table 1. Effective mobilities of R-Flu and β-CD, preconcentration factors (F) and conductivity signal enhancement factors (EF) characterizing the sweeping power of the model system at various concentrations of β-CD

c_{CD} mM	$\mu_{A,eff}$ 10^{-9} m^{2}s^{-1}V^{-1}	$\mu_{CD,eff}$ 10^{-9} m^{2}s^{-1}V^{-1}	F_{sim}	$F_{(Eq 3)}$	$F_{(Eq 5)}$	F_{exp}[a]	EF_κ	EF_{tot}	$EF_{tot,exp}$[b]
0.1	−20.61	−3.68	1.22	1.23	1.22	1.14 ± 0.01	8.84	10.8	10.2 ± 0.2
0.5	−15.35	−2.42	1.65	1.69	1.60	1.48 ± 0.01	24.4	39.0	38.7 ± 0.3
1	−13.93	−1.61	1.83	1.86	1.76	1.58 ± 0.01	30.4	53.5	52.5 ± 0.1
2	−12.94	−0.96	1.93	1.96	1.89	1.64 ± 0.01	35.3	66.7	63.0 ± 0.1
5	−12.33	−0.44	2.01	2.02	1.98	1.66 ± 0.01	38.8	76.8	68.2 ± 0.9

a) Experimental preconcentration factor obtained from UV detection.
b) Experimental enhancement factor obtained by conductivity detection.

neutral-CD sweeping system. pK_A values and limiting mobilities are the necessary input parameters for the calculations. The TAPS and LiOH constituents were picked up from the PeakMaster database. The *R*-Flu has a pK_A of 4.19. Its limiting mobility was set to the effective mobility of the *R*-Flu, $\mu_{A,eff}$, in the presence of a particular concentration of the β-CD (Table 1). The predicted conductivity enhancement factor, EF_κ (Table 1), was calculated as a ratio between the conductivity signal at the given concentration of the β-CD and that obtained without any sweeping agent. The conductivity enhancement factor is then fortified by the sweeping preconcentration factor, *F*, into the total enhancement factor. By using the values of $F_{(eq\ 5)}$ and EF_κ, the total enhancement factor, EF_{tot}, can be predicted from the mere physical-chemical properties of an analyte, a sweeping agent, and BGE constituents ask

$$EF_{tot} = F_{(eq5)} \cdot EF_\kappa \tag{8}$$

The predicted total enhancement factors EF_{tot} are listed in Table 1. Clearly, the EF_κ values appreciably contribute to the signal amplification, which fully justifies the use of the conductivity detection over UV-Vis detection in these electrophoretic sweeping systems.

4.3 Experimental verification

The same model system as for simulations was investigated experimentally to verify a theoretical description of preconcentration with a neutral sweeping agent. Due to the presence of a rapid cationic EOF, the experimental setup was reversed as it is depicted in Fig. 1E. A plug of 0.1 mM *R*-Flu was hydrodynamically injected into the capillary filled with pure TAPS/LiOH buffer. Large plug of sample was injected into capillary to achieve maximum preconcentration factor and neglect diffusion effect. A vial with TAPS/LiOH buffer containing the β-CD was set as an inlet vial prior to the voltage application. When the voltage is on, the EOF drags the CD zone. The sweeping process takes place as the negatively charged *R*-Flu reaches the CD boundary. Since the mobility of the EOF is higher in absolute value than the mobility of the *R*-Flu, the *R*-Flu reaches the detector after passing through

the CD boundary. As sweeping is independent of EOF [8], all equations derived before remain valid. The resulting electropherograms for the concentrations of the β-CD varied from 0 to 5 mM are given in Fig. 3. Fig. 3A shows the UV-Vis signal at a wavelength of 247 nm.

The experimental preconcentration factors, F_{exp}, were calculated as a ratio of the *R*-Flu zone height at every given concentration of the β-CD to the *R*-Flu zone height obtained without any sweeping agent. The resulting values of F_{exp} are listed in Table 1 together with their theoretical predictions. Unlike theoretical calculations and simulations, the experiments are influenced by ionic strength and viscosity changes. The effect of the ionic strength is not too pronounced in our system as the BGE used has an ionic strength of only 5 mM. The higher viscosity of the CD-containing zone decreases the $\mu_{A,eff}$ and should actually lead to an increase in the *F* value (see the Eq. (3)). Nevertheless, the F_{exp} values are lower than those obtained by simulations. This fact might be attributed to changes in the molar extinction coefficient of *R*-Flu at 247 nm in the presence of the β-CD. This hypothesis is supported by measurements of absorption spectra of 0.1 mM *R*-Flu in the TAPS/LiOH buffer, and after an addition of 2 mM β-CD. The absorbance of the *R*-Flu decreased from 2.17 to 1.93 AU at 247 nm in the presence of the β-CD.

Figure 3B shows the conductivity signal of the swept *R*-Flu. In accordance with the theoretical considerations outlined above, enhancement in the conductivity signal is significantly higher compared to the UV absorbance signal of the same experiments (Fig. 3A). No analyte peak is detectable without the presence of the β-CD while a concentration of the β-CD as low as 0.1 mM amplifies the signal to the visible extent. The total experimental amplification of the conductivity signal was evaluated and listed in Table 1 as $EF_{tot,exp}$. The values of $EF_{tot,ext}$ were calculated from CCD records as the ratio of the amplitude of the conductivity signal of the *R*-Flu at every given concentration of the β-CD to 3 times the height of the noise of the conductivity signal without sweeping, as no visible *R*-Flu signal is available in the latter case (see Fig. 3B). LOD of *R*-Flu in the TAPS/LiOH buffer is 1.7 μM when sweeping with 5 mM β-CD and contactless conductivity detection is used.
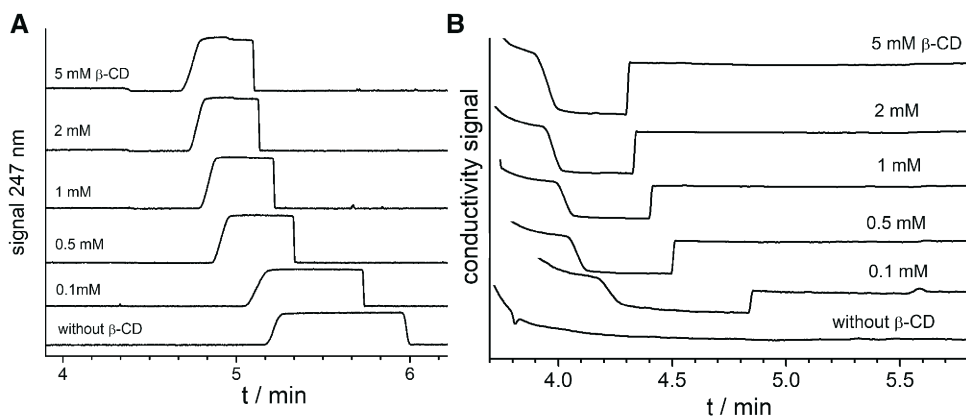

Figure 3. Experimental electropherograms showing the compression of R-Flu zones injected and the enhancement of R-Flu signal caused by sweeping with various concentrations of β-CD. (A) UV detection at 247 nm (B) conductivity signal. Curves are marked by the concentration of β-CD. BGE consisting of 10 mM TAPS and 5 mM LiOH. 10 kV/49.8 cm capillary length.

4.4 Conductivity signal enhancement in a drug sample

Cyclodextrins (as well as other selectors) are often encountered in affinity capillary electrophoresis where they assist in separations of structurally similar solutes, often enantiomers [62]. To the contrary, the main advantage of using these compounds as sweeping agents is seen in a targeted amplification of a conductivity signal of a molecule of interest. This is achieved in systems where the other molecules (matrix components) do not interact with the selector. We demonstrate this possibility on a specific amplification of a conductivity signal of flurbiprofen in a commercially available strepfen pastille. Information leaflet of strepfen declares 8.75 mg of flurbiprofen in a pastille. Strepfen pastille was diluted in 20 ml of TAPS/LiOH buffer and filtrated, which gives a concentration of 1.79 mM in a sample. Strepfen sample was then injected without any further pre-treatment (see Fig. 4).

Figure 4A shows a conductivity signal of the strepfen sample without sweeping. A signal from matrix components is present but flurbiprofen is barely visible (zoomed part, flurbiprofen identified according to its electrophoretic mobility). When the same sample was swept by neutral CD (Fig. 4B), conductivity signal of flurbiprofen was specifically amplified without amplifying signals of the other components. Migration time of flurbiprofen has changed due to the change of mobility of flurbiprofen in the presence of the neutral CD during sweeping. The conductivity signal was amplified sixty times, which is a bit less than sixty-eight times signal amplification observed with injecting a rectangular profile (Fig. 3). This is attributed to peak dispersion, while the rectangular profile was used in the theoretical part of this study to overcome such effect.
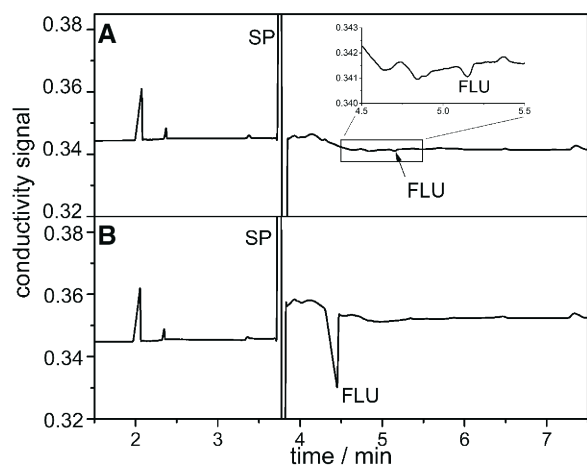
4.5 System zones

As the electrophoretic mobility of an analyte is changed abruptly at the boundary between a pure BGE and a BGE containing sweeping agent, the original situation in the separation system is disrupted and system zones must readjust. Thus, new system zones are excited at the boundary as it is shown by means of experiment and simulation at Fig. 5A and 5B, respectively. For the investigations of system zones, the setup (Fig. 1E) was slightly modified. A short plug of the *R*-Flu was injected and the zone was driven into the capillary at a pressure of 35 mbar for 120 s followed by the pure BGE further to isolate the injection position from the CD boundary. When voltage is applied, two almost stationary overlapping system peaks are excited in the position of injection. The PeakMaster software evaluates their mobilities to $0.00 \cdot 10^{-9}$ $m^2s^{-1}V^{-1}$ and $-0.08 \cdot 10^{-9}$ $m^2s^{-1}V^{-1}$. The EOF drifts these system zones toward the CCD detector and they appear in the record as the two peaks denoted as SP_{inj} in Fig. 5.

As the *R*-Flu reaches the CD-containing zone, a second pair of system zones arises. These new zones have the same mobilities as SP_{inj} zones but they have different amplitudes. When the EOF transports the CD boundary into the CCD detector, two (herein overlapped) system peaks appear in the record, marked as $SP_{boundary}$ in Fig. 5. Simulation was done by Simul 5 Complex with a setup corresponding to the that described above. We deliberately modified the experimental setup in order to visualize the system peaks generated at the CD boundary. When CD is present in the BGE directly followed by an injection zone (original setup, Fig. 1), the generated system peaks can easily merge with that as expected in a BGE without the presence of a selector. Thus no extra system peaks are present in Fig. 4. Nevertheless, the number
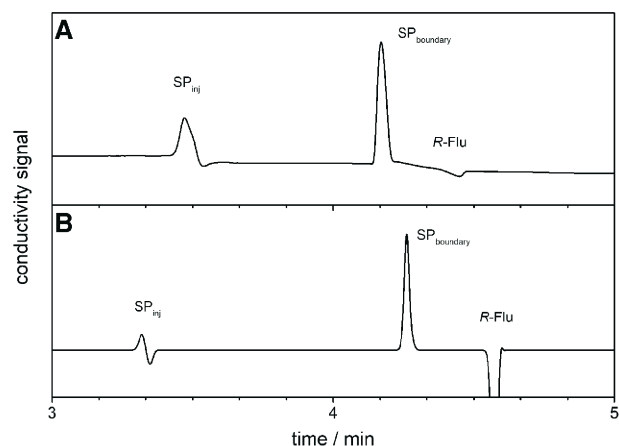

Figure 4. Conductivity signals of strepfen samples (A) without and (B) with sweeping by neutral CD showing specific amplification of flurbiprofen signal. BGE consisting of 10 mM TAPS and 5 mM LiOH and 5 mM β-CD. 10 kV/49.8 cm capillary length.

Figure 5. Conductivity signals of (A) experimental and (B) simulated electropherograms showing original system peaks (SPinj) and system peaks arising due to the R-Flu sweeping with the β-CD (SPboundary) in the TAPS/LiOH 10 mM/5 mM BGE.

of system zones may double in sweeping separation systems. This must be considered to prevent incomprehension and misinterpretation of resulting electropherograms.

5 Concluding remarks

The presence of a neutral sweeping agent does not affect the electric field intensity along the capillary. The homogeneous electric field allows the utilization of conductivity detection without any complications. The preconcentration in systems with a neutral sweeping agent aproaches to μ_A/μ_{ACD}, the ratio of mobilities of a free analyte and an analyte-agent complex. As the mobility of the *R*-Flu-β-CD complex is only about half that of the mobility of the free *R*-Flu, only a weak intrinsic preconcentration power was observed in our model system. On the other hand, not only the preconcentration factor but also the conductivity signal is enhanced when the analyte interacts with the sweeping agent. Both effects work in a synergic manner and the latter can significantly contribute to the overall enhancement in the conductivity response. Thus a total enhancement factor of 68 could be achieved with *R*-flu as the analyte and β-CD as the sweeping agent resulting in the LOD in the micromolar range.

The overall enhancement factor can be advantageously predicted by combining Eqs. (4) and (5) with calculations by means of our PeakMaster freeware. Sweeping with neutral CD was utilized to amplify conductivity signal of flurbiprofen in a pharmaceutical sample. The main potential of this technique is seen in specific amplification of conductivity signal of the compounds of interest that interact with the sweeping agent, as demonstrated. Finally, the study revealed a formation of a new set of system peaks as an analyte reaches the boundary between a sweeping agent and a pure BGE. This phenomenon is to be further studied but should be taken into account in the process of the interpretation of the resulting signal trace.

The authors have declared no conflict of interest.

6 References

[1] Breadmore, M. C., *Electrophoresis* 2007, *28*, 254–281.

[2] Breadmore, M. C., Thabano, J. R. E., Dawod, M., Kazarian, A. A., Quirino, J. P., Guijt, R. M., *Electrophoresis* 2009, *30*, 230–248.

[3] Breadmore, M. C., Dawod, M., Quirino, J. P., *Electrophoresis* 2011, *32*, 127–148.

[4] Breadmore, M. C., Shallan, A. I., Rabanes, H. R., Gstoettenmayr, D., Keyon, A. S. A., Gaspar, A., Dawod, M., Quirino, J. P., *Electrophoresis* 2013, *34*, 29–54.

[5] Breadmore, M. C., Tubaon, R. M., Shallan, A. I., Phung, S. C., Keyon, A. S. A., Gstoettenmayr, D., Prapatpong, P., Alhusban, A. A., Ranjbar, L., See, H. H., Dawod, M., Quirino, J. P., *Electrophoresis* 2015, *36*, 36–61.

[6] Breadmore, M. C., Wuethrich, A., Li, F., Phung, S. C., Kalsoom, U., Cabot, J. M., Tehranirokh, M., Shallan, A. I., Keyon, A. S. A., See, H. H., Dawod, M., Quirino, J. P., *Electrophoresis* 2017, *38*, 33–59.

[7] Quirino, J. P., Terabe, S., *Science* 1998, *282*, 465–468.

[8] Quirino, J. P., Terabe, S., *Anal. Chem.* 1999, *71*, 1638–1644.

[9] Quirino, J. P., Kim, J. B., Terabe, S., *J. Chromatogr. A* 2002, *965*, 357–373.

[10] Aranas, A. T., Guidote, A. M., Quirino, J. P., *Anal. Bioanal. Chem.* 2009, *394*, 175–185.

[11] Isoo, K., Terabe, S., *Anal. Chem.* 2003, *75*, 6789–6798.

[12] Markuszewski, M. J., Britz-McKibbin, P., Terabe, S., Matsuda, K., Nishioka, T., *J. Chromatogr. A* 2003, *989*, 293–301.

[13] Quirino, J. P., Terabe, S., *Chromatographia* 2001, *53*, 285–289.

[14] Quirino, L. P., Terabe, S., Otsuka, K., Vincent, J. B., Vigh, G., *J. Chromatogr. A* 1999, *838*, 3–10.

[15] Kirschner, D. L., Jaramillo, M., Green, T. K., *Anal. Chem.* 2007, *79*, 736–743.

[16] Rabanes, H. R., Quirino, J. P., *Electrophoresis* 2013, *34*, 1319–1326.

[17] Britz-McKibbin, P., Ichihashi, T., Tsubota, K., Chen, D. D. Y., Terabe, S., *J. Chromatogr. A* 2003, *1013*, 65–76.

[18] Song, G. Q., Peng, Z. L., Lin, J. M., *J. Sep. Sci.* 2006, *29*, 2065–2071.

[19] Cheng, C. Y., Tsai, H. R., *J. Pharm. Biomed. Anal.* 2011, *56*, 728–735.

[20] Wang, C. C., Chen, J. L., Chen, Y. L., Cheng, H. L., Wu, S. M., *Anal. Chimi. Acta* 2012, *744*, 99–104.

[21] El-Awady, M., Belal, F., Pyell, U., *J. Chromatogr. A* 2013, *1309*, 64–75.

[22] El-Awady, M., Pyell, U., *Electrophoresis* 2014, *35*, 605–616.

[23] Otsuka, K., Matsumura, M., Kim, J. B., Terabe, S., *J. Pharm. Biomed. Anal.* 2003, *30*, 1861–1867.

[24] Ibrahim, W. A. W., Hermawan, D., Sanagi, M. M., *J. Chromatog. A* 2007, *1170*, 107–113.

[25] Ibrahim, W. A. W., Hermawan, D., Sanagi, M. M., Aboul-Enein, H. Y., *Chromatographia* 2010, *71*, 305–309.

[26] Martinez-Giron, A. B., Crego, A. L., Gonzalez, M. J., Marina, M. L. *J. Chromatogr. A* 2010, *1217*, 1157–1165.

[27] Lin, E. P., Lin, K. C., Chang, C. W., Hsieh, M. M., *Talanta* 2013, *114*, 297–303.

[28] Mikuma, T., Iwata, Y. T., Miyaguchi, H., Kuwayama, K., Tsujikawa, K., Kanamori, T., Kanazawa, H., Inoue, H., *Electrophoresis* 2016, *37*, 2970–2976.

[29] Scriba, G. K. E., Zhu, Q., *Chromatographia* 2016, *79*, 1403–1435

[30] Xu, X. Y., Jia, Z. M., Shu, Y., Liu, L. H., *J. Chromatogr. B* 2015, *980*, 20–27.

[31] Fan, L. Y., Yan, W., Cao, C. X., Zhang, W., Chen, Q., *Anal. Chim. Acta* 2009, *650*, 111–117.

[32] Quirino, J. P., Terabe, S., *J. High Res. Chrom.* 1999, *22*, 367–372.

[33] Quirino, J. P., Terabe, S., Bocek, P., *Anal. Chem.* 2000, *72*, 1934–1940.

[34] Breadmore, M. C., Quirino, J. P., Thormann, W., *Electrophoresis* 2009, *30*, 570–578.

[35] Thormann, W., Caslavska, J., Mosher, R. A., *Electrophoresis* 2015, *36*, 773–783.

[36] Jin, J., Shao, J., Li, S., Zhang, W., Fan, L. Y., Cao, C. X., *J. Chromatogr. A* 2009, *1216*, 4913–4922.

[37] Jaros, M., Soga, T., van de Goor, T., Gas, B., *Electrophoresis* 2005, *26*, 1948–1953.

[38] Kubáň, P., Hauser, P. C., *Electrophoresis* 2017, *38*, 95–114.

[39] Kubáň, P., Hauser, P. C., *Electrophoresis* 2015, *36*, 195–211.

[40] Coltro, W. K. T., Lima, R. S., Segato, T. P., Carrilho, E., de Jesus, D. P., do Lago, C. L., da Silva, J. A. F., *Anal. Methods* 2012, *4*, 25–33.

[41] Nuchtavorn, N., Suntornsuk, W., Lunte, S. M., Suntornsuk, L., *J. Pharm. Biomed. Anal.* 2015, *113*, 72–96.

[42] Xu, Y., Wang, W. L., Li, S. F. Y. *Electrophoresis* 2007, *28*, 1530–1539.

[43] Lau, H. F., Quek, N. M., Law, W. S., Zhao, J. H., Hauser, P. C., Li, S. F. Y., *Electrophoresis* 2011, *32*, 1190–1194.

[44] Xu, L., Hauser, P. C., Lee, H. K., *J. Chromatogr. A* 2009, *1216*, 5911–5916.

[45] See, H. H., Hauser, P. C., Ibrahim, W. A. W., Sanagi, M. M., *Electrophoresis* 2010, *31*, 575–582.

[46] Wei, R. X., Li, W. H., Yang, L. R., Jiang, Y. X., Xie, T. Y., *Talanta* 2011, *83*, 1487–1490.

[47] Anouti, S., Vandenabeele-Trambouze, O., Cottet, H., *Electrophoresis* 2010, *31*, 1029–1035.

[48] Gas, B., Zuska, J., Coufal, P., van de Goor, T., *Electrophoresis* 2002, *23*, 3520–3527.

[49] Hruska, V., Benes, M., Svobodova, J., Zuskova, I., Gas, B., *Electrophoresis* 2012, *33*, 938–947.

[50] Svobodova, J., Benes, M., Hruska, V., Uselova, K., Gas, B., *Electrophoresis* 2012, *33*, 948–957.

[51] Riesova, M., Svobodova, J., Uselova, K., Tosner, Z., Zuskova, I., Gas, B., *J. Chromatogr. A* 2014, *1364*, 276–288.

[52] Benes, M., Svobodova, J., Hruska, V., Dvorak, M., Zuskova, I., Gas, B., *J. Chromatogr. A* 2012, *1267*, 109–115.

[53] Hruska, V., Svobodova, J., Benes, M., Gas, B., *J. Chromatogr. A* 2012, *1267*, 102–108.

[54] https://echmet.natur.cuni.cz/download.

[55] Monton, M. R. N, Quirino J. P., Otsuka K., Terabe S., *J. Chromatogr. A* 2001, *939*, 99–108

[56] Dubsky P., Dvorak M., Ansorge M., *Anal. Bioanal. Chem.* 2016, *30*, 8623–8641

[57] Wren, S. A. C., Rowe, R. C., *J. Chromatogr.* 1992, *603*, 235–241.

[58] Tazaki, M., Hayashita, T., Fujino, Y., Takagi, M., *Bull. Chem. Soc. Jpn.* 1986, *59*, 3459–3464.

[59] Dubrovcakova, E., Gas, B., Vacik, J., Smolkova-Keulemansova, E., *J. Chromatogr.* 1992, *623*, 337–344.

[60] Almeida, V. K., Larive, C. K., *Magn. Reson. Chem.* 2005, *43*, 755–761.

[61] Stedry, M., Jaros, M., Hruska, V., Gas, B., *Electrophoresis* 2004, *25*, 3071–3079.

[62] Stavrou I. J., Mavroudi M. C., Kapnissi-Christodoulou C. P., *Electrophoresis* 2015, *36*, 101–123.

II

Online preconcentration of weak electrolytes at the pH boundary induced by system a zone in capillary zone electrophoresis

M. Boublík, M. Riesová, J. Šteflová, V. Hruška

Online preconcentration of weak electrolytes at the pH boundary induced by a system zone in capillary zone electrophoresis

Milan Boublík [a], Martina Riesová [a, *], Vlastimil Hruška [b], Jana Šteflová [a, b]

[a] Department of Physical and Macromolecular Chemistry, Faculty of Science, Charles University, Albertov 6, Prague 2, 128 43, Czech Republic
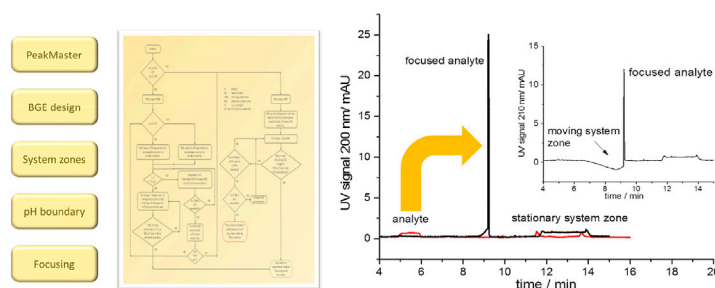[b] Agilent Technologies GmbH, Waldbronn, Germany

HIGHLIGHTS

- System zone is introduced as source of pH boundary for dynamic pH junction in CE.
- Both moving and stationary system zones can be employed.
- PeakMaster software helps to design focusing systems.
- Flowchart for method development is presented.

GRAPHICAL ABSTRACT

ABSTRACT

Within the frame of the dynamic pH junction preconcentration technique in capillary electrophoresis, we introduce a novel approach based on the use of the pH boundary of a system zone for the preconcentration of general, multivalent, weak analytes in a system of binary, uni-univalent, background electrolytes (BGE). For such purpose, in addition to presenting a comprehensive flowchart for the development of a method for BGE preconcentration, we showed several model cases using acidic, basic and ampholytic analytes. Furthermore, we combined the flowchart with calculations in electrophoretic software Peak-Master to determine all necessary information such as analyte mobility, system zones and the amplitude of the pH boundary of a system zone as a function of the sample matrix. For an even more detailed understanding of the process, we also investigated changes in the pH boundary through computer simulations with Simul 5, providing an in-depth characterization of all model analytes according to the steps of the flowchart and to PeakMaster calculations for experimental verification of the final BGE preconcentration.

© 2019 Elsevier B.V. All rights reserved.

1. Introduction

Online preconcentration techniques enhance the detection sensitivity of capillary electrophoresis (CE) and are currently an integral part of almost every CE analytical application. Various online preconcentration approaches, their improvements, limitations and applications are periodically reviewed by Breadmore et al. [1—7]. Several specialized reviews focused on online preconcentration in CE analysis of chiral compounds [8], peptides [9] and proteins [10] or in CE-MS and online derivatization techniques [11—13] have also been recently published.

Dynamic pH junction, an online preconcentration technique commonly applied in CE, uses changes in the ionization of weak electrolytes due to differences in pH between the sample and the background electrolyte (BGE). This approach was introduced in CE by Aebersold and Morrison [14] and further developed and applied by the Britz-McKibbin research group [15–18]. Moreover, comprehensive theoretical and practical studies on moving reaction boundaries have been conducted by the Cao group, which have significantly contributed to this field, as summarized in a critical review [19]. Kazarian et al. [20] recapped the mechanism of dynamic pH junction and provided an overview of its applications from 1990 to 2010. These applications are summarized each 2 years in the corresponding section of the Breadmore's review series [4–7].

In most applications listed in Ref. [20], pH discontinuity is induced by analyte injection in a sample matrix solution with different constituents (and with a different pH) from those of the BGE solution. Usually, a preconcentration system is specifically designed for a target analyte based on buffers previously shown to effectively focus an analyte of similar acid-base properties. The most commonly used combinations are borate buffer as the BGE and formate, acetate or phosphate buffer as the sample matrix solution [20].

Although conceptually very simple, the precise mechanism of dynamic pH junction can be quite complicated because it depends on all sample and BGE components, their concentrations, acid-base properties and electrophoretic mobilities. Thus, the pH boundary origin, its velocity and amplitude of pH change are only rarely discussed in publications on dynamic pH junction applications. Mechanistic details of the pH junction focusing process in the borate buffer/acetate sample matrix boundary have been investigated by Kim et al. [21]. For such purpose, these researchers used computer simulations in Simul 4 software [22] to elucidate the focusing mechanism of m-nitrophenol injected into the borate buffer (pH 10) from the acetate sample matrix (pH 4.5). The dynamic pH boundary is formed in the capillary through migration of a high amount (450 mM) of acetic acid. Persistently low pH within the acetic acid zone prevents the mobility of m-nitrophenol, thus focusing m-nitrophenol on this pH boundary. The mechanism of Trp focusing, when it is injected from a sample matrix consisting of 200 mM ammonium acetate and 15 mM NaCl (pH 7) into 1 M formic acid (pH 1.8) BGE, was elucidated via Simul 5.0 [23] simulations. Trp is focused on the dynamic pH boundary formd by migrating zones of ammonium and sodium ions [24]. Similarly, the computer program developed by Bier et al. [25] and further modified by Mosher and Thormann [26] was used to elucidate the pH stacking process of several sugars in a CE separation and derivatization system consisting of borate BGE and of a formate sample matrix [27]. Cao et al. [28] calculated theoretically velocities of a pH boundary formed in simple systems, where only formic or acetic acid solutions were used as BGE, and sample matrices were composed of various concentrations of sodium formate and sodium acetate, respectively. The model analyte, Trp, was focused on the pH boundary formed by the migrating zone of the sodium ions. Based on the comparison between the calculated velocities of Trp and the pH boundary movement, appropriate sample matrix concentrations and general pH conditions are recommended for the successful preconcentration of a zwitterionic analyte.

All approaches analyzed in detail in the aforementioned publications [21,24,27,28], as well as most dynamic pH junction applications published [20], can be regarded as techniques for target analyte preconcentration at the boundary between the BGE and the zone of an auxiliary co-ion, which is simultaneously injected in a high concentration with the target analyte. The constituents of a sample matrix absent from the BGE are regarded as auxiliary ions.

In such systems, acetic acid [21], ammonium or sodium ions [24,27,28] function as auxiliary co-ions and form the pH boundaries for the analytes.

Interestingly, in several reports, authors used the same components for both BGE and sample matrix preparation. Such simplifications of dynamic pH junction focusing systems aimed to theoretically describe the moving pH boundary [29], to simulate its dynamics [30] or to couple CE to MS [31]. Similarly to their previous work [28], Zhu et al. calculated the theoretical pH boundary velocity induced in a CE system consisting of formic acid/NaOH (pH 2.85) as acidic BGE and of sodium formate as sample matrix [29]. Breadmore et al. [30] systematically investigated the focusing of 24 weak bases at the moving pH boundary induced by the use of a formic acid/NaOH sample matrix solution at pH 8.6 together with formic acid/NaOH buffer, at pH 2.85, as BGE. Based on computer simulations of the preconcentration system, the relationships between analyte velocity and pH boundary velocity are formulated for maximum focusing efficiency. The effect of the sample matrix pH on focusing performance was experimentally investigated when optimizing the CE-MS method for four peptides mixture [31]. Formic acid/ammonium hydroxide solutions at pH = 2 and pH 2–10 were used as BGE and sample matrix, respectively. In Refs. [29–31], differences in pH are made only by varying the concentration of constituents in BGE and in sample matrix solutions because the auxiliary co-ions that create moving pH boundaries are absent. Thus, pH discontinuities for target analyte stacking must have a different origin.

Provided that the capillary zone electrophoresis (CZE) arrangement of the method is preserved, $i.e.$, the sample zone is hydrodynamically injected into the capillary filled with BGE, pH discontinuities must be caused by traveling (or stationary) disturbances in BGE components concentration profiles - system zones [32]. System zones are a phenomenon inherent to every electrophoretic measurement. Currently, system zones are well understood and mathematically described [33]; accordingly, their mobilities, polarities [34] and even amplitudes and shapes [35] are accurately predicted. The number of system zones is equal to the number of BGE constituents, and system zone mobility is governed by the concentrations and limiting electrophoretic mobilities of all BGE constituents; thus, the number and mobilities of system zones are characteristic properties of each BGE. The amplitudes of the system zone depend on the initial (injected) disturbances in the concentration profiles of BGE constituents. All predictions and calculations concerning system zones and other electrophoretic system properties can be easily made using PeakMaster software [36], wherein the linearized theory of electromigration [33] is implemented and solved analytically. The dynamics of the electromigration process, including the origin and development of system peaks, can be comfortable investigated via numerical simulation software, such as Simul [23,37]. Although system peaks are considered disturbing phenomena, when used wisely, they can help to determine the critical micellar concentration [38] or to detect additional equilibria in the separation system [39].

In this paper, system zones in binary uni-univalent BGEs are employed as moving (dynamic) or stationary pH discontinuities for focusing weak electrolyte analytes within the electrophoretic process running in the capillary. Based on calculations performed in PeakMaster software, we developed a complete method for finding a suitable CE preconcentration system for any weak electrolyte analyte. We designed three preconcentration systems for model acidic, basic and ampholytic weak electrolytes according to the flowchart we compiled. In addition, we showed in detail the stacking mechanism through computer simulations in Simul software and experimentally proved the ability of the designed systems to focus target analytes.

2. Experimental

All chemicals were of analytical grade purity. Lithium hydroxide monohydrate and *p*-cresol were purchased from Fluka (Steinheim, Germany). Formic acid, chloroacetic acid, triethylamine (TEA), hydrochloric acid, 2-(N-Morpholino)ethanesulfonic acid (MES) monohydrate, *p*-nitrophenol, 4-aminophenyl acetic acid (APAA) and 4-aminophenyl butyric acid (APBA) were purchased from Sigma Aldrich (Steinheim, Germany). Water for the preparation of all solutions was deionized using a Watrex Ultrapur system (Prague, Czech Republic). All running buffers were filtered using Minisart syringe filters (Sartorius Stedim Biotech, Goettingen, Germany), with a pore size of 0.45 μm.

All CE experiments were performed using an Agilent 7100 capillary electrophoresis instrument operated under ChemStation software (Agilent Technologies, Waldbronn, Germany). Detection was performed using a built-in diode array detector (DAD). Fused silica capillaries (50 μm i.d., 375 μm o.d.) were purchased from Polymicro Technologies (Phoenix, AZ, USA). The experiments were performed in bare capillaries with total (L_{tot}) and effective (L_{eff}) lengths to the DAD of 50.0 and 41.5 cm, respectively. The new capillary was flushed with deionized water for 10 min and then for 20 min with the actual BGE. Commonly used, initial flushing of the capillary by sodium hydroxide solution was omitted for the possible carryover effect of sodium ions on the number of system zones and on their mobilities in the separation systems. Hydrodynamic injection was used.

PeakMaster 5.4 software [40] was used to design suitable CE systems and to calculate their fundamental properties such as pH, buffering capacity, system zone mobilities and effective electrophoretic mobility of the analyte under the specific conditions tested in this study. PeakMaster 5.4 was also used to calculate pH disturbances at system zones as a function of the injected concentration of sample matrix components to search for the proper sample composition. Acidic dissociation constants, as well as the limiting electrophoretic mobilities of BGE components and of all model analytes, were obtained from the PeakMaster database. All calculations were performed with ionic strength correction. BGEs and sample matrices selected for the preconcentration of model analytes shown in this paper are summarized in Table 1.

Simulations in Simul 5 Complex were used to verify the preconcentration abilities of CE systems designed based on Peak-Master calculations. The simulated capillary filled with BGE was 50 mm long (3000 grid points), and a 4-mm-wide sample zone (peak edge 0.5 mm) was injected into the middle of the capillary. The simulated sample was composed of 0.01 or 0.1 mM analyte in a particular sample buffer matrix designed in PeakMaster 5.4 (see Table 1). Voltage was always positive 200 V; no electroosmotic flow (EOF) was set; simulations were performed with ionic strength correction.

All BGEs, as well as the sample matrix, were prepared by mixing appropriate amounts of buffer component stock solutions with deionized water. The particular sample matrix was further used as a solvent for to prepare samples of model analytes with the following compositions: 0.1 mM *p*-cresol in 60/60 mM TEA/HCl, 0.1 mM *p*-nitrophenol in 5/5 mM or 50/50 mM MES/LiOH, 0.01 mM APAA and 0.01 mM APBA in 35/27 mM formic acid/LiOH. The experimental pH of each BGE was measured and is outlined in Table 1, in addition to other experimental conditions for individual preconcentration systems. Additional pressure was applied when necessary to modulate the velocity of EOF. The preconcentration performance of each system was evaluated in comparison with the run where the same amount of analyte was injected with the original BGE. Measurements were performed in triplicates.

OriginPro 2016 software (OriginLab Corporation, Northampton, USA) was used for data evaluation and visualization.

3. Results and discussion

Generally, the technique proposed in this study is based on analyte accumulation on the pH boundary formed by a system zone. The simplest binary buffers consisted of a univalent buffering constituent and of a univalent strong counterion. Based on the linear theory of electromigration [33], two system zones develop in such separation systems. One of them always has almost zero mobility, *i.e.*, there is one stationary system zone in the uni-univalent BGE [41,42]. The second system zone can acquire various electrophoretic mobilities depending on the pH of the BGE; close to zero mobility in the region of pH 5–9 and cationic or anionic mobility in the acidic or alkaline pH range, respectively

Table 1
Calculated PeakMaster characteristics of CE systems designed for preconcentration of model analytes and conditions of their experimental verifications.

Model analyte (pK$_A$[a])		*p*-cresol (10.96)	aniline (4.60)	APAA (3.36; 5.13)	*p*-nitrophenol (7.15)
PeakMaster parameters	BGE	TEA/HCl	chloroacetic a./LiOH	formic a./LiOH	MES/LiOH
	/mM	60/40	50/40	40/20	50/20
	pH	10.62	3.42	3.70	5.86
	β/mM	32.03	18.82	23.53	27.64
	u_1; u_2/10^{-9} m^2 s^{-1} V^{-1}	0.00; −8.09	0.00; +17.55	0.00; +6.92	0.00; +0.05
	$u_{eff,A}$/10^{-9} m^2 s^{-1} V^{-1}	−9.81	+23.01	+7.88	−1.60
	sample solution	TEA/HCl	chloroacetic a./LiOH	formic a./LiOH	MES/LiOH
	/mM	60/60	60/60	35/27	5/5 (50/50)
	pH resp.$_1$; pH resp.$_2$	0.02; −7.83	−0.10; +8.24	−0.02; +0.59	+5.81; −0.14 (−0.07; +6.08)
	$u_{EMD,1}$; $u_{EMD,2}$ /10^{-9} m^2 s^{-1} V^{-1}	−0.00; 11.57	0.00;-9.03	0.00; −6.57	0.00; 0.03 (0.00; −0.23)
Experimental conditions	pH$_{exp}$	10.61	_[b]	3.71	5.96
	voltage/kV	+20	—	+25	+20
	injection/mbar × s	30 × 90	—	60 × 60	60 × 60
	sample plug/% of L_{eff}	10	—	13	13
	EOF	fast cationic	—	slow cationic	fast cationic
	additional pressure	−50 mbar	—	—	—
	analyte concentration/mM	0.1	—	0.01	0.1
	detection wavelength	280 nm	—	200; 210 nm	320 nm
	P_{exp}	6	—	50	8 (3)

[a] From PeakMaster database.
[b] Experimentally unverified system.

[33,41,42]. Both types of system zones, stationary or moving, can be used for analyte pH stacking. Weak acids with pK_A higher than 9, weak bases with pK_A lower than 5 and ampholytes with pI outside the 5–9 range are good candidates for focusing using moving system zones because they are usually analyzed in rather high or low pH buffers with mobile system zones. Uni-univalent electrolytes help to reduce the overall complexity of the proposed method. Weak acids with a pK_A lower than 5 and weak bases with a pK_A higher than 9 cannot be stacked on moving system zones because they lack the required co-migrating system peak. However, these compounds and weak ampholytes with a pI in the 5–9 range can be stacked on the pH boundary created by the stationary system zone. The electrophoretic mobility of strong electrolytes does not change with pH, and they cannot be captured and concentrated by any pH disturbance. The flowchart of the focusing system design is shown in Fig. 1. This flowchart makes it possible to find a suitable system for analyte preconcentration at any pK_A using the system zone.

3.1. Preconcentration by moving system zone

An analyte migrating in the same direction as the system zone can be stacked by mobile system zone if it is faster than the system zone in BGE but slower than the system zone when passing it, *i.e.*, within the system zone, the original pH must be disturbed in a way that reduces the effective mobility of the analyte to a value lower than the system zone mobility. When this condition is met, the analyte is focused on the migrating system zone boundary. The selection of the preconcentration (separation) system requires knowing the dissociation constant(s) of the target analyte. The pH of the BGE must be close to pK_A or pI of the analyte, *i.e.*, must lie in the region where the effective mobility of the analyte varies the most with the ambient pH.

Based on calculations performed in PeakMaster 5.4 [36], we designed the following model separation systems, detailing the strategy for BGE selection and the importance of adequately choosing the sample zone composition. Prior experiments, the stacking mechanism, as well as the preconcentration potential and limitations of the proposed technique, and particular separation systems designed were investigated through computer simulations in Simul 5 Complex software.

3.1.1. Weak acid analyte with $pK_A > 9$: p-cresol

We have chosen *p*-cresol with a pK_A of 10.96 as a model analyte of a very weak acid with a pK_A higher than 9. As discussed above, in
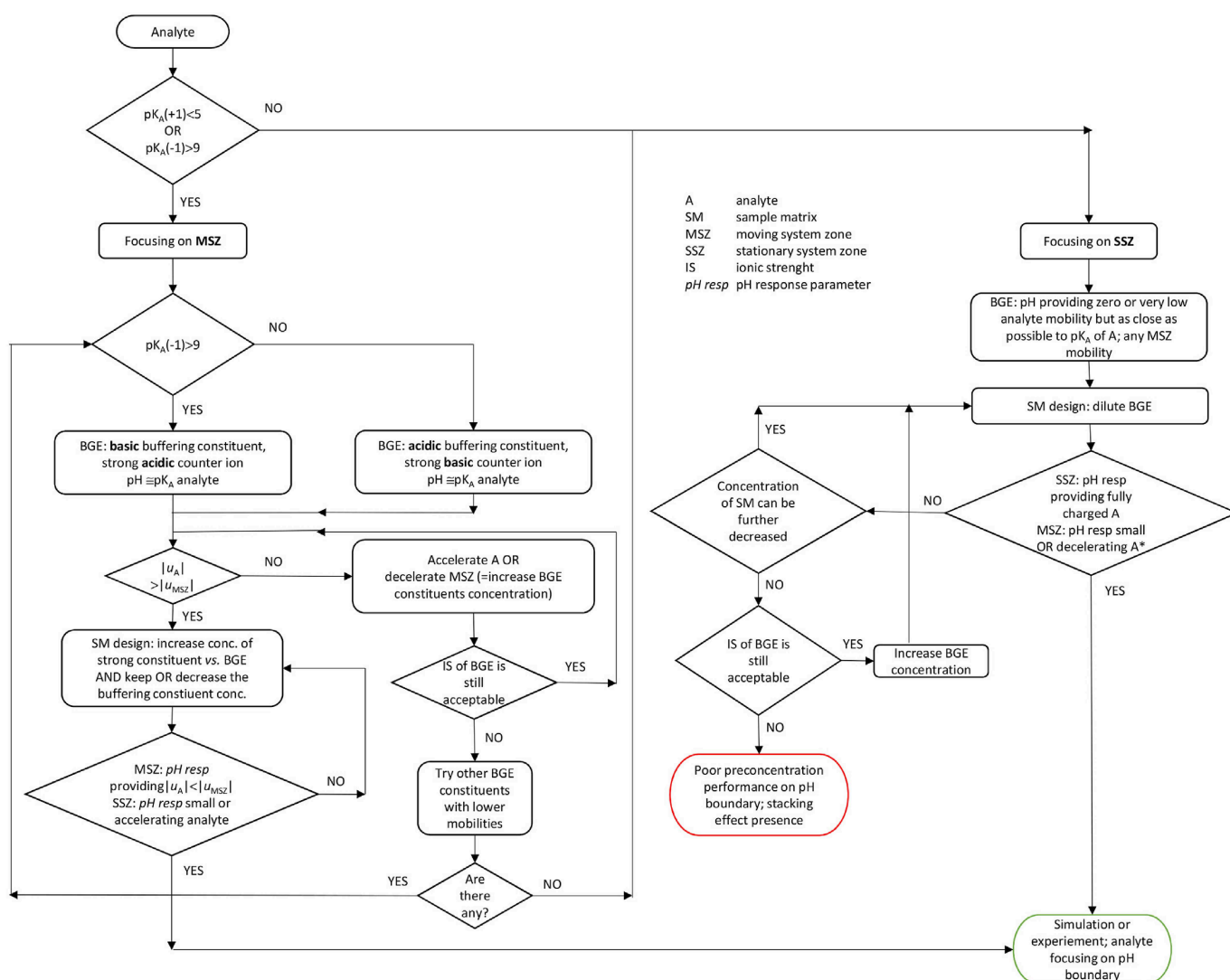

Fig. 1. Flowchart guiding the selection of preconcentration uni-univalent BGE and sample matrix electrolyte system for weak electrolyte analyte.

alkaline binary uni-univalent electrolytes, an anionic system zone is formed. This system zone can be used for anionic analyte stacking. To sufficiently affect the effective mobility of the analyte via pH disturbance of the system zone, BGE of pH close to the pK$_A$ of *p*-cresol should be designed. For this purpose, TEA (pK$_A$ 10.86) was selected as suitable basic buffering compound and hydrochloric acid as counterion. In PeakMaster 5.4, various ratios and concentrations of these two buffer components were fine-tuned to determine a composition in which the effective mobility of *p*-cresol is higher than the mobility of the anionic system zone (see flowchart at Fig. 1).

Simultaneously, both analyte and system zone should be mobile enough to be separated from the injection position (stationary system zone) in a reasonable time. Although the ratio between TEA an HCl (*i.e.* pH of BGE) determines the dissociation state and thus the effective electrophoretic mobility of *p*-cresol, the absolute concentrations of both components significantly affect the mobility of the anionic system zone; the higher the concentration is, the slower the system zone will be. This effect independently affects the ionic strength. We tuned the system within several iterations and selected BGE consisting of 60 mM TEA and 40 mM HCl. The calculated characteristics of this system are outlined in Table 1. As required, the anionic zone mobility of the 60/40 mM TEA/HCl system ($u = -8.09 \times 10^{-9}\,\mathrm{m^2\,V^{-1}\,s^{-1}}$) is slower than the effective electrophoretic mobility ($u_{\mathrm{eff,A}}$) of *p*-cresol ($-9.81 \times 10^{-9}\,\mathrm{m^2\,V^{-1}\,s^{-1}}$). When this criterion is met, the sample matrix composition invoking the appropriate pH disturbances in system zones must be found; the pH of the mobile system zone should reduce the analyte effective mobility so as to prevent the passing of the analyte through the system zone while simultaneously disturbing the pH of the stationary system zone as little as possible (this disturbance can be even high when accelerating the analyte) to prevent capturing the analyte at the injection position. Previously [35,43], we investigated the polarity and the amplitude of system peaks as a function of disturbances of the injected BGE sample and implemented the "Amplitudes and Shape" tool in our PeakMaster software. This PeakMaster plugin is perfectly suitable for sample composition optimization [35]. In the context of this study, we updated the previous version of PeakMaster [35] and released version 5.4 [40], which enables us to more comfortably predict the system zone pH. For such purpose, the parameter termed "pH response" should be used in PeakMaster 5.4 software. Although the sign of this parameter corresponds to the polarity of pH disturbances in comparison with the pH of BGE, the value of the pH response corresponds to the pH difference between the system zone and BGE at the beginning of the electromigration process. The pH value of the system zone is calculated from its composition given by amplitudes. The real amplitude is then lowered by diffusion and electromigration dispersion (EMD) of the system zone. Importantly, completely new PeakMaster software, PeakMaster 6 [44,45], is being developed in our lab. All calculations and predictions made within this work can also be calculated in this new software.

Electromigration dispersion (EMD) causes the triangular shape of electromigrating zones (peaks) whether it is an analyte or a system zone. The triangular shape of the peak decreases the peak height at its apex. Similarly, a system zone undergoing EMD has a lower maximal amplitude of pH disturbance than that which leads to insufficient preconcentration performance. Thus, EMD should be regarded when designing the preconcentrating system. EMD is characterized by the electromigration dispersion mobility parameter, u_{EMD}, defined as $v_{\mathrm{(EMD,i)}}/E_{\mathrm{(BGE)}}$, where $E_{\mathrm{(BGE)}}$ is the applied intensity of the electric field in BGE and $v_{\mathrm{(EMD,i)}}$ is a measure of the electromigration dispersion of the *i*-th zone for given initial conditions (*i.e.*, sample composition) [35]. The parameter u_{EMD} is also

calculated at the "Amplitudes and Shape" window in PeakMaster 5.4. The composition of the sample should be selected to provide sufficient pH disturbance of the preconcentrating system zone while its u_{EMD} remains optimal. If the u_{EMD} is too high (in the order of hundreds; usually when testing the composition providing the as high/low pH as possible), the triangulation decreases the pH apex of the boundary, which is insufficient for sample stacking. Conversely, optimal triangulation of the system zone ensures the formation of a sharp boundary. Stacking the analyte on this sharp boundary increases the efficiency of the focusing process. To ensure the correct orientation of the system zone in relation to the analyte, the u_{EMD} of the system zone has the opposite sign of the effective mobility of the analyte (in all presented possibilities of binary uni-univalent preconcentrating systems, the orientations of the triangular shape are inherently correct). Based on the above, we chose the 60/60 mM TEA/HCl composition as the most suitable sample matrix solution. The values of linear pH response and u_{EMD} of both stationary and moving (focusing) system zones are outlined in Table 1. The whole selection procedure of the preconcentration system for *p*-cresol using the flowchart and PM calculations is summarized in detail in Supplementary data. Furthermore, we verified the proposed preconcentration system through simulations in Simul 5 Complex [37]. Simulations provide a direct insight into system zone formation and analyte stacking and show changes in their actual amplitudes due to diffusion and EMD within the preconcentration process.

Fig. 2 A shows the course of the preconcentration process of a 4-mm-wide zone of 0.01 mM *p*-cresol by the anionic system zone of 60/40 mM TEA/HCl BGE. Before applying voltage (t = 0 s), the initial pH disturbance given by the sample matrix solution pH (60/60/ 0.01 mM TEA/HCl/*p*-cresol) and by the concentration profile of *p*-cresol is shown. When positive voltage is switched on for 100 s, both *p*-cresol and anionic system zone start migrating to the anode. The pH disturbance caused by the migrating system zone forms a pH boundary through which *p*-cresol cannot pass, and thus *p*-cresol is stacked on the system zone boundary. After 300 s, the preconcentration process is completed, but the pH disturbance is still high enough to prevent *p*-cresol from migrating through the system zone. Thus, *p*-cresol peak sharpening continues even during its electromigration. To evaluate the preconcentration efficiency of our systems, we define a simulated preconcentration factor, P_{sim}, as the ratio between peak height (in mM scale) under preconcentration conditions and peak height in simulations in which the analyte is injected from undisturbed BGE. THe P_{sim} of our model system for *p*-cresol was approximately 17. Our simulations further showed that the designed TEA/HCl system maintains its performance even when the initial concentration of *p*-cresol is increased 10x to 0.1 mM, as shown in Supplementary data, Fig. S1.

3.1.2. Weak basic analyte with pK$_A$ < 5: aniline

Aniline was selected as the model basic analyte with pK$_A$ lower than 5 (pK$_A$ 4.60). This type of compounds is suited for preconcentration by a cationic system zone in the acidic pH region. At first, we tested acetate and formate BGEs maintaining the pH around the pK$_A$ of the aniline. Such pH is close to the pH region 5–9, wherein the cationic system zone is rather slow, even at low BGE constituent concentrations. Therefore, we selected a 50/40 mM chloroacetic acid (pK$_A$ 2.87)/LiOH system with pH 3.42 and a cationic system zone mobility $u = +17.6 \times 10^{-9}\,\mathrm{m^2V^{-1}s^{-1}}$. In this BGE, aniline is already more than 90% protonated ($u_{\mathrm{eff,A}} = +23.0 \times 10^{-9}\,\mathrm{m^2V^{-1}s^{-1}}$). Nevertheless, the sample matrix of 60/60 mM chloroacetic acid/LiOH still provides a sufficiently high pH barrier for aniline to migrate through the cationic system zone.

Calculated characteristics of the system are outlined in Table 1. The simulated online preconcentration of 0.01 mM aniline is
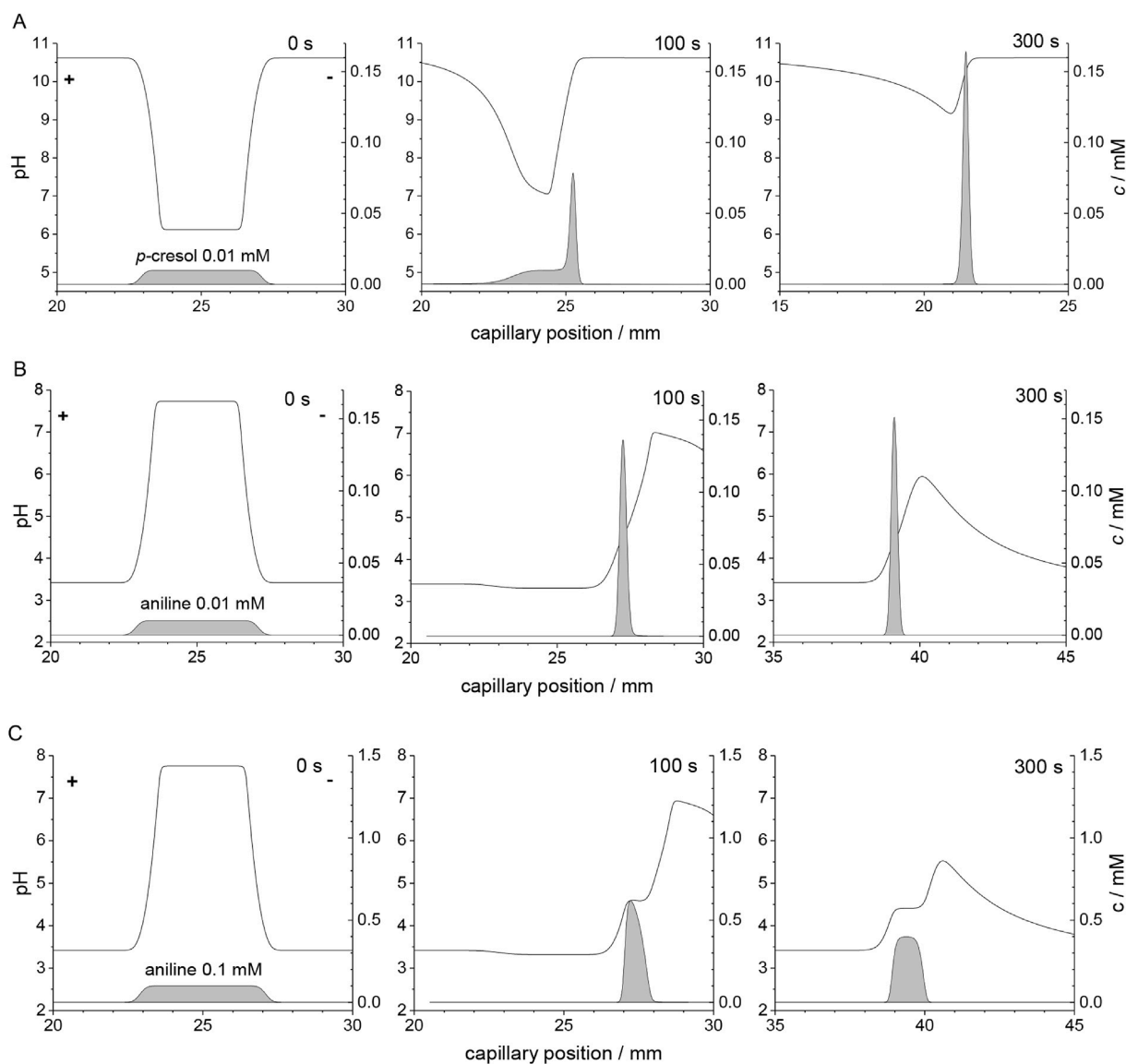
Fig. 2. Three consecutive time-labeled simulated pH profiles (black line; left axes) and analyte concentration profiles (filled by grey, right axes) of preconcentration by a moving system zone. A) 0.01 mM *p*-cresol in 60/60 mM TEA/HCl, BGE: 60/40 mM TEA/HCl; B) 0.01 mM aniline in 60/60 mM chloroacetic a./LiOH; BGE: 50/40 mM chloroacetic a./LiOH; C) same as B) but with 0.1 mM aniline. The polarity of the inserted voltage is depicted.

depicted in Fig. 2B. The P_{sim} of aniline was similar to that of *p*-cresol, *i.e.*, approximately 15. When an analyte is stacked on a zone boundary, the analyte zone matches its electrophoretic mobility to that of the system zone, which is in principle isotachophoresis. When increasing the concentration of the analyte in the sample above a specific level, its isotachophoretic zone becomes visible and the analyte height no longer increases. Fig. 2B shows a hint of the analyte zone at 300 s. When using a higher initial concentration of aniline (0.1 mM), this zone becomes clearly visible, as shown in Fig. 2C. The analyte zone height is limited by the ITP and therefore so is the preconcentration performance. The maximum P_{sim} was only 6 (panel 100 s, Fig. 2C). As the leading mobile system zone diminishes over time, mainly due to its high electromigration dispersion, and the analyte zone fully develops, the focusing performance becomes even poorer, as shown in the 300-s panel of Fig. 2C. Therefore, every analyte concentration has its limits above which such a sample overload behavior starts to play a role and the focusing performance is ruined [46].

3.1.3. Ampholytes with pI out of the 5–9 range: APAA and APBA

The selection of a suitable preconcentration system for ampholytes is governed by the same rules as those indicated in previous cases. Advantageously, when the pH profile is changing around the pI of the ampholyte, not only its velocity but also the direction of its electromigration can be altered. When designed thoroughly, separation systems can use this pH-driven switching between the cationic and anionic direction of electromigration of ampholytes for their highly effective separation and selective preconcentration even if both ampholytes have similar acid-base properties. To demonstrate this behavior, we have selected APAA (pI = 4.24) and APBA (pI = 4.73) as two model ampholytic analytes of similar physicochemical properties. Fig. S2 in Supplementary data shows the calculated curves of their effective mobilities as a function of pH. Using PeakMaster 5.4 calculations, we tuned the separation system so that APBA migration remains unaffected because pH disturbance of the system peak is insufficient for APBA stacking, whereas APAA is concentrated by the cationic system

zone and is separated from the APBA. The BGE was simple and consisted of formic acid/LiOH 40/20 mM, pH 3.70. The calculated effective electrophoretic mobility of APAA and APBA in this BGE is $7.88 \times 10^{-9}\,\mathrm{m^2\,s^{-1}\,V^{-1}}$ and $19.05 \times 10^{-9}\,\mathrm{m^2\,s^{-1}\,V^{-1}}$, respectively. The injection of a sample composed of formic acid/LiOH/APAA/APBA 35/27/0.01/0.01 mM only slightly (in comparison with aniline and *p*-cresol) but sufficiently increases the original pH, thereby switching APAA mobility to a negative value and reducing APBA mobility, which nevertheless remains positive (see Fig. 3 for t = 0 s). As a result, both ampholytes are separated, and APAA focusing within the cationic system peak formation is shown in Fig. 3 at t = 100 s. The last panel of Fig. 3, t = 300 s, shows the concentrated peak of APAA and the dispersed peak of APBA. Overall, our simulations proved the applicability of this strategy for the selective preconcentration of ampholytes. Simulated and experimental results of a slightly different formic acid/LiOH preconcentration system designed for focusing the second ampholyte, APBA, are shown in Supplementary data, in Figs. S3 and S4, respectively.

3.2. Preconcentration of weak analytes and ampholytes by a stationary system zone

As demonstrated in the flowchart, focusing via a mobile system zone is suitable only for compounds with specific properties. For analytes that fail to meet the requirements of stacking on a mobile system zone, stacking on stationary system zones at the injection site of the capillary can be employed. The pH of BGE is selected to keep the analyte uncharged or to limit the electrophoretic mobility to very low values. In turn, pH disturbance at the stationary system zone should accelerate the analyte as much as possible. In such a separation system, the analyte is swept from the wide injected zone (coinciding with the stationary system zone) to its boundary with the BGE and thus stacking occurs. The theoretical preconcentration performance is given by the ratio of velocities of the analyte in the stationary system zone and in the BGE. When stacking is finished, the analyte leaves the injection site and slowly migrates toward the detector or stagnates at the system zone/BGE boundary if the mobility of the analyte in BGE is slow or zero, respectively. No further continuous sharpening occurs, in contrast to preconcentration on a migrating system zone, and thus the preconcentration efficiency is decreased by diffusion or other dispersion phenomena. Another important process that affects the theoretical preconcentration factor is stacking/destacking [47,48] at the BGE/system zone boundary caused by step changes in electric field intensity (*E*). Therefore, not only the pH of the system zone but also its conductivity must be considered when designing a sample matrix solution.

Preconcentration on a stationary system zone is applicable for any weak electrolyte analytes, albeit most beneficially for analytes with a pK$_A$ around neutral pH at which the aforementioned strategies fail given the lack of a binary uni-univalent BGE with a sufficiently mobile system zone. We chose *p*-nitrophenol, a weak acid with pK$_A$ 7.15, as a representative example of this group of analytes. The 50/20 mM MES/LiOH buffer, pH 5.86, at which the effective electrophoretic mobility of *p*-nitrophenol is only $-1.60 \times 10^{-9}\,\mathrm{m^2\,s^{-1}\,V^{-1}}$, was selected as a suitable BGE. The first and second system zone mobilities of BGE are $0.00 \times 10^{-9}\,\mathrm{m^2\,s^{-1}\,V^{-1}}$ and $0.05 \times 10^{-9}\,\mathrm{m^2\,s^{-1}\,V^{-1}}$, respectively. Thus, both system zones overlap and can be considered one stationary zone, which does not migrate from the original injection position. To obtain the highest possible preconcentration factor, the pH disturbance at the injection zone should provide the fastest possible effective mobility of *p*-nitrophenol. Simultaneously, it is equally important to choose a sample composition at which the *E* of the injection zone is higher than (or at least equal to) *E* of the BGE, which leads to synergistically working stacking effects.

We simulated a preconcentration of 0.01 mM *p*-nitrophenol injected at two sample solutions to assess the effect of various *E* step changes at the injection zone/BGE boundary. At first, the MES/LiOH 5/5 mM solution was used as a sample matrix. The initial pH at the injection site was 8.6, which provided a *p*-nitrophenol effective mobility of $-29.9 \times 10^{-9}\,\mathrm{m^2\,s^{-1}\,V^{-1}}$. Although the electric field intensity in the BGE-filled part of the capillary (E_{BGE}) was $3.3\,\mathrm{kV\,mm^{1}}$, the electric field intensity within the injection site was nearly 4 times higher; $E_{inj} = 12.3\,\mathrm{kV\,m^{-1}}$. Thus, the migration velocity of *p*-nitrophenol within the stationary system zone was approximately 4 times faster, which further enhanced the preconcentration effect of changing the effective electrophoretic mobility. Fig. 4A depicts the pH, *E* and concentration profile of p-nitrophenol after 10 s of simulated preconcentration of an originally 4-mm-wide zone of 0.01 mM *p*-nitrophenol in 5/5 mM MES/LiOH. The maximal P_{sim} observed (P_{sim} when analyte leaves the injection site) was 13. Conversely, when using 50/50 mM MES/LiOH as the sample solution, the pH at the injection site was 9.2, similarly to the previous case (effective mobility of *p*-nitrophenol was $-26.6 \times 10^{-9}\,\mathrm{m^2\,s^{-1}\,V^{-1}}$). However, *E* is distributed differently from the previous case and changes from $E_{BGE} = 4.2\,\mathrm{kV\,m^{-1}}$ to $E_{inj} = 1.8\,\mathrm{kV\,m^{-1}}$ at the BGE/injection site boundary, and thus the preconcentration process is slower and its efficiency is reduced due to the destacking effect. In our simulation, *p*-nitrophenol passed the boundary within 100 s, and maximal P_{sim} is only 5, as shown at Fig. 4B. Although the stacking effect can play a key role when the analyte is concentrated by a stationary system zone, substantial pH disturbances induced by the system zone and respective changes in
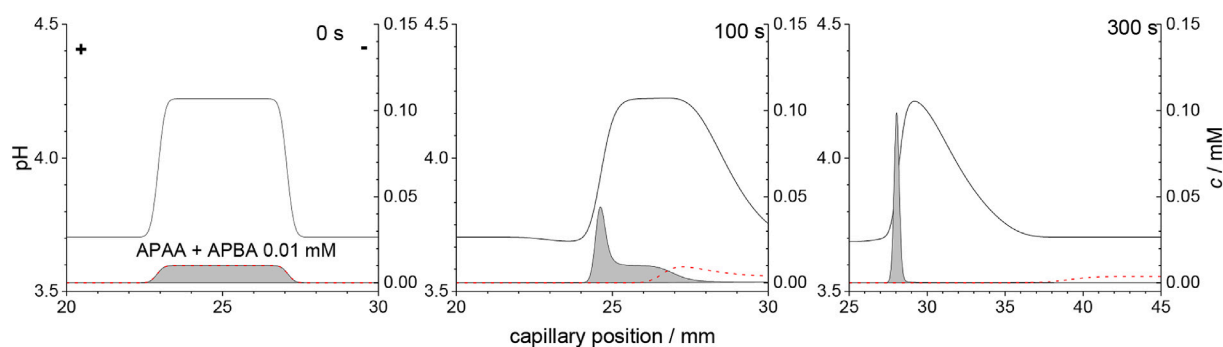

Fig. 3. Three consecutive time-labeled simulated pH profiles (black line; left axes), APAA concentration profile (filled by grey, right axes) and APBA concentration profile (red dash line, right axes) of the selective preconcentration of 0.01 mM APAA together with 0.01 mM APBA. BGE: 40/20 mM formic a./LiOH, sample solution: 35/27 mM formic a./LiOH. The polarity of the inserted voltage is depicted. (For interpretation of the references to colour in this figure legend, the reader is referred to the Web version of this article.)
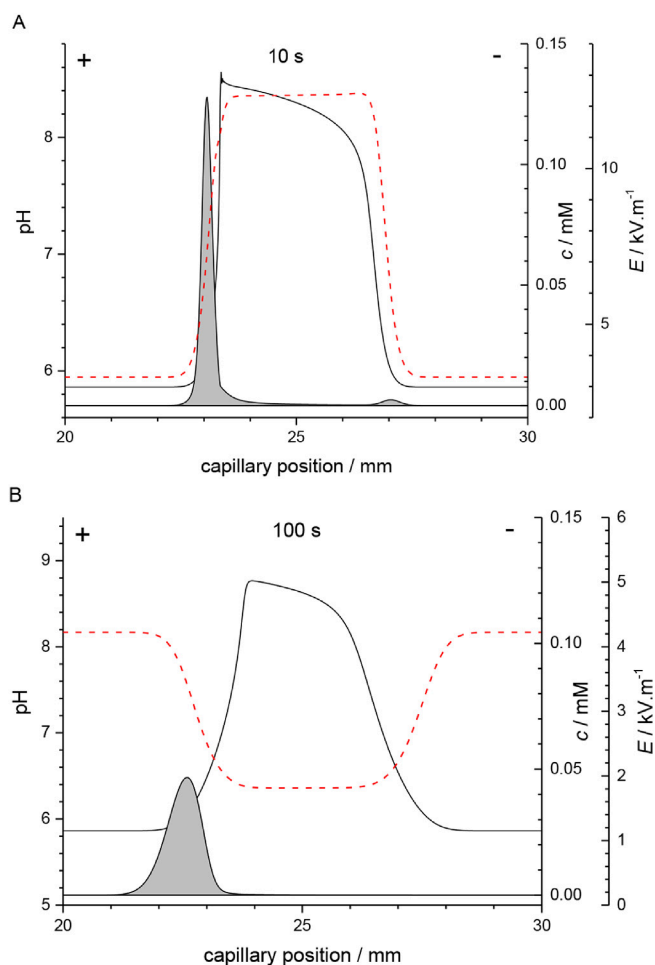
Fig. 4. Simulated result of the preconcentration of 0.01 mM *p*-nitrophenol (profile filled by grey, first right axis) by a pH barrier (black line, left axis) caused by the stationary system zone of 50/20 mM MES/LiOH BGE. *p*-nitrophenol is injected from A) 5/5 mM MES/LiOH solution; B) 50/50 mM MES/LiOH. Electric field intensity (*E*) profiles are depicted as red dashed lines. The polarity of the inserted voltage is depicted. (For interpretation of the references to colour in this figure legend, the reader is referred to the Web version of this article.)

effective mobility remain the main preconcentration mechanism.

3.3. Experimental verification

The experimental verification was performed for the following setups i) *p*-cresol preconcentration by a moving system zone of TEA/HCl 60/40 mM BGE (see part 3.1.1); ii) selective stacking of APAA and APBA through thoroughly tuned injection disturbance of a 40/20 mM formic acid/LiOH system (see 3.1.3); iii) preconcentration of *p*-nitrophenol by stationary system zones of 50/20 mM MES/LiOH BGE in two different sample matrices providing various distributions of electric field intensity along the capillary (see 3.2). Experimental parameters must be selected to focus the analyte into the detector in a reasonable time; not before focusing step is completed but before the pH barrier is dissipated or the focused peak is broadened by diffusion. The parameters used in the experimental verification are outlined in Table 1. To express the experimental preconcentration efficiency, we defined the experimental preconcentration factor, P_{exp}, as the ratio between the S/N of an analyte under stacking conditions and the S/N of an analyte injected from an undisturbed BGE. The P_{exp} values of all experiments performed are presented in Table 1.

Our simulations showed that the 60/40 mM TEA/HCl system is suitable for preconcentration of 0.01 mM *p*-cresol, and this system remains effective at a rather high 0.1 mM concentration of *p*-cresol in the sample. A wide, unfocused zone of 0.1 mM *p*-cresol is observed when *p*-cresol is injected from a sample matrix identical to BGE (Fig. 5). Changing the sample matrix composition to 60/60 mM TEA/HCl narrows the *p*-cresol peak, and the S/N ratio improves from 23 to 142; thus, P_{exp} is 6. In these experiments, an additional pressure of −50 mbar was applied to decrease the EOF velocity and to ensure sufficient time for full *p*-cresol stacking (see Experimental conditions in Table 1).

Furthermore, we experimentally tested the system and the sample composition designed for selective APAA preconcentration together with a very similar ampholyte, APBA, by a cationic system zone. Firstly, we evaluated the ability of the 40/20 mM formic acid/LiOH system to focus 0.01 mM APAA alone. Fig. 6A shows the comparison between electropherograms obtained without a preconcentration step, *i.e.*, APAA is injected from an undisturbed BGE, and APAA focused by the pH boundary of a system zone induced by the composition of the 35/27 mM formic acid/LiOH sample. The latter experiment provides an APAA peak with a S/N ratio of 500, which is 50 times higher than that of the unfocused zone of APAA. The panel inserted in Fig. 6A shows the record at a wavelength of 210 nm, wherein the cationic system zone is also visible. The APAA peak is focused behind this system peak, as simulated by Simul 5 Complex. Moreover, Fig. 6B proved that the designed sample composition selectively captures APAA. The simultaneously injected APBA migrates unaffectedly before the cationic system zone. Thus, the appropriate choice of sample composition enables a very effective separation of both analytes and an efficient preconcentration of the selected compound with close electromigration properties (see Fig. S2 in Supplementary data).

Preconcentration of *p*-nitrophenol by the combined stacking/destacking effect and the pH barrier created by the stationary system zone were experimentally examined. We used MES/LiOH 50/20 mM BGE and measured the same three experiments previously investigated by Simul 5 Complex simulations; 0.1 mM *p*-nitrophenol injection from i) undisturbed BGE, ii) MES/LiOH 50/50 mM where destacking effects decrease the preconcentration efficiency and iii) MES/LiOH 5/5 mM with a synergic stacking effect.
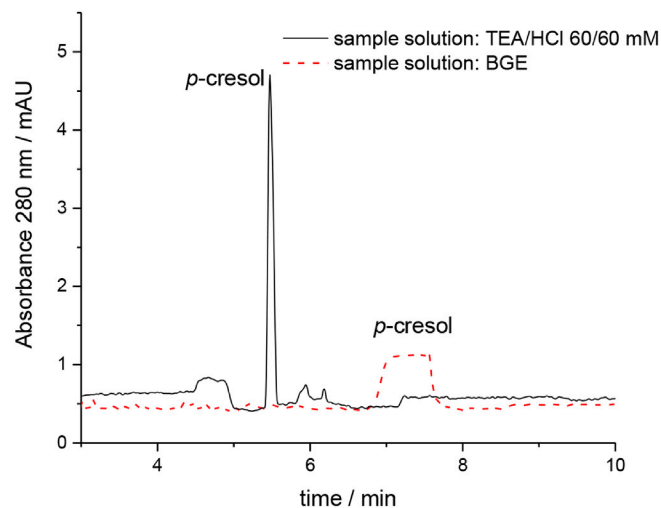

Fig. 5. Experimental electropherograms of the 0.1 mM *p*-cresol analysis in 60/40 mM TEA/HCl BGE with (black line, sample solution TEA/HCl 60/60 mM) and without (red dashed line, injection from undisturbed BGE) preconcentration; see Experimental section and Table 1 for detailed conditions. (For interpretation of the references to colour in this figure legend, the reader is referred to the Web version of this article.)
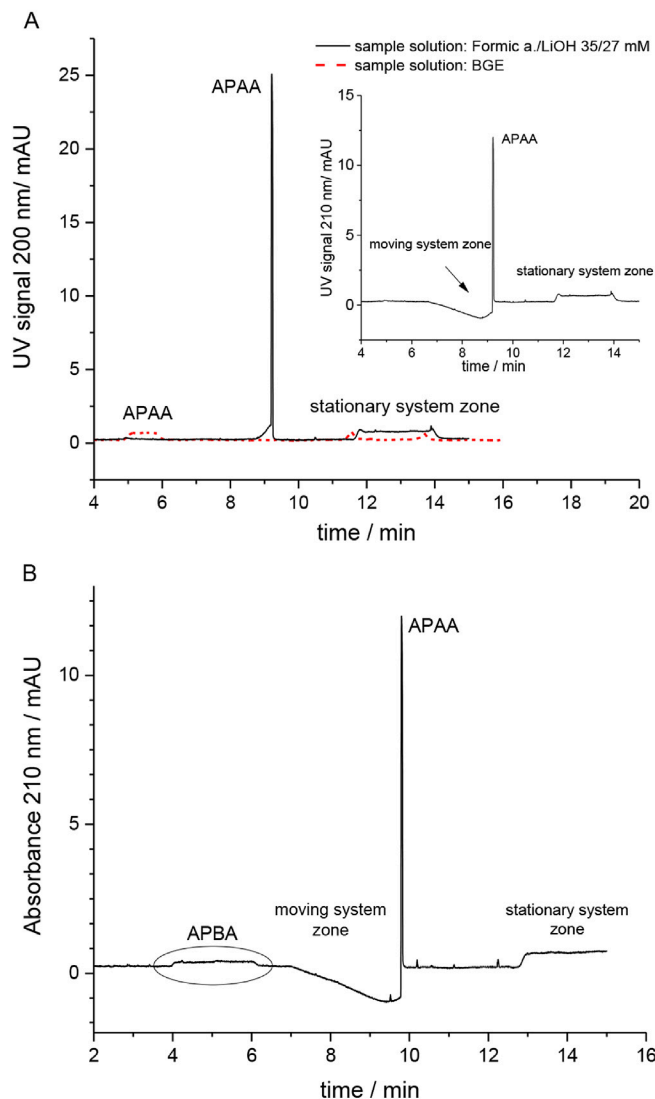
Fig. 7. Comparison between *p*-nitrophenol analysis in MES/LiOH 50/20 mM BGE and three different sample solutions: undisturbed BGE, 50/50 mM MES/LiOH and 5/5 mM MES/LiOH. Voltage +20 kV, presence of fast cationic EOF; see Experimental section and Table 1 for detailed conditions.

Fig. 6. A) Experimental electropherograms of the 0.01 mM APAA analysis in 40/20 mM formic a./LiOH BGE with (black line, 35/27 mM formic a./LiOH sample solution) and without (red dashed line, injection from undisturbed BGE) preconcentration at 200 nm and 210 nm (inserted graph), respectively; B) electropherogram of the selective preconcentration of APAA together with APBA at 210 nm, BGE: 40/20 mM formic a./LiOH; sample solution: 35/27 mM formic a./LiOH; see Experimental section and Table 1 for detailed conditions. (For interpretation of the references to colour in this figure legend, the reader is referred to the Web version of this article.)

Relevant electropherograms are shown at Fig. 7. As predicted, the best preconcentration performance was observed in the 5/5 mM MES/LiOH sample matrix where P_{exp} was approximately 8. The 50/50 mM MES/LiOH sample matrix provided only $P_{exp} = 3$. The distribution of electric field intensity along the capillary slows down the *p*-nitrophenol within the stationary zone and thus reduces the preconcentration efficiency. All experiments fully proved the simulated results.

4. Concluding remarks

The new approach of how to prepare a pH boundary for dynamic pH junction preconcentration was introduced in this study. pH discontinuities essential for weak electrolyte analyte stacking are created by moving or stationary system zones. The well-established mathematical description of the electromigration process and its
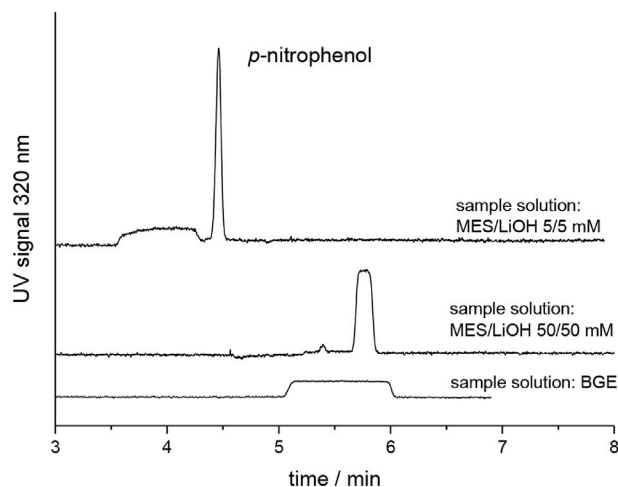
implementation in user-friendly software PeakMaster allows us to predict not only the mobilities of system zones but also the respective pH changes. Although the number and mobility of system peaks depends only on BGE itself, their amplitudes depend on sample matrix. Thus, the design of a preconcentration method for the analyte consists of properly selecting the composition of both BGE and sample matrix solutions. The flowchart guiding the method for uni-univalent BGEs and for weak electrolytes with specific acid-base properties was also presented in this study.

Moving or stationary system zones can be employed for analyte stacking. Both approaches were demonstrated on various weak analytes (even for two structurally similar ampholytes together), thus showing the wide applicability of this method. If possible, a moving pH boundary is recommended because, until the pH barrier is dissipated, the analyte co-migrates with the system zone and its peak is continuously sharpened. Numerical simulations in Simul 5 Complex made it possible to elucidate mechanistic details of the preconcentration methods presented. Dynamic pH junction techniques are suitable for many real samples of high salinity (or complexity) [20]. The new approaches based on system zone-induced pH boundaries can be used for such applications as well. The high content of a salt in the sample matrix usually only affects the pH discontinuities designed to a small extent [29]. Moreover, when the real sample matrix is known or can be estimated, the resulting effect on the designed pH boundaries can be predicted using the software PeakMaster.

Appendix A. Supplementary data

Supplementary data to this article can be found online at https://doi.org/10.1016/j.aca.2019.08.004.

Conflicts of interest

The authors declared no conflict of interest.

References

[1] M.C. Breadmore, Recent advances in enhancing the sensitivity of electrophoresis and electrochromatography in capillaries and microchips, Electrophoresis 28 (2007) 254—281.

[2] M.C. Breadmore, J.R.E. Thabano, M. Dawod, A.A. Kazarian, J.P. Quirino, R.M. Guijt, Recent advances in enhancing the sensitivity of electrophoresis and electrochromatography in capillaries and microchips (2006-2008), Electrophoresis 30 (2009) 230—248.

[3] M.C. Breadmore, M. Dawod, J.P. Quirino, Recent advances in enhancing the sensitivity of electrophoresis and electrochromatography in capillaries and microchips (2008-2010), Electrophoresis 32 (2011) 127—148.

[4] M.C. Breadmore, A.I. Shallan, H.R. Rabanes, D. Gstoettenmayr, A.S.A. Keyon, A. Gaspar, M. Dawod, J.P. Quirino, Recent advances in enhancing the sensitivity of electrophoresis and electrochromatography in capillaries and microchips (2010-2012), Electrophoresis 34 (2013) 29—54.

[5] M.C. Breadmore, R.M. Tubaon, A.I. Shallan, S.C. Phung, A.S.A. Keyon, D. Gstoettenmayr, P. Prapatpong, A.A. Alhusban, L. Ranjbar, H.H. See, M. Dawod, J.P. Quirino, Recent advances in enhancing the sensitivity of electrophoresis and electrochromatography in capillaries and microchips (2012-2014), Electrophoresis 36 (2015) 36—61.

[6] M.C. Breadmore, A. Wuethrich, F. Li, S.C. Phung, U. Kalsoom, J.M. Cabot, M. Tehranirokh, A.I. Shallan, A.S.A. Keyon, H.H. See, M. Dawod, J.P. Quirino, Recent advances in enhancing the sensitivity of electrophoresis and electrochromatography in capillaries and microchips (2014-2016), Electrophoresis 38 (2017) 33—59.

[7] M.C. Breadmore, W. Grochocki, U. Kalsoom, M.N. Alves, S.C. Phung, M.T. Rokh, J.M. Cabot, A. Ghiasvand, F. Li, A.I. Shallan, A.S.A. Keyon, A.A. Alhusban, H.H. See, A. Wuethrich, M. Dawod, J.P. Quirino, Recent advances in enhancing the sensitivity of electrophoresis and electrochromatography in capillaries and microchips (2016-2018), Electrophoresis 40 (2019) 17—39.

[8] E. Sanchez-Lopez, M.L. Marina, A.L. Crego, Improving the sensitivity in chiral capillary electrophoresis, Electrophoresis 37 (2016) 19—34.

[9] V. Kasicka, Recent developments in capillary and microchip electroseparations of peptides (2013-middle 2015), Electrophoresis 37 (2016) 162—188.

[10] S. Stepanova, V. Kasicka, Recent applications of capillary electromigration methods to separation and analysis of proteins, Anal. Chim. Acta 933 (2016) 23—42.

[11] G.J. Zhu, L.L. Sun, N.J. Dovichi, Dynamic pH junction preconcentration in capillary electrophoresis-electrospray ionization-mass spectrometry for proteomics analysis, Analyst 141 (2016) 5216—5220.

[12] T. Kawai, Recent studies on online sample preconcentration methods in capillary electrophoresis coupled with mass spectrometry, Chromatography 38 (2017) 1—8.

[13] Z. Glatz, On-capillary derivatisation as an approach to enhancing sensitivity in capillary electrophoresis, Electrophoresis 36 (2015) 744—763.

[14] R. Aebersold, H.D. Morrison, Analysis of dilute peptide samples by capillary zone electrophoresis, J. Chromatogr. 516 (1990) 79—88.

[15] P. Britz-Mckibbin, A.R. Kranack, A. Paprica, D.D.Y. Chen, Quantitative assay for epinephrine in dental anesthetic solutions by capillary electrophoresis, Analyst 123 (1998) 1461—1463.

[16] P. Britz-McKibbin, D.D.Y. Chen, Selective focusing of catecholamines and weakly acidic compounds by capillary electrophoresis using a dynamic pH junction, Anal. Chem. 72 (2000) 1242—1252.

[17] P. Britz-McKibbin, G.M. Bebault, D.D.Y. Chen, Velocity-difference induced focusing of nucleotides in capillary electrophoresis with a dynamic pH junction, Anal. Chem. 72 (2000) 1729—1735.

[18] A.S. Ptolemy, P. Britz-McKibbin, New advances in on-line sample preconcentration by capillary electrophoresis using dynamic pH junction, Analyst 133 (2008) 1643—1648.

[19] C.X. Cao, L.Y. Fan, W. Zhang, Review on the theory of moving reaction boundary, electromigration reaction methods and applications in isoelectric focusing and sample pre-concentration, Analyst 133 (2008) 1139—1157.

[20] A.A. Kazarian, E.F. Hilder, M.C. Breadmore, Online sample pre-concentration via dynamic pH junction in capillary and microchip electrophoresis, J. Sep. Sci. 34 (2011) 2800—2821.

[21] J.B. Kim, P. Britz-McKibbin, T. Hirokawa, S. Terabe, Mechanistic study on analyte focusing by dynamic pH junction in capillary electrophoresis using computer simulation, Anal. Chem. 75 (2003) 3986—3993.

[22] C. Schwer, B. Gas, F. Lottspeich, E. Kenndler, Computer-simulation and experimental evaluation of on-column sample preconcentration in capillary zone electrophoresis by discontinuous buffer systems, Anal. Chem. 65 (1993) 2108—2115.

[23] V. Hruska, M. Jaros, B. Gas, Simul 5 - free dynamic simulator of electrophoresis, Electrophoresis 27 (2006) 984—991.

[24] R. Lee, A.S. Ptolemy, L. Niewczas, P. Britz-McKibbin, Integrative metabolomics for characterizing unknown low-abundance metabolites by capillary electrophoresis-mass spectrometry with computer simulations, Anal. Chem. 79 (2007) 403—415.

[25] M. Bier, O.A. Palusinski, R.A. Mosher, D.A. Saville, Electrophoresis - Mathematical-modeling and computer-simulation, Science 219 (1983) 1281—1287.

[26] R.A. Mosher, D. Dewey, W. Thormann, D.A. Saville, M. Bier, Computer-Simulation and experimental validation of the electrophoretic behavior of proteins, Anal. Chem. 61 (1989) 362—366.

[27] A.A. Kazarian, E.F. Hilder, M.C. Breadmore, Utilisation of pH stacking in conjunction with a highly absorbing chromophore, 5-aminofluorescein, to improve the sensitivity of capillary electrophoresis for carbohydrate analysis, J. Chromatogr. A 1200 (2008) 84—91.

[28] C.X. Cao, W. Zhang, W.H. Qin, S. Li, W. Zhu, W. Liu, Quantitative predictions to conditions of zwitterionic stacking by transient moving chemical reaction boundary created with weak electrolyte buffers in capillary electrophoresis, Anal. Chem. 77 (2005) 955—963.

[29] W. Zhu, W. Zhang, L.Y. Fan, J. Shao, S. Li, J.L. Chen, C.X. Cao, Study on mechanism of stacking of zwitterion in highly saline biologic sample by transient moving reaction boundary created by formic buffer and conjugate base in capillary electrophoresis, Talanta 78 (2009) 1194—1200.

[30] M.C. Breadmore, R.A. Mosher, W. Thormann, High-resolution computer simulations of stacking of weak bases using a transient pH boundary in capillary electrophoresis. 1. Concept and impact of sample ionic strength, Anal. Chem. 78 (2006) 538—546.

[31] K. Imami, M.R.N. Monton, Y. Ishihama, S. Terabe, Simple on-line sample preconcentration technique for peptides based on dynamic pH junction in capillary electrophoresis-mass spectrometry, J. Chromatogr. A 1148 (2007) 250—255.

[32] B. Gas, E. Kenndler, System zones in capillary zone electrophoresis, Electrophoresis 25 (2004) 3901—3912.

[33] M. Stedry, M. Jaros, V. Hruska, B. Gas, Eigenmobilities in background electrolytes for capillary zone electrophoresis: III Linear theory of electromigration, Electrophoresis 25 (2004) 3071—3079.

[34] B. Gas, V. Hruska, M. Dittmann, F. Bek, K. Witt, Prediction and understanding system peaks in capillary zone electrophoresis, J. Sep. Sci. 30 (2007) 1435—1445.

[35] V. Hruska, M. Riesova, B. Gas, A nonlinear electrophoretic model for Peak-Master: I. Mathematical model, Electrophoresis 33 (2012) 923—930.

[36] B. Gas, M. Jaros, V. Hruska, I. Zuskova, M. Stedry, PeakMaster - a freeware simulator of capillary zone electrophoresis, LC-GC Eur. 18 (2005) 282—288.

[37] V. Hruska, M. Benes, J. Svobodova, I. Zuskova, B. Gas, Simulation of the effects of complex- formation equilibria in electrophoresis: I. Mathematical model, Electrophoresis 33 (2012) 938—947.

[38] J. Lokajova, V. Hruska, E. Tesarova, B. Gas, System peaks in micellar electrophoresis: 1. Utilization of system peaks for determination of critical micelle concentration, Electrophoresis 29 (2008) 1189—1195.

[39] M. Benes, M. Riesova, J. Svobodova, E. Tesarova, P. Dubsky, B. Gas, Complexation of buffer constituents with neutral complexation agents: Part II. Practical impact in capillary zone electrophoresis, Anal. Chem. 85 (2013) 8526—8534.

[40] https://web.natur.cuni.cz/gas/peakmaster.html.

[41] M. Stedry, M. Jaros, K. Vcelakova, B. Gas, Eigenmobilities in background electrolytes for capillary zone electrophoresis: II. Eigenpeaks in univalent weak electrolytes, Electrophoresis 24 (2003) 536—547.

[42] J.L. Beckers, P. Bocek, The preparation of background electrolytes capillary zone electrophoresis: golden rules and pitfalls, Electrophoresis 24 (2003) 518—535.

[43] V. Hruska, M. Stedry, K. Vcelakova, J. Lokajova, E. Tesarova, M. Jaros, B. Gas, Eigenmobilities in background electrolytes for CZE. V. Intensity (amplitudes) of system peaks, Electrophoresis 27 (2006) 4610—4617.

[44] M. Maly, M. Doyhunoya, M. Dvorak, G.S. Gerlero, P.A. Kler, V. Hruska, P. Dubsky, Generalized model of the linear theory of electromigration and its application to electrokinetic chromatography: theory and software Peak-Master 6-next generation, Electrophoresis 40 (2019) 683—692.

[45] https://echmet.natur.cuni.cz/software/download#peakmaster.

[46] H. Poppe, Overloading and interaction phenomena in electrophoretic separations, Anal. Chem. 64 (1992) 1908—1919.

[47] F.E.P. Mikkers, F.M. Everaerts, T. Verheggen, High-performance zone electrophoresis, J. Chromatogr. 169 (1979) 11—20.

[48] J.P. Quirino, S. Terabe, Sample stacking of cationic and anionic analytes in capillary electrophoresis, J. Chromatogr. A 902 (2000) 119—135.

III

Determination of thermodynamic acidity constants and limiting ionic mobilities of weak electrolytes by capillary electrophoresis using a new free software AnglerFish

M. Malý, M. Boublík, M. Pocrnić, M. Ansorge, K. Lorinčíková, J. Svobodová, V. Hruška, P. Dubský, B. Gaš

Michal Malý[1]
Milan Boublík[1]
Marijana Pocrnić[2]
Martin Ansorge[1] (ID)
Kateřina Lorinčíková[1]
Jana Svobodová[3]
Vlastimil Hruška[3]
Pavel Dubský[1]
Bohuslav Gaš[1] (ID)

[1]Faculty of Science, Department of Physical and Macromolecular Chemistry, Charles University in Prague, Prague, Czech Republic
[2]Department of Chemistry, Faculty of Science, University of Zagreb, Zagreb, Croatia
[3]Agilent Technologies Deutschland GmbH & Co. KG, Liquid Phase Separations Division, Waldbronn, Germany

Research Article

Determination of thermodynamic acidity constants and limiting ionic mobilities of weak electrolytes by capillary electrophoresis using a new free software AnglerFish

Thermodynamic acidity constants (acid or acid-base dissociation constants, sometimes called also as ionization constants) and limiting ionic mobilities (both of them at defined temperature, usually 25°C) are the fundamental physicochemical characteristics of a weak electrolyte, that is, weak acid or weak base or ampholyte. We introduce a novel method for determining the data of a weak electrolyte by the nonlinear regression of effective electrophoretic mobility versus buffer composition dependence when measured in a set of BGEs with various pH. To correct the experimental data for zero ionic strength we use the extended Debye-Hückel model and Onsager-Fuoss law with no simplifications. Contrary to contemporary approaches, the nonlinear regression is performed on limiting mobility data calculated by PeakMaster's correction engine, not on the raw experimental mobility data. Therefore, there is no requirement to perform all measurements at a constant ionic strength of the set of BGEs. We devised the computer program AnglerFish that performs the necessary calculations in a user-friendly fashion. All thermodynamic pKa values and limiting electrophoretic mobilities for arbitrarily charged substances having any number of ionic forms are calculated by one fit. The user input consists of the buffer composition of the set of BGEs and experimentally measured effective mobilities of the inspected weak electrolyte.

Keywords:

Capillary electrophoresis / Dissociation constant / Limiting mobility / Nonlinear regression / Software DOI 10.1002/elps.201900283

1 Introduction

An acidity dissociation constant and electrophoretic mobilities are the fundamental physicochemical constants that characterize an ionic constituent (by ionic constituent we understand a weak electrolyte, i.e., a weak acid or base). Both of the constants determine the effective mobility of the constituent in the electromigration movement and in this way have a direct impact on the quality of separation in electromigration separation methods–CZE and ITP. In fact, both constants depend on the ionic strength of the solution. The ionic strength I is the quantity assessing the contributions of Coulombic interaction of all ionic species in the solution, including H^+ and OH^- ions, and is defined as: $I = 1/2 \sum_{i=1}^{n} c_i z_i^2$, where c_i and z_i is the concentration and the charge number of the i-th ionic species, n is the number of all ionic species in solution. The mobility and acidity dissociation constant (pKa) converge to

some values when decreasing the ionic strength, that is, when decreasing the concentration of ionic species to zero. Such limiting values are called limiting ionic mobilities and thermodynamic pKa constants and characterize the particular constituent. They are defined for infinitely diluted solutions and therefore are unavailable to be measured directly.

Accurate and precise knowledge of limiting mobilities and thermodynamic constants is however essential in multiple fields of chemistry, not only in electromigration, and much scientific effort has been devoted to development of methods for their determination. Most of these methods do not utilize the set of the measurements of quantities with gradually decreasing ionic strength, but rather rely on a theoretical model of the dependence of the quantities on ionic strength.

The development of such models goes back to the history of physical chemistry. It was Debye and Hückel who proposed the theory of activity coefficients dependent on ionic strength [1, 2]. The theory has been used with various modifications to the present time. It explains how to obtain the activity

Correspondence: Michal Malý, Faculty of Science, Department of Physical and Macromolecular Chemistry, Charles University in Prague, Prague, Czech Republic
E-mail: michal.maly@natur.cuni.cz

Abbreviation: GMP, guanosine monophosphate

Color online: See article online to view Figs. 13 in color.

coefficient γ_i of the ion to calculate the activity $a_i = \gamma_i\,c_i$ of the i-th ionic species from the concentrations c_i at a finite ionic strength I. When the activities of the ionic species are known, the true thermodynamic dissociation constants of the ionic constituents (acid or bases) can be determined.

The dependence of the electrophoretic mobility on ionic strength is, however, more complicated. While the activity coefficient regards only the static influence of the ionic atmosphere, the electrophoretic mobility has to take into consideration also the dynamics of forming an ionic atmosphere, as the ionic constituents are in forced movement. The theory by Onsager and Fuoss [3] takes into account two phenomena connected with the electromigration of ionic constituents: the electrophoretic and relaxation effects. It even derives for electrolytes composed of more than two ionic species that the relaxation effect depends not only simply on ionic strength but also on the mobility ratios and on the ratios of concentrations in which the various ions are present. Onsager and Fuoss call this phenomenon the "mixture effect" and show that the mixture effect is greater the more the mobility ratios deviate from unity. The mixture effect plays an inevitable role in electrolytes in CE, where typically three ions are present in the peak: the separated ion, the co-ion and the counter ion of the BGE. The mixture effect is significant in highly acidic or alkaline electrolytes, as the mobilities of hydroxonium and hydroxide ions are extraordinarily high when compared to other ions.

Long before CE and isotachophoresis, the methods for the direct determination of mobilities and dissociation constants were introduced, a number of papers were published on the dependence of molar conductivity and transport numbers on ionic strength. This is reviewed in the classic book by Robinson and Stokes [4].

As mentioned above, the electromigration separation methods, ITP and CZE, can be used not only for the separation of analytes but also for the determination of the mobilities and pKa constants of various constituents. Here a substantial contribution was made by Hirokawa and coworkers [5–13], who published a great deal of reliable data obtained by ITP. The advantage of ITP is its separation ability, which enables us to determine the mobilities of several constituents at once, even without purification. Further advantage of ITP for such measurements is its accuracy, as it works in a hydrodynamically closed system, which eliminates bulk electroosmotic flow, a possible source of experimental errors. Due to a stacking effect the edges of the zones remain sharp. The approach by Hirokawa involved computer-assisted data fitting and then correcting both pKa and limiting mobilities for ionic strength. The Debye-Hückel law [1, 2] was used to calculate the true thermodynamic pKa constants, while the limiting mobilities were calculated using the Onsager equation [14].

One of the first approaches based on CZE measurements was proposed by Beckers et al. [15]. Beckers' method naturally uses the fact that effective electrophoretic mobility is the weighted average of the actual ionic mobilities of all dissociation states of a given compound where the weights are molar fractions of each dissociation state. Beckers showed that the pKa and limiting mobility of a monovalent acid or base can be calculated by measuring its effective mobility in two systems with different pH, provided that the pH and ionic strength of both systems is known. True pKa values are again calculated using the Debye-Hückel law and the limiting mobilities are calculated from ionic equivalent conductance.

Cai et al. from the group of El Rassi [16] were the first to combine effective mobility measurements by CZE with non-linear regression. In this case, the effective mobility of the analyte is measured in several buffers with different pH. The obtained set of pH versus effective mobility data points is then fitted with a model appropriate for the analyte. Ionic mobilities and pKa constants are parameters of the fit. A considerable advantage of this approach is the fact that the overall procedure remains the same regardless of the number of dissociation states of the analyte. The only thing that needs to be adjusted is the equation describing the theoretical dependence of the effective mobility on pH. Such an equation is, however, fairly simple to derive so long as the possible dissociation states of the studied substance are known. Other advantages include high robustness against experimental error, proper error estimation of the fitted parameters and the ease of automation. Even though ionic mobilities are also obtained from the fit, Cai proposed no means of how to calculate limiting mobilities from the experimental data. Cai's approach has been further extended for multivalent substances [17] and applied to wide variety of substances [18, 19].

For the purposes of true thermodynamic pKa determination it is convenient to define a sort of acidity constants as so-called mixed constant [20, 21]. The mixed acidity constant is defined as a function of activity of hydroxonium ions and concentrations of the two consecutive ionic forms of a given compound. This is advantageous because activity of hydroxonium ions can be measured directly by calibrated pH electrodes. As such, this mixed constant is already partially corrected for ionic effects.

Andrassi et al. [22] performed a comparative study of pKa determination using CZE and potentiometric titration. They concluded that CZE is advantageous due to its ability to both separate and characterize a substance, thus greatly reducing the effect of any impurities that might be present in a sample. Additionally, it can work with very small sample volumes and even allows for the characterization of multiple substances simultaneously.

While calculation of true pKa using the Debye-Hückel law is straightforward, there is no equally simple and universal formula for the calculation of limiting mobilities. Presently used methods for determination of limiting mobilities that utilize CZE use some form of the Pitts equation [23,24]. The Pitts equation, Ref. [25], is an extension of the Onsager-Fuoss [3] law and uses various additional parameters whose value must be determined beforehand. The means of how to get the values of these parameters vary from semi-empirical approaches to rather complicated experiments that require specialized equipment.

There were many attempts to use CZE to determine both pKa and ionic mobilities, see, for example, Refs. [26–28]. Šlampová et al. [27, 28] attempted to correct both pKas and ionic mobilities for ionic effects. Šlampová's approach was limited to singly charged weak electrolytes and required that all experimental data be measured at the same ionic strength. A Microsoft Excel spreadsheet has been provided for automatic data evaluation.

All the works on the determination of limiting ionic mobilities and thermodynamic pKa constants by electromigration methods have used the following approach: determination of the actual ionic mobilities and apparent pKa constants from the sets of experimental data and then correcting them for zero ionic strength using the Debye-Hückel theory and some modification of the Onsager equation for mobilities. Such an approach requires using a set of measurements at constant ionic strength, which is difficult or even impossible to reach at very low or very high pH, where either hydroxonium or hydroxide ions significantly contribute to the ionic strength. In fact, the approach is principally incorrect, as the experimentally available effective mobility is dependent both on the ionic mobility and pKa constant. Moreover, it is difficult to make a proper correction of mobilities when two pKa constants of a constituent are close together because in this case the pKa constants also influence each other and so do the limiting mobilities.

Our group introduced two software tools for the simulation and prediction of electromigration behavior and for method development–PeakMaster [29–32] and Simul [33]. Both tools use as the input data the set of limiting ionic mobilities and thermodynamic pKa constants, which is known as the Hirokawa database [6]. Both software tools also enable one to perform the correction of (i) activity coefficients influencing pKa using the Debye-Hückel theory [1, 2] and (ii) mobilities using the theory by Onsager and Fuoss [3]. This way they can simulate the real behavior of ions quite precisely.

In the present work, we propose adapting the ionic strength corrections used in PeakMaster for the inverse task: to determine the limiting mobilities and true thermodynamic pKa constants of a constituent from the set of experimental data of effective mobilities of the constituent obtained by electrophoresis using a set of background electrolytes with various pH. The procedure for obtaining the limiting mobilities and thermodynamic pKa constants will be a nonlinear regression of the set of experimental mobility data. Contrary to contemporary approaches, the nonlinear regression is performed on limiting mobility data calculated by the PeakMaster's correction engine, not on the raw experimental mobility data. This enables us to calculate by one fit both the true thermodynamic pKa values and limiting electrophoretic mobilities for arbitrarily charged substances with any number of ionic forms. There is no requirement to perform all measurements at the same ionic strength of the set of BGEs.

We have developed the freeware program AnglerFish for the user-friendly input of experimental data and the comfortable obtaining of results.

2 Theory

2.1 Corrections for ionic strength

As was shown by Debye and Hückel [1, 2] and Onsager and Fuoss [3], even low concentrations of ions in a solution lead to observable deviation of the expected ideal behavior of solutions. These deviations cause differences between the observed and expected dissociation constants and changes in conductivity, which in turn are a result of the reduced ionic mobilities of all ions. The Debye-Hückel and Onsager-Fuoss theories consider ions to be infinitely small uniformly charged particles.

In our software tools PeakMaster and Simul we apply the Davies' [34] modification of the extended Debye-Hückel formula for the ionic activity coefficient γ_z of an ion with the charge number z at a temperature of 25°C:

$$\log \gamma_z = -\frac{0.50925\, z^2\, \sqrt{I}}{1 + 1.5\, \sqrt{I}} + 0.1\, z^2 I, \tag{1}$$

where z is the charge number of the ion and I is the ionic strength expressed in mol/L.

For the correction of mobility for ionic strength, u_j, we use the equations derived by Onsager and Fuoss [3] taking into account effects stemming from nonequilibrium thermodynamics. We have rewritten the equations into contemporary notation and presently used units for better clarity:

$$u_j = u_j^\infty - \left(B_1 z_j u_j^\infty \sum_{n=0}^{5} C_n R_j^{(n)} + B_2 |z_j| \right) \frac{\sqrt{\Gamma}}{1 + Ba\sqrt{\frac{\Gamma}{2}}}$$

$$B_1 = \frac{e^3}{12\pi} \sqrt{\frac{N_A \nu}{(\varepsilon kT)^3}}, \quad B_2 = \frac{e^2}{6\pi \eta} \sqrt{\frac{N_{Av}}{\varepsilon kT}}, \quad \Gamma = \sum_{i=1}^{s} \Gamma_i,$$

$$\Gamma_i = c_i z_i^2, \tag{2}$$

where u_j^∞ and z_j are the limiting ionic mobility and charge number of the j-th ionic species, respectively, c_j is the concentration of the j-th ionic species, e is the elementary charge, N_{Av} is the Avogadro constant, ϵ and η is the permittivity and dynamic viscosity of the solution, respectively, k is the Boltzmann constant, T is the absolute temperature, and s is the overall number of all ionic species in the solution. For the $Ba/\sqrt{2}$ term, the value of 1.5 mol$^{-1/2}$dm$^{3/2}$ is employed.

C_n are the coefficients of the series

$$C_0 = \frac{1}{2}\left(2 - \sqrt{2}\right) \text{ and } C_n = -\frac{\sqrt{2}}{2}\binom{1/2}{n} \text{ for } n \geq 1 \tag{3}$$

Column vectors $R^{(n)}$ are defined by means of the recursion formulas

$$R_j^{(n)} = \sum_{\sigma=1}^{s} (2\mathbf{H} - \mathbf{I})_{j\sigma} R_\sigma^{(n-1)}$$

$$R_j^{(0)} = z_j - \frac{\sum_{i=1}^{s} z_i \mu_i}{\sum_{i=1}^{s} \left|\frac{z_i}{u_i^\infty}\right| \mu_i} \left|\frac{z_j}{u_j^\infty}\right|$$

$$\mu_i = \frac{\Gamma_i}{\Gamma} \tag{4}$$

H is the matrix with the elements h_{ji}

$$h_{ji} = \delta_{ji} \left(\sum_i \mu_i \frac{\omega_i}{\omega_i + \omega_j} \right) + \mu_i \frac{\omega_i}{\omega_i + \omega_j}, \omega_j = \frac{u_j^\infty}{|e_j|} \tag{5}$$

where δ_{ji} is the Kronecker delta, e_j is the charge of j-th ion, $e_j = e\, z_j$, where e is the elementary charge, and **I** is the unit matrix.

This way it is possible to calculate the so-called actual effective mobilities of an analyte when all parameters of the BGE and the analyte are known–their limiting ionic mobilities and the thermodynamic pKa constants of all constituents included.

But our task is inversed:

i. We have an analyte, the thermodynamic pKa constant(s) and mobility(ies) of which are to be determined.

ii. We have a background electrolyte with a known composition, where all limiting mobilities and thermodynamic constants pKa of all its constituents are known. This enables us to calculate using PeakMaster: (a) the pH based on the activity of the hydroxonium ions and (b) ionic strength of the background electrolyte.

iii. We prepare a set of such BGE s with various pH.

iv. We measure by CZE the effective mobilities of the analyte in the set of the background electrolytes above.

v. Using a nonlinear regression, we fit the set of the mobilities of the analyte by the Henderson-Hasselbalch equation, in the analogous way, as in Ref. [16]. The substantial difference is that we correct the measured mobilities of the analyte for ionic strength effects using the PeakMaster correction engine, Eqs. (1–5), inversely. The correction is hardcoded in the fitting function, so in our approach the Henderson-Hasselbalch equation fits directly the limiting ionic mobilities and thermodynamic constants of the compound. In the single fitting procedure, the fitted parameters are both the limiting ionic mobilities and thermodynamic pKa constants of the analyte. These parameters are the results.

2.2 AnglerFish computer program

One obvious drawback of treating the entire buffer as an independent variable by multi-purpose tools such as Origin, MATLAB, QtiPlot, Gnuplot, etc. that are commonly used in the electrophoretic community for the nonlinear fitting of experimental mobility, is that the fitting cannot simply use both the Henderson-Hasselbalch equation and correction procedure by Debye-Hückel and Onsager-Fuoss. Specifically, the Onsager-Fuoss correction is nontrivial and it requires knowledge of the exact buffer composition. A specialized computer program that accepts experimentally obtained effective mobilities and composition of buffers as input is needed.

To take full advantage of the approach suggested above we have devised the computer program AnglerFish. Input

data for the program consists of (i) the composition of a series of buffers, (ii) effective mobilities measured experimentally in each entered buffer and (iii) initial estimates of the pKa and limiting mobilities. The program then performs a nonlinear regression using the Levenberg-Marquardt algorithm [35, 36] to calculate the thermodynamic pKa constants and limiting ionic mobilities. Since the program knows the exact composition of every buffer, the proper correction for ionic effects using the Debye-Hückel law for pKa and the Onsager-Fuoss law for limiting mobilities is applied at every step of the regression. This enables the calculation of the true thermodynamic values of all pKa constants and eliminates the need to perform the entire series of measurements in buffers of the same ionic strength. The AnglerFish program is derived from the PeakMaster 6 [32] program and both programs provide a common user interface which allows for the user-friendly input and output of parameters and displaying a graph with the experimental and fitted values of mobilities.

The expected procedure of use is to design a series of buffers by means of PeakMaster, run the experiments, import the composition of buffers and measured actual effective mobilities into AnglerFish, and fit the results. The program and a user guide can be downloaded from the ECHMET group website [37], the source code is available on GitHub [38].

3 Materials and methods

3.1 Chemicals

All used chemicals were of analytical grade purity. Lithium hydroxide monohydrate, β-alanine, CHES, MOPS, MES, glycine, acetic acid, formic acid, phosphoric acid, histidine, guanosine monophosphate (GMP), all of them from Sigma Aldrich. Water for preparation of all solutions was deionized by Watrex Ultrapur system (Prague, Czech Republic). All running buffers were filtrated using Minisart syringe filters (Sartorius Stedim Biotech, Goettingen, Germany), pore size 0.45 mm.

All experiments were performed using Agilent 7100 CE equipment operated under ChemStation software (Agilent Technologies, Waldbronn, Germany). Detection was performed with the built-in DAD. Fused silica capillary (50 μm i.d. 375 μm o.d.) was provided by Polymicro Technologies (Phoenix, AZ). The experiments were performed in bare capillaries with a total lengths and effective lengths to the DAD detector around 50 and 41.5 cm, respectively. The new capillary was flushed first with 1 M sodium hydroxide and then with de-ionized water for 10 min and 10 min with actual BGE.

A sets of 33 buffers with calculated properties by PeakMaster was prepared. Buffers covered pH range of 1.5–12 in ionic strengths of 10 mM. pH coverage for all the buffers is summarized in Table 1. All BGEs as well as sample matrix were prepared by mixing appropriate amounts of buffer component stock solutions and deionized water. Injected samples composed of 0.1–0.5 mM of GMP and DMSO were dissolved in the measured BGE. DMSO was used to track the velocity

Buffer composition	pH range
Phosphoric acid	1.5–2.3
Phosphoric acid/LiOH	2–3.1
Formic acid/LiOH	2.9–4.1
Acetic acid/LiOH	3.8–5
MES/LiOH	5.3–6.2
MOPS/LiOH	6.2–7.4
Tricine/LiOH	7.3–8.6
Glycine/LiOH	8.9–10.4
CHES/LiOH	8.5–9.3
β-Alanine/LiOH	9.7–11.7
LiOH	11.6–12.6

of electroosmotic flow. Hydrodynamic injection of 10 mbar × 15 s was applied. Additional pressure was used if there was a need to modulate the velocity of EOF. Applied voltage was 15 kV keeping flowing current below 15 µA. Measurements were performed in triplicates and evaluated by CEval 0.6h6 [39] computer program.

3.2 Data fit algorithm

The software performs a nonlinear fit to calculate the thermodynamic pKa and limiting mobilities. The algorithm performs sanity checks of the fitted parameters to ensure that they are physically sensible. The first check is to make sure that pKa(n) > ⋯ > pKa(p), where pK(n) is pK of the form with the lowest charge and pK(p) the pK of the form with the highest charge.

The second check concerns limiting mobilities and can be described as follows: $0.55\,u_{base} + u_{z-1} < u_z < 1.2\,u_{base} + u_{z-1}$ for basic and as $0.55\,u_{base} + u_{z+1} < u_z < 1.2\,u_{base} + u_{z+1}$ for acidic ionic forms, where u_{base} is either u_{-1} or u_{+1} depending on whether the acidic or basic forms are evaluated. This reflects the generally valid rule that each additional charge increases the overall mobility of a substance by approximately the same amount. AnglerFish provides the option of disabling the limiting mobilities sanity check. The sanity check of pKas cannot be disabled. Initial estimates for fits, both in Origin and AnglerFish, were estimated from experimental curves.

4 Results and discussion

It is not the purpose of this paper to present thermodynamic pKa constants and limiting mobilities of a number of various compounds. Instead, we will demonstrate the abilities of AnglerFish by calculating the data for one multivalent ionic constituent–GMP, which is a trivalent weak anionic compound. The set of buffers summarized in Table 1 was prepared to have the same ionic strength close to 10 mM. Buffers of the same ionic strength were prepared to allow

for the fair comparison between the "classic" procedure and AnglerFish.

Our intention here is to compare the classic procedure for the determination of thermodynamic pKa constants and limiting mobilities of an ionic compound by electrophoresis with the new one based on the new approach.

(i) The classic procedure we used was based on this approach: we measured the set of effective mobility data of the compound for various pH of the BGEs and fitted these raw experimental mobility data by the Henderson-Hasselbalch equation with the Origin software. This way obtained apparent mixed pKa constants we corrected for zero ionic strength using the Debye-Hückel equation, Eq. (1). To make the comparison with AnglerFish fair, we corrected the actual mobilities for zero ionic strength by "manual iteration" by means of the PeakMaster software. This "manual iteration" procedure is explained further below.

(ii) The procedure by AnglerFish is based simply on the input of the compositions of the set of BGEs and corresponding measured effective mobilities.
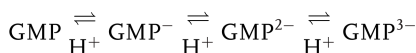
4.1 Classic procedure

The set of 99 couples of the measured pH of 33 BGEs (every measurement was repeated three times) and the corresponding measured effective mobilities of GMP were entered into the Origin environment into the so-called Book. The data were analyzed and depicted by one of Origin's tools, the Nonlinear Curve Fit, using the Henderson-Hasselbalch function, which was manually inserted. The Levenberg-Marquardt algorithm was used for the nonlinear fit. The output in the form of a Graph is shown in Fig. 1.

All effective mobilities dependent on pH are depicted by crosses. The figure also displays the fitting Henderson-Hasselbalch curve in red and the fitted parameters calculated by Origin in the inlay: the actual ionic mobilities and apparent mixed pKa constants. These values are to be corrected for ionic strength.

4.1.1 Correction of pKa constants

The dissociation steps of GMP are as follows:

$$\text{GMP} \underset{\text{H}^+}{\rightleftharpoons} \text{GMP}^- \underset{\text{H}^+}{\rightleftharpoons} \text{GMP}^{2-} \underset{\text{H}^+}{\rightleftharpoons} \text{GMP}^{3-}$$

and corresponding dissociation equations for mixed dissociation constants K_z^{mix} are:

$$K_1^{mix} = \frac{c\left(\text{GMP}^-\right) \cdot a\left(\text{H}^+\right)}{c\left(\text{GMP}\right)}$$

$$K_2^{mix} = \frac{c\left(\text{GMP}^{2-}\right) \cdot a\left(\text{H}^+\right)}{c\left(\text{GMP}^-\right)} \tag{6}$$

$$K_3^{mix} = \frac{c\left(\text{GMP}^{3-}\right) \cdot a\left(\text{H}^+\right)}{c\left(\text{GMP}^{2-}\right)}$$

Model	Henderson-Hasselbalch function
Equation	(uA1*10^(x-pK1)+uA2*10^(x+x-pK1-pK2)+uA3*10^(x+x+x-pK1-pK2-pK3))/(1+10^(x-pK1)+10^(x+x-pK1-pK2)+10^(x+x+x-pK1-pK2-pK3))
Plot	B
uA1	-17.77207 ± 0.10947
uA2	-31.04987 ± 0.14503
uA3	-44.45983 ± 0.16793
pK1	2.65818 ± 0.01631
pK2	6.70323 ± 0.02546
pK3	10.23941 ± 0.02862
Reduced Chi-Sqr	0.22073
R-Square(COD)	0.9984
Adj. R-Square	0.99832
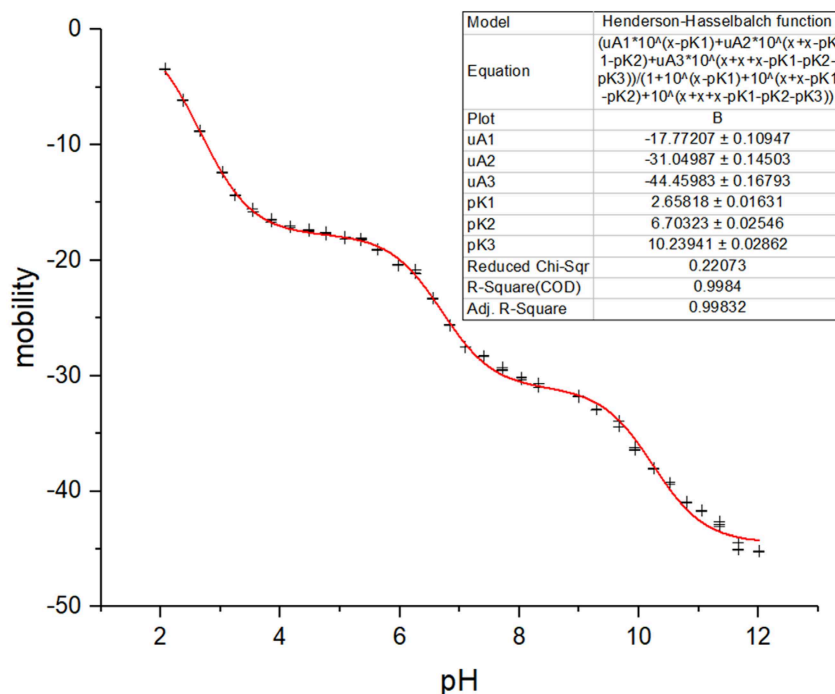
Figure 1. Origin's output of nonlinear regression analysis of effective mobility dependence on pH of the BGE for GMP. Crosses: experimental data. Curve: fitting function. The Henderson-Hasselbalch fitting function and fitted parameters are depicted in the inlay.

According to equation Eq. (1), the activity coefficients for mono-, di- and three-valent ions for the electrolytes with ionic strengths I of 0.01 mol/L are: $\gamma_1 = 0.9051$, $\gamma_2 = 0.6712$, $\gamma_3 = 0.4078$, respectively. The true thermodynamic dissociation constants are expressed exclusively by means of activities, $a_i = \gamma c_i$, instead of concentrations. The relation between the thermodynamic K_z and apparent K_z^{mix} mixed dissociation constants is therefore $K_1 = \gamma_1 K_1^{mix}$, $K_1 = \frac{\gamma_2}{\gamma_1} K_2^{mix}$, $K_3 = \frac{\gamma_3}{\gamma_2} K_3^{mix}$, so correspondingly for pKa constants

$$pK_1 = pK_1^{mix} - \log(\gamma_1)$$
$$pK_2 = pK_2^{mix} - \log(\gamma_2) + \log(\gamma_1) \quad\quad (7)$$
$$pK_3 = pK_3^{mix} - \log(\gamma_3) + \log(\gamma_2)$$

Using formulas in Eqs. (7) the corrected pKa values for GMP are: $pK_1 = 2.7015$, $pK_2 = 6.8331$, $pK_3 = 10.4558$.

4.1.2 Correction of mobilities

All data on mobilities in this paper is given in electrophoretic units, that is, 10^{-9} m^{2}V/s. The correction of mobilities for zero ionic strength was accomplished by manual iteration by means of the PeakMaster software. In PeakMaster we first input as the BGE a highly alkaline electrolyte composed of lithium hydroxide to assure that any anionic analyte will be fully dissociated. The concentration of lithium used was 10.130 mM to achieve an ionic strength of 10.000 mM. Then we build the GMP as the analyte by steps, starting from a hypothetical univalent form. We entered the value 2.7015 obtained in the above paragraph as the pKa(-1) and manually iteratively adjusted the limiting mobility u(-1) to obtain the effective mobility of the compound of −17.772, as fitted by

Origin, see Fig. 1. The resulting limiting mobility u(-1) was 20.538. These actions were repeated when adding the second and third valency with pKa 6.8331 and 10.4558, successively. The resulting corrected mobilities are u(-1) = 20.538, u(-2) = 37.178, u(-3) = 55.620.

4.2 Procedure by AnglerFish

The same set of 99 couples of the measured pH of 33 BGEs including their compositions and corresponding measured effective mobilities of GMP were placed into the window of the AnglerFish environment, see Fig. 2.

The software then requires initial estimates of mobilities of all ionic forms, here say 45, 27, and 17, and pKa constants, here say 10.4, 6.7, and 2.8. The calculation of limiting mobilities and thermodynamic constants is carried out by simply clicking the Fit button. The resulting graphical window is shown in Fig. 3, the fitted parameters in Fig. 4.

Notice that the blue squares in Fig. 3 are the fitted values of the actual effective mobilities. They do not have to necessarily form a smooth curve (when using BGEs with different ionic strengths) as it was in the classic procedure, where the fitting function was the Henderson-Hasselbalch function.

The comparison of the limiting values obtained by both approaches is shown in Table 2.

4.3 Discussion

It is obvious from Table 2 that all results obtained by AnglerFish have lower standard deviations. It is a natural consequence of the fact that the Henderson-Hasselbalch function is exact only for true thermodynamic dissociation
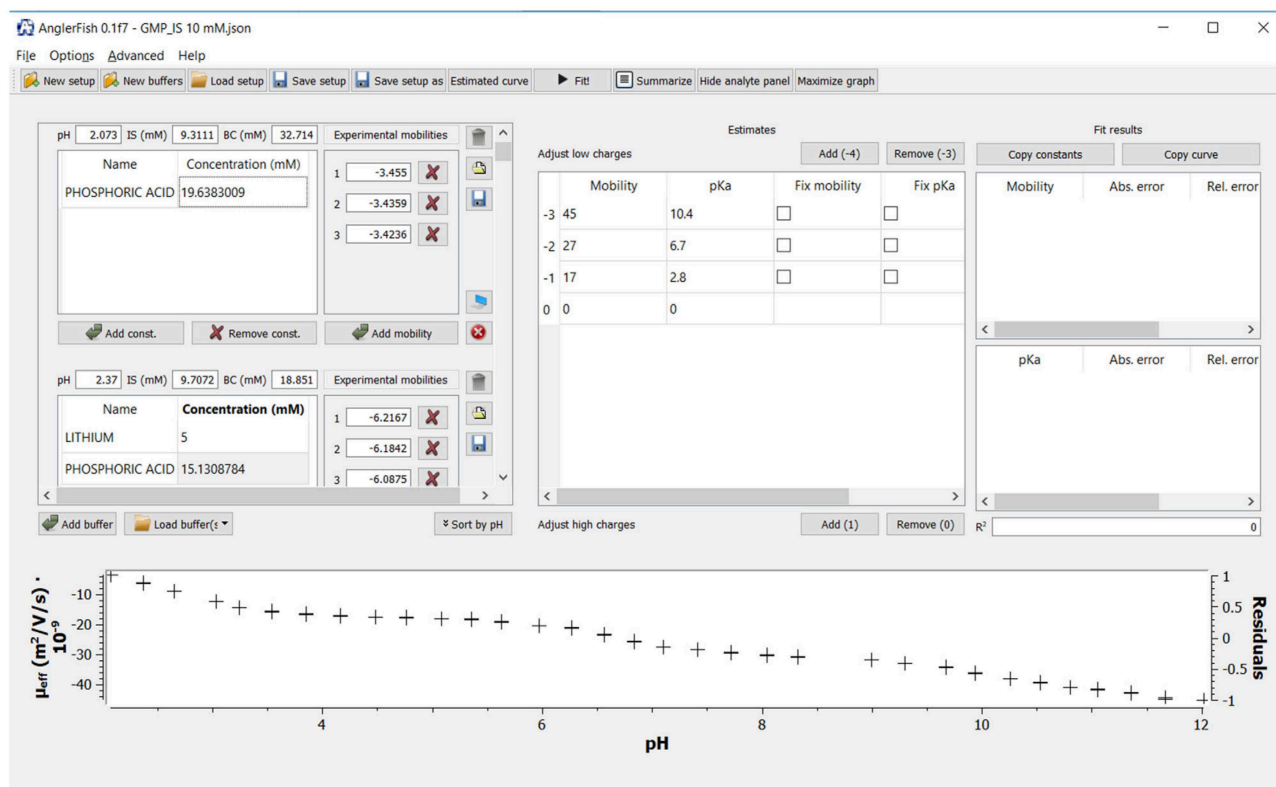

Figure 2. Input window of AnglerFish. Crosses: experimental data. Subwindows in the upper left corner: compositions of BGEs. Subwindow in the middle upper part: initial estimates.

Table 2. Limiting ionic mobilities and thermodynamic pKa constants. In the classic approach: first fitted by Origin, then manually corrected. In the AnglerFish approach: fitted directly

	Classic approach		AnglerFish	
	Mobility	S.D.	Mobility	S.D.
u_1	20.538	0.109	20.696	0.034
u_2	37.178	0.145	38.140	0.050
u_3	55.620	0.168	57.458	0.051
	pKa	S.D.	pKa	S.D.
pK_1	2.7015	0.0163	2.6986	0.0048
pK_2	6.8331	0.0255	6.7638	0.0080
pK_3	10.4558	0.0286	10.2056	0.0093
R^2		0.99832		0.99947

R^2: coefficient of determination.

constants and limiting ionic mobilities. Thus, it does not fit the experimental data correctly before its correction to the thermodynamic (limiting) values.

Moreover, as a matter of fact, any effective mobility obtained by measurement is dependent more or less on all parameters of the compound. Therefore, it is not entirely right to correct the values of the actual ionic mobilities and appar-

ent pKa constants for zero ionic strength independently, one by one, as is done in the classic procedure.

There is one more important aspect of using AnglerFish which employs the Onsager-Fuoss correction procedure described in Ref. [3]. As already mentioned, this procedure considers the mixture effect. In alkaline BGEs at pH around 12 or more, the anions are composed mostly of highly mobile hydroxide ions. The mixture effect of fast hydroxide ions speeds up the negative GMP^{3-} ions, so their mobility is extraordinarily higher. This is well recognized by AnglerFish and the fitted points lie close to experimental points at a high pH of around 12. On the other hand, in the classic approach by Origin the fitted curve deviates from the experimental points in this region; compare Figs. 1 and 3.

Another advantage of the proposed approach is that the buffers in the set need not necessarily have the same ionic strength as each of them is treated individually. This is especially useful for buffers with either highly acidic or highly alkaline pH, for example, it is principally impossible to prepare a buffer for pH less than two having the ionic strength equal to or less than 0.01 mol/L.

As mentioned above, the input data for AnglerFish regarding buffers is simply the compositions of these buffers. The software includes the same database of pKa constants and mobilities of many constituents, as Simul and PeakMaster have–the Hirokawa database. From the composition of the buffer can be then calculated its corresponding pH. However,
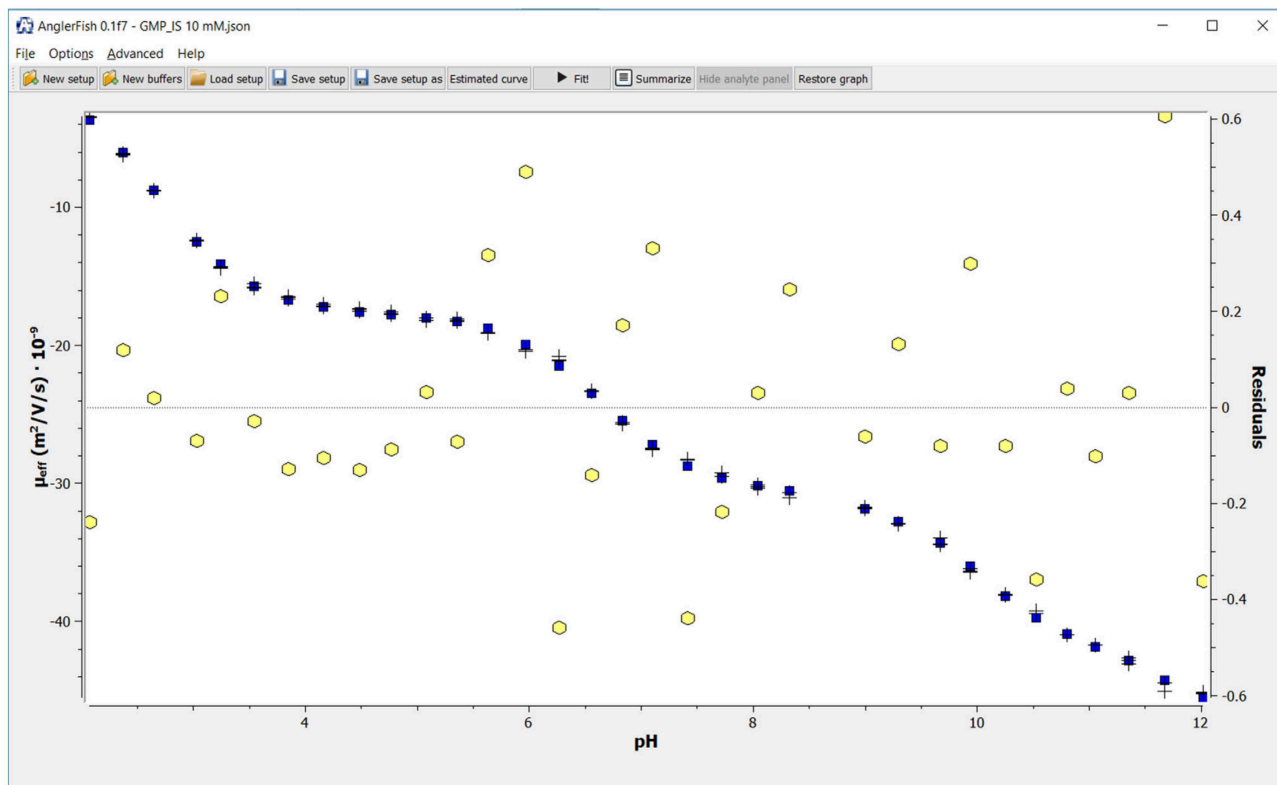
Figure 3. Output graphical window of AnglerFish. Crosses: experimental data. Full squares: fitted mobilities, values on left axis. Hexagons: residuals of the fit, values on right axis.

Figure 4. Output window of AnglerFish – fitted limiting mobilities and thermodynamic constants together with their standard deviations. R^2: coefficient of determination.

the calculated pH may differ from the pH measured. Moreover, often some chemicals used for the preparation of buffers cannot be weighed with maximum precision, especially liquid chemicals, such as phosphoric or acetic acid. Therefore,

we decided to adopt the following strategy: (i) the pH measured by a calibrated pH meter and (ii) the amount of one of the constituents of the buffer, the one which can be reliably weighed, are the basic entries of the buffer composition. The corresponding amount of the second constituents of the buffer is calculated by the software. This way we are able to reach the maximum correctness of the input data.

To the authors' best knowledge, when utilizing the Onsager-Fuoss correction, Eqs. (2–5), the ionic strength of all used buffers should not exceed 20 mM to achieve acceptable accuracy. As we came to recognize, for a higher ionic strength and charge numbers of measured compounds higher than two the correction can fail and yield deviated results.

5 Concluding remarks

We have introduced an improved method for the determination of thermodynamic acidity dissociation constants and limiting ionic mobilities by the nonlinear fit of effective mobility versus buffer composition dependence. The method uses the extended Debye-Hückel model and Onsager-Fuoss law with no simplifications and does not require maintaining constant ionic strength in all experiments. We devised a computer program that performs the necessary calculations in a fully automated fashion. The user input consists of the buffer composition and experimentally measured effective mobilities.

The authors have declared no conflict of interest.

6 References

[1] Debye, P., Hückel, E., *Physik. Z.* 1923, *24*, 185–206.

[2] Debye, P., Hückel, E., *Physik. Z.* 1923, *24*, 305–325.

[3] Onsager, L., Fuoss, R. M., *J. Phys. Chem.* 1932, *36*, 2689–2778.

[4] Robinson, R. A., Stokes, R. H., *Electrolyte Solutions*, Dover Publications, Mineola, New York, 2nd revised ed., 2002.

[5] Hirokawa, T., Kiso Y., *J. Chromatogr.* 1982, *248*, 341–362.

[6] Hirokawa, T., Nishimo, M., Aoki, N., Kiso, Y., Sawamoto, Y., Yagi, T., Akiyama, J., *J. Chromatogr.* 1983, *271*, D1–D106.

[7] Hirokawa, T, Kiso, Y., *J. Chromatogr.* 1982, *252*, 33–48.

[8] Hirokawa, T., Nishino, M., Kiso, Y., *J. Chromatogr.* 1982, *252*, 49–65.

[9] Hirokawa, T., Kobayashi, S., Kiso, Y. *J. Chromatogr.* 1985, *318*, 195–210.

[10] Hirokawa, T., Gojo, T., Kiso, Y., *J. Chromatogr.* 1986, *369*, 59–81.

[11] Hirokawa, T., Tsuyoshi, T., Kiso, Y., *J. Chromatogr.* 1978, *408*, 27–41.

[12] Hirokawa, T., Gojo, T., Kiso, Y., *J. Chromatogr.* 1987, *390*, 201–223.

[13] Hirokawa, T., Kiso, Y., Gaš, B., Zusková, I., Vacík, J., *J. Chromatogr.* 1993, *628*, 283–308.

[14] Onsager, L., *Phys. Z.* 1927, *28*, 277.

[15] Beckers, J. L., Everaerts, F. M., Ackermans, M. T., *J. Chromatogr.* 1991, *537*, 407–428.

[16] Cai, J., Smith, J. T., El Rassi, Z., *J. High Resol. Chromatogr.* 1992, *15*, 30–32.

[17] Poole, S. K., Patel, S., Dehring, K., Workman, H., Poole, C. F., *J. Chromatogr. A* 2004, *1037*, 445–454.

[18] Šolínová, V., Kašička, V., Koval, D., Česnek, M., Holý, A., *Electrophoresis* 2006, *27*, 1006–1019.

[19] Nowak, P., Wozniakiewicz, M., Koscielniak, P., *J. Chromatogr A* 2015, *1377*, 1–12.

[20] Koval D., Kašička, V., Jiráček, V., Collinsová, M., *Electrophoresis* 2003, *24*, 774–781.

[21] Včeláková, K., Zusková, I., Kenndler, E., Gaš, B., *Electrophoresis* 2004, *25*, 309–317.

[22] Andrasi, M., Buglyo, P., Zekany, L., Gaspar, A., *J. Pharm. Biomed. Analysis* 2007, *44*, 1040–1047.

[23] Aupiais, J., Delorme, A., Baglan, N., *J. Chromatogr. A* 2003, *994*, 199–206.

[24] Li, D., Fu, S., Lucy, C. A., *Anal. Chem.* 1999, *71*, 687–699.

[25] Pitts, D., *Proc. R. Soc. Lond. A* 1953, *217*, 43–70.

[26] Tůmová, T., Monincová, L., Čeřovský, V., Kašička, V., *Electrophoresis* 2016, *37*, 3186–3195.

[27] Šlampová, A., Boček, P., *Electrophoresis* 2008, *29*, 538–541.

[28] Šlampová, A., Křivánková, L., Gebauer, P., Boček, P., *J. Chromatogr. A* 2009, *1216*, 3637–3641.

[29] Jaroš, M., Včeláková, K., Zusková, I., Gaš, B., *Electrophoresis* 2002, *23*, 2667–2677.

[30] Jaroš, M., Hruška, V., Štědrý, M., Zusková, I., Gaš, B., *Electrophoresis* 2004, *25*, 3080–3085.

[31] Hruška, V., Riesová, M., Gaš, B., *Electrophoresis* 2012, *33*, 923–930.

[32] Malý, M., Dovhunová, M., Dvořák, M., Gerlero, G. S., Kler, P. A., Hruška V., Dubský, P., *Electrophoresis* 2019, *40*, 683–692.

[33] Hruška, V., Jaroš, M., Gaš, B., *Electrophoresis* 2006, *27*, 984–991.

[34] Davies, C. W., *Ion Association*, Butterworths, London, 1962.

[35] Levenberg, K., *Quart. Appl. Math.* 1944, *2*, 164–168.

[36] Marquardt, D. W., *J. Soc. Indust. Appl. Math.* 1963, *11*, 431–441.

[37] https://echmet.natur.cuni.cz/

[38] https://github.com/echmet/AnglerFish

[39] Dubský, P., Ördögová, M., Malý, M., Riesová, M., *J. Chromatogr. A* 2016, *1445*, 158–165.

IV

The effect of buffer concentration and cation type in the mobile phase on retention of amino acids and dipeptides in hydrophilic interaction liquid chromatography

K. Kalíková, M. Boublík, G. Kučerová, P. Kozlík

CrossMark

SHORT COMMUNICATION

The effect of buffer concentration and cation type in the mobile phase on retention of amino acids and dipeptides in hydrophilic interaction liquid chromatography

Květa Kalíková[1] · Milan Boublík[1] · Gabriela Kučerová[1] · Petr Kozlík[2,3]

Abstract The current work is focused on exploring the effect of buffer cation type and its concentration on retention of amino acids, dipeptides and their blocked analogues on two stationary phases, i.e., bare silica and amide-based in hydrophilic interaction liquid chromatography. Five different buffers of pH 4.0 composed of Tris/acetic acid, triethylamine/acetic acid, ammonium/acetic acid, Li^+/acetic acid and Ba^{2+}/acetic acid were used in various concentrations. Interestingly, an increase of the buffer concentration caused increasing, decreasing or stable retention of analytes, according to the cation type in the buffer. The buffers containing barium cations provided the highest retention of all the analytes in comparable mobile phases, i.e., buffers with the same ionic strength and pH on both columns. Moreover, using buffers with barium cation different selectivity for dipeptides was observed. The chromatographic systems with buffers consisting of triethylamine behaved differently compared to others.

✉ Květa Kalíková
  kalikova@natur.cuni.cz

[1] Department of Physical and Macromolecular Chemistry, Faculty of Science, Charles University, Hlavova 8, 128 43 Prague 2, Czech Republic

[2] Department of Analytical Chemistry, Faculty of Science, Charles University, Hlavova 8, 128 43 Prague 2, Czech Republic

[3] Department of Oncology, Lombardi Comprehensive Cancer Center, Georgetown University, 3970 Reservoir Road NW, Washington, DC 20007, USA

Hydrophilic interaction liquid chromatography (HILIC) has attracted increasing attention in the recent years due to its application for the separation of polar compounds that are poorly or not retained using reversed phase (RP) chromatography (Zhang et al. 2017; Tircová and Kozlík 2017; Noga et al. 2013; Kozlík et al. 2013; Špačková and Pazourek 2013). Different predominant retention mechanism in HILIC can be observed if different analytes and/or stationary and mobile phases are applied. It is a combination of solute partition between a water layer held on the surface of the stationary phase (SP) and the bulk mobile phase (MP), and by adsorption onto polar groups that may be partially deactivated by the presence of the water layer (Hemstrom and Irgum 2006). Investigation of HILIC separation mechanism is still under the interest of several research groups (Kozlík et al. 2012; Schuster and Lindner 2013; Kalíková et al. 2013; Česla et al. 2016; West and Auroux 2016; Jandera and Janás 2017; McCalley 2017).

Typical HILIC SPs consist of classical bare silica or silica gel modified with many polar functional groups, e.g., amide, diol, cyano, and sulfoalkylbetaine groups, or polar molecules, e.g., cyclodextrins, cyclofructans (Jandera 2016; Qiao et al. 2016). MPs for HILIC consist of water-miscible polar organic solvents such as acetonitrile and a small amount of some aqueous solution, i.e., pure water or aqueous buffers. The primary effect of the pH of the MP is on the charged state of both the SP and polar solutes. Charged solutes are more hydrophilic than their neutral forms and thus more strongly retained in HILIC. Electrostatic interactions with positive charged analytes, such as amino compounds, are dramatically increased on silica

phases with increasing pH of the MP (McCalley and Neue 2008). Buffers are added to the MP to control electrostatic interactions between charged analytes and SP. Buffer concentration modifies the thickness of the water layer (Soukup and Jandera 2014). It was described that increasing the salt concentration led to an increase of the water layer resulting in stronger retention (Guo 2015). In addition to buffer concentration, the type of buffer also influences the retention. The effect of ammonium buffers, i.e., ammonium formate and ammonium acetate on the retention of polar compounds has been investigated by Guo and Gaiki (2005). However, only a few papers focus on exploring the effect of the buffer cation and its concentration on retention (Douša et al. 2014; McCalley 2010). Douša et al. (2014) investigated the retention behavior of amino acids (AAs) on various SPs in two buffers differing in cation type and concentration. They found that analyte retention increases with increasing potassium formate/citrate buffer concentration. On the other hand, triethylammonium buffer concentration had no influence on the AA retention.

A major purpose of this study was to investigate the effect of buffer concentration and the type of cation in the MP on the retention of selected polar compounds and gain some insights into the chromatographic process of HILIC. The buffers composed of five different cations, i.e., lithium, ammonium, barium, tris(hydroxymethyl)aminomethane (Tris), triethylamine (TEA), and acetic acid in various concentrations were tested. Retention of AAs, *tert*-butyloxycarbonyl (*t*-BOC)-AAs, dipeptides and benzyloxycarbonyl (*Z*)-dipeptides on the two SPs including amide and silica was investigated in detail.

All chromatographic measurements were performed on Waters Alliance system (Waters Chromatography, Milford, MA, USA) consisting of 2695 Separation Module, 2996 Photodiode Array Detector, 717 plus autosampler, and Alliance Series column heater. Empower software was used for data acquisition and analyses. Two chromatographic columns used were: TSK gel Amide-80 from Tosoh (Tokyo, Japan) and Kromasil 60-5SIL from Eka Chemicals AB (Bohus, Sweden). Both columns sized 250 × 4.6 mm i.d., particle size 5 μm. Acetonitrile (ACN, gradient grade), ammonium acetate (purity ≥99%), acetic acid (HAc, purity >99.8%), triethylamine (minimum 99%), barium acetate (purity ≥99%), lithium hydroxide monohydrate and Trizma® base (purity ≥99.9%) were supplied by Sigma-Aldrich (St. Louis, MO, USA). Standards of *t*-BOC-L-Phe, *t*-BOC-L-Trp, *t*-BOC-L-Tyr, L-Phe, L-Trp, L-Tyr and Tyr-Phe were obtained from Sigma-Aldrich (St. Louis, MO, USA). Standards of H-Tyr-Phe, H-Phe-Tyr, Z-Trp-Phe, Z-Phe-Trp, H-Phe-Trp and H-Trp-Phe were purchased from BACHEM AG (Bubendorf, Switzerland). Deionized water was purified with a Rowapur and Ultrapur

Fig. 1 Dependence of logarithm of retention factors of AAs on the ▶ logarithm of concentration and buffer types on the two columns: **A** amide column, **B** silica column; MP ACN/buffer 90/10 (v/v). *Tyr* tyrosine, *Boc-Tyr tert*-butyloxycarbonyl tyrosine, *Trp* tryptophan, *Boc-Trp tert*-butyloxycarbonyl tryptophan, *Phe* phenylalanine, *Boc-Phe tert*-butyloxycarbonyl phenylalanine

system from Watrex (Prague, Czech Republic). Stock solutions of the individual compounds at a concentration of 1 mg mL^{-1} were prepared by dissolving the compounds in ACN or in a mixture of ACN/water depending on the solubility.

All measurements were performed in triplicates. Toluene was used as a dead time marker. The buffers used were composed of LiOH/HAc, NH$_4^+$/HAc, Tris/HAc or TEA/HAc. The concentrations of buffers were: cation/HAc 5/32 mM (ionic strength $I = 5.11$, pH 4.00), 10/62 mM ($I = 10.11$, pH 4.00), 20/120 mM ($I = 20.11$, pH 4.00), 25/148 mM ($I = 25.12$, pH 4.00) and 50/285 mM ($I = 50.12$, pH 4.01). The buffers containing barium were composed of Ba^{2+}/HAc in the following concentrations: 1.7/21.3 mM ($I = 5.12$, pH 4.01), 3.3/41.5 mM ($I = 10.10$, pH 4.00), 6.7/80.6 mM ($I = 20.12$, pH 4.00) and 8.3/98 mM ($I = 25.10$, pH 4.01). The concentrations of barium cations in buffers differed from the other cation concentrations as we wanted to use buffers with the same ionic strength and pH values for comparison. Program PeakMaster (for more information see http://echmet.natur. cuni.cz/peakmaster) was used for calculation of buffer constituents' concentrations, ionic strengths and pH values. Marvin software (product of ChemAxon company) was used for calculation of log D values of analytes at pH 4. The measurements were performed under the following experimental conditions: the MPs used were ACN/buffer 80/20 (v/v) and 90/10 (v/v), flow rate 1 mL min^{-1}, column temperature 25 °C, injection volume 10 μL and UV detection at 280 nm.

The influence of buffer concentration and cation type in MPs on the retention of small polar compounds was tested on the two columns under HILIC conditions. Amide-based and bare silica SPs were used. Analytes, i.e., AAs, dipeptides and their *N*-blocked analogues, well visible in UV, were chosen as representatives of biological important compounds. These analytes show some similarities in the structure, but differences in polarity and size. Two volume ratios of ACN and buffer were used as MPs, i.e., 80/20 and 90/10.

The retention behavior of three native (tyrosine, tryptophan, phenylalanine) and three *N*-blocked (*t*-BOC-Phe, *t*-BOC-Trp, *t*-BOC-Tyr) AAs in different buffers was studied. As can be expected *N*-blocked AAs showed significantly lower retention than native AAs due to lower polarity in all the separation systems tested—see Fig. 1
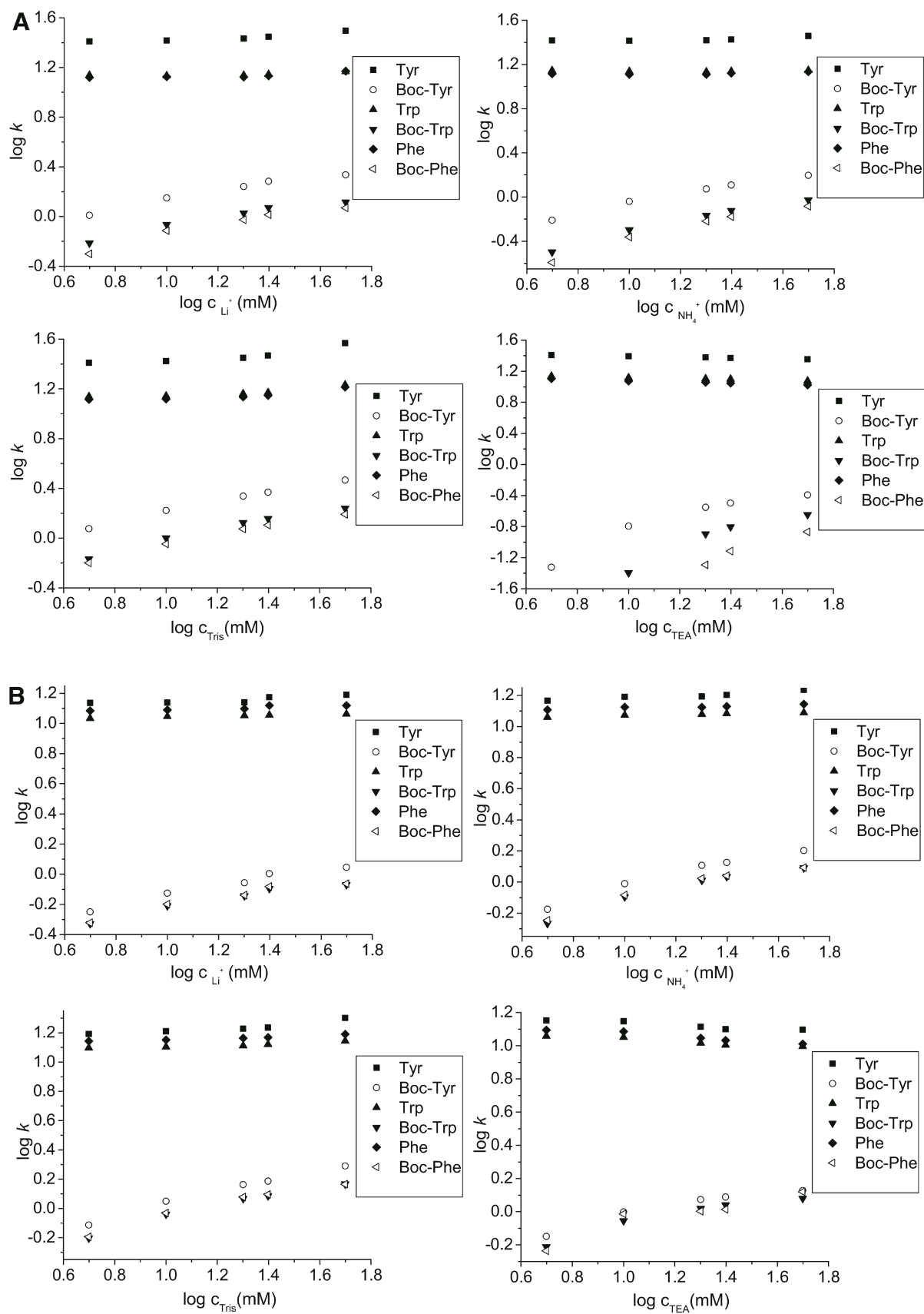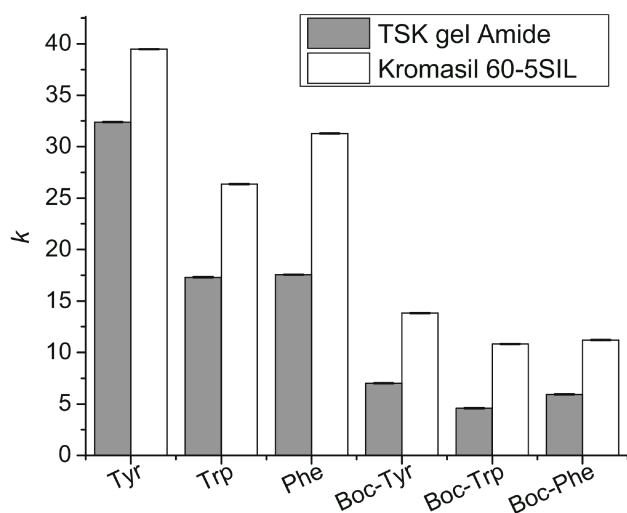
Fig. 2 Retention factors with their standard deviations of AAs and their *N*-blocked analogues on both tested columns. MP ACN/(Ba^{2+}/HAc, 1.7/21.3 mM) buffer, pH 4.01 90/10 (v/v)

Fig. 3 Dependence of logarithm of retention factors of dipeptides on the logarithm of concentration and buffer types on the two columns: **A** amide column, **B** silica column; MP ACN/buffer 90/10 (v/v). *H-Tyr-Phe* tyrosyl-phenylalanine, *H-Phe-Tyr* phenylalanyl-tyrosine, *Z-Trp-Phe* benzyloxycarbonyl tryptophanyl-phenylalanine, *Z-Phe-Trp* benzyloxycarbonyl phenylalanyl-tryptophan, *H-Phe-Trp* phenylalanyl-tryptophan, *H-Trp-Phe* tryptophanyl-phenylalanine

(dependence of log *k* vs log *c* of cation in buffer) and Table S1 in Supporting Information. The values of linear regression equations as well as coefficients of determination are summarized in Table S3 in Supporting Information. It can be seen that linear fits were not obtained for all analytes, especially on amide column. In these cases the retention rather fluctuates with changing concentration of cation in the buffer.

Tyrosine (log $D = -1.49$ at pH 4), the most polar compound showed the highest retention. Much higher retention of Tyr was obtained on the amide-based SP compared to the bare silica SP under the same chromatographic conditions while the retention of Phe and Trp is almost identical. The elution order of native AAs were Tyr > Phe > Trp on the silica column in all the MPs tested. The retention behavior correlates with the polarity of AAs. Different elution order, i.e., Tyr > Trp > Phe was observed using the amide column. An increasing retention does not correlate unequivocally with the polarity which increases in the order—tryptophan (log $D = -1.10$ at pH 4), phenylalanine (log $D = -1.19$ at pH 4) and tyrosine (log $D = -1.49$ at pH 4). This behavior can be attributed to the fact that retention mechanism in HILIC is complex (Kalíková et al. 2013; Guo 2015) and the retention does not depend only on the polarity of an analyte. Moreover, the amide column can possess more interaction types than the bare silica column.

The obtained data indicate that increasing salt concentration in MP results in an increase of the retention of all *N*-blocked AAs on both columns in all the MPs tested (Table S1 in Supporting Information). Higher salt concentration behaves as a driving force for transition of more

solvated salt ions into the water-rich liquid layer. This would result in an increase in volume or hydrophilicity of the liquid layer, leading to stronger retention of the solutes (Guo and Gaiki 2005). Despite the fact that these compounds are typical RP analytes they showed HILIC behavior (increasing retention with increasing ACN content in the MP; data not shown). In the case of the amide column, the lowest retention of all *N*-blocked AAs (and also native AAs) was observed in the MPs containing buffer with TEA (the same behavior was observed for all tested buffer concentrations). In comparison, the silica column provided the lowest retention of *N*-blocked AAs using MPs containing buffer with Li$^+$. For both columns all concentrations of Tris buffers gave significantly the highest retention. It can be related to the structure of Tris. It contains three hydroxyl groups and one amino group in the molecule while the others have only one hydroxyl or amino group. In the case of native AAs the retention of the analytes increased, decreased or did not change with increasing buffer concentration according to the cation type in the buffer. First, we will describe the retention behavior on the amide column. The highest positive shift of retention with increasing buffer concentration showed Tyr using Tris buffer. Tris buffer also gave the highest positive shift of retention for the other native AAs in comparison with other buffers. Interestingly, using buffer containing TEA led to a decrease of retention with increasing buffer concentration of all the AAs. This behavior was previously explained as follows: TEA cation could compete for negatively charged active sites which results in the reduced electrostatic attraction of solutes (Douša et al. 2014). This is in accordance with the results obtained for *N*-blocked AAs. They do not contain positive charge and thus their retention did not decrease with increasing TEA concentration in buffer. However, at pH 4 the concentration of negative charges at SPs should not be so important (Maier et al. 2014). Nevertheless, the small but significant effect of residual silanols on retention was observed. The lowest shift of retention was observed for native AAs in the buffers containing NH$_4^+$ cations. The highest and positive shift of retention was observed for Tyr. Trp and Phe showed almost no change of retention. The retention of all *N*-blocked AAs increased with increasing buffer concentration (NH$_4^+$). Nevertheless, the retention times were significantly lower than that for native AAs. Unless otherwise indicated, the
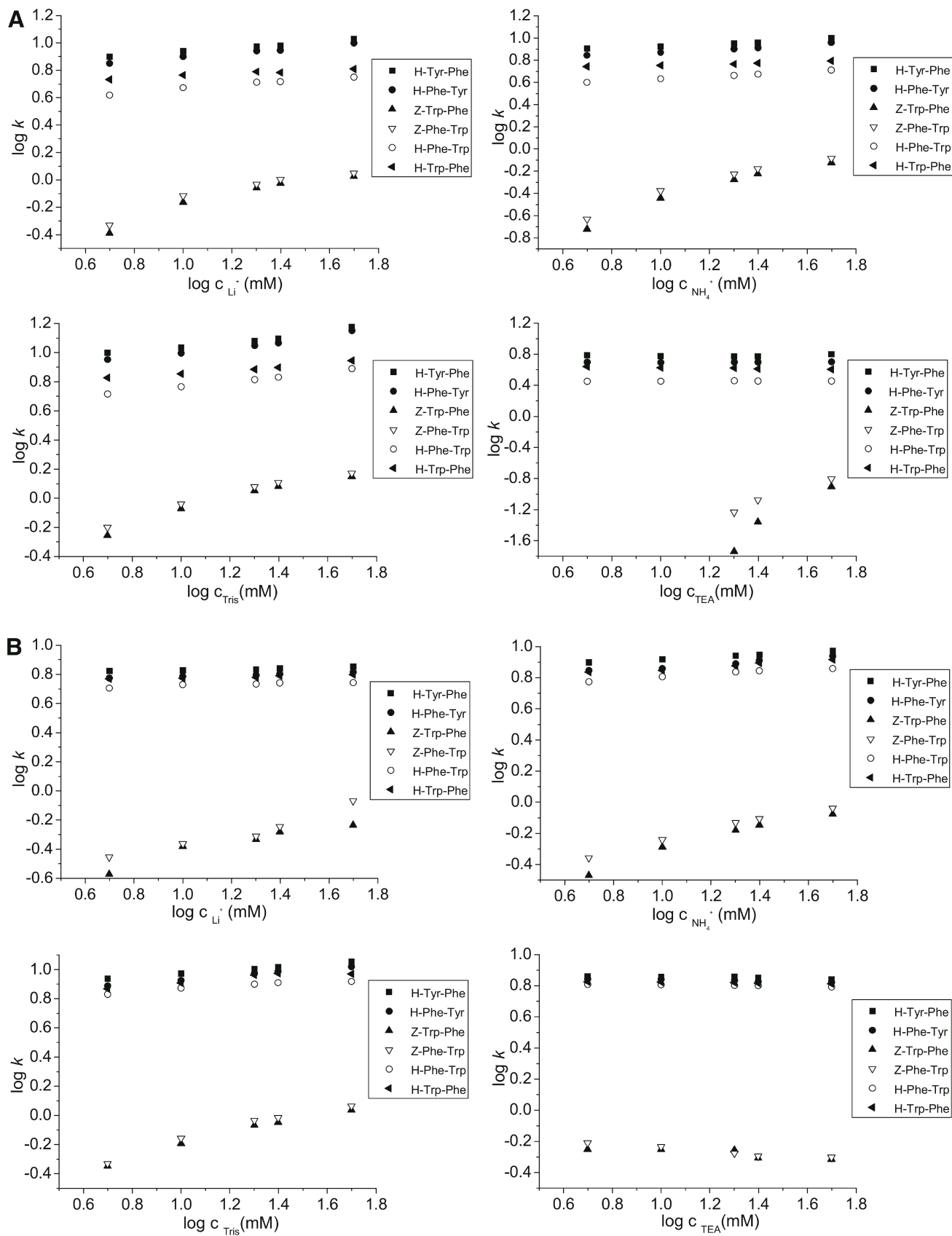
retention trends of these analytes on the silica column were similar to that of the amide column.

In addition, we also tested buffers containing Ba^{2+} cations. Previously, it was shown that addition of Ba^{2+} to the MP increased retention of some binaphthyl atropisomers in RP HPLC (Maier et al. 2014). The concentration of Ba^{2+} cations ranged from 1.7 to 8.3 mM in the MP ACN/buffer 80/20 (v/v). These concentrations were selected to have the same ionic strengths and pH values as other buffers. In the MP ACN/buffer 90/10 (v/v), only a concentration of 1.7 mM was used to protect the columns. Much higher retention of both native and N-blocked AAs was observed in comparison with the other buffers of the same ionic strength and pH on both columns. This can be caused by "strong" sorption of barium cations on the SP and thus ion-exchange interaction mechanism significantly influences the retention. It is well known that ion exchangers favor the bonding of ions of higher charge, decreased hydrated radius and increased polarizability (Heaton et al. 2014). The retention factors with their standard deviations of AAs in MP ACN/buffer (1.7 mM Ba^{2+}) 90/10 (v/v) are depicted in Fig. 2. Moreover, the retention of all analytes is significantly higher on the silica column compared to that on the amide column. This behavior was not observed for the other buffers with the same ionic strength and pH.

The influence of cation type and its concentration in MP buffer on retention of some dipeptides and their N-blocked analogues was also tested. All non-blocked dipeptides exhibited significantly lower retention than native AAs under the same chromatographic conditions. It can be explained by their lower polarity and bigger molecule size. N-Blocked dipeptides showed similar retention as N-blocked AAs in the same MPs—see Fig. 3 (dependence of log k vs log c of cation in buffer) and Table S2 in Supporting Information. The values of linear regression equations as well as coefficients of determination are summarized in Table S4 in Supporting Information. We obtained the similar observations as for AAs and their N-blocked analogues. From this group of analytes, H-Tyr-Phe showed the highest retention (in comparable MPs) followed by H-Phe-Tyr. The lowest retained non-blocked dipeptide on both columns was H-Phe-Trp. Similarly as for AAs, Tris buffers gave the highest retention of dipeptides. This is true for both tested columns. Interestingly, using Tris buffers the amide column exhibited higher retention for H-Tyr-Phe and H-Phe-Tyr than silica column while the silica column showed higher retention for H-Phe-Trp and H-Trp-Phe—see Table S2 in Supporting Information. The lowest retention of all analytes on the amide column was achieved in TEA/HAc buffers while on the silica column the Li^+/HAc buffers showed the lowest retention for the majority of analytes.

The retention behavior of these analytes slightly differs on the individual columns. Using the amide column the retention of all analytes increased with increasing buffer concentrations except for some dipeptides in TEA/HAc buffers. The slight decrease of retention with increasing buffer concentration was observed for H-Trp-Phe and almost constant retention for H-Phe-Trp. Using TEA/HAc buffers with the silica column led to slight decrease of retention with increasing buffer concentration for all the analytes. This can confirm the idea that TEA cation is able to compete for negatively charged active sites on the SP. Higher number of these sites is present on the bare silica. The other buffers exhibited opposite effect on retention of all the analytes.

The buffers containing Ba^{2+} cations were also used. The retention factors of dipeptides observed on both columns in MP ACN/buffer (1.7 mM Ba^{2+}) 90/10 (v/v) are shown in Fig. 4. As in the case of AAs much higher retention of all the analytes was observed compared to the other buffers with the same ionic strength and pH on both columns. Besides, different elution order was observed, i.e., H-Phe-Tyr > H-Tyr-Phe > H-Phe-Trp > H-Trp-Phe, which indicates diverse retention mechanism. This applies to both tested columns.

Moreover, the retention of non-blocked dipeptides was higher than native AAs under these conditions, which is reversed in comparison with the other tested buffers.

To see the correlation of retention of analytes with their polarity, the dependencies of log k versus log D for 20 mM cations in buffers were plotted—see Fig. 5. For other concentrations similar dependencies were obtained. t-BOC-AAs are significant outliers (points in the ring) for both
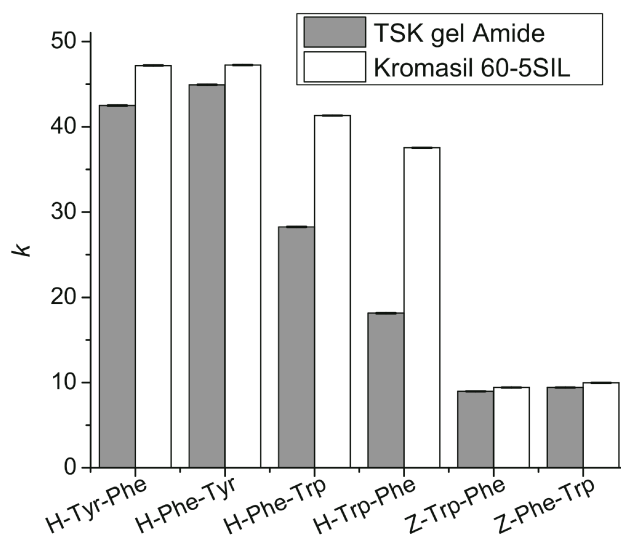

Fig. 4 Retention factors with their standard deviations of dipeptides and their blocked analogues on both tested columns. MP ACN/(Ba^{2+}/HAc, 1.7/21.3 mM) buffer, pH 4.01 90/10 (v/v)

Fig. 5 Dependence of logarithm of retention factor on log D on the two columns: **A** amide column, **B** silica column; MP ACN/20 mM cation in buffer 90/10 (v/v). **a** All data (retention factors of AAs, *t-BOC*-AAs, dipeptides and their *N*-blocked analogues) are included in the linear fit; **b** data in the ring (log k of *t-BOC*-AAs) are not included in the linear fit
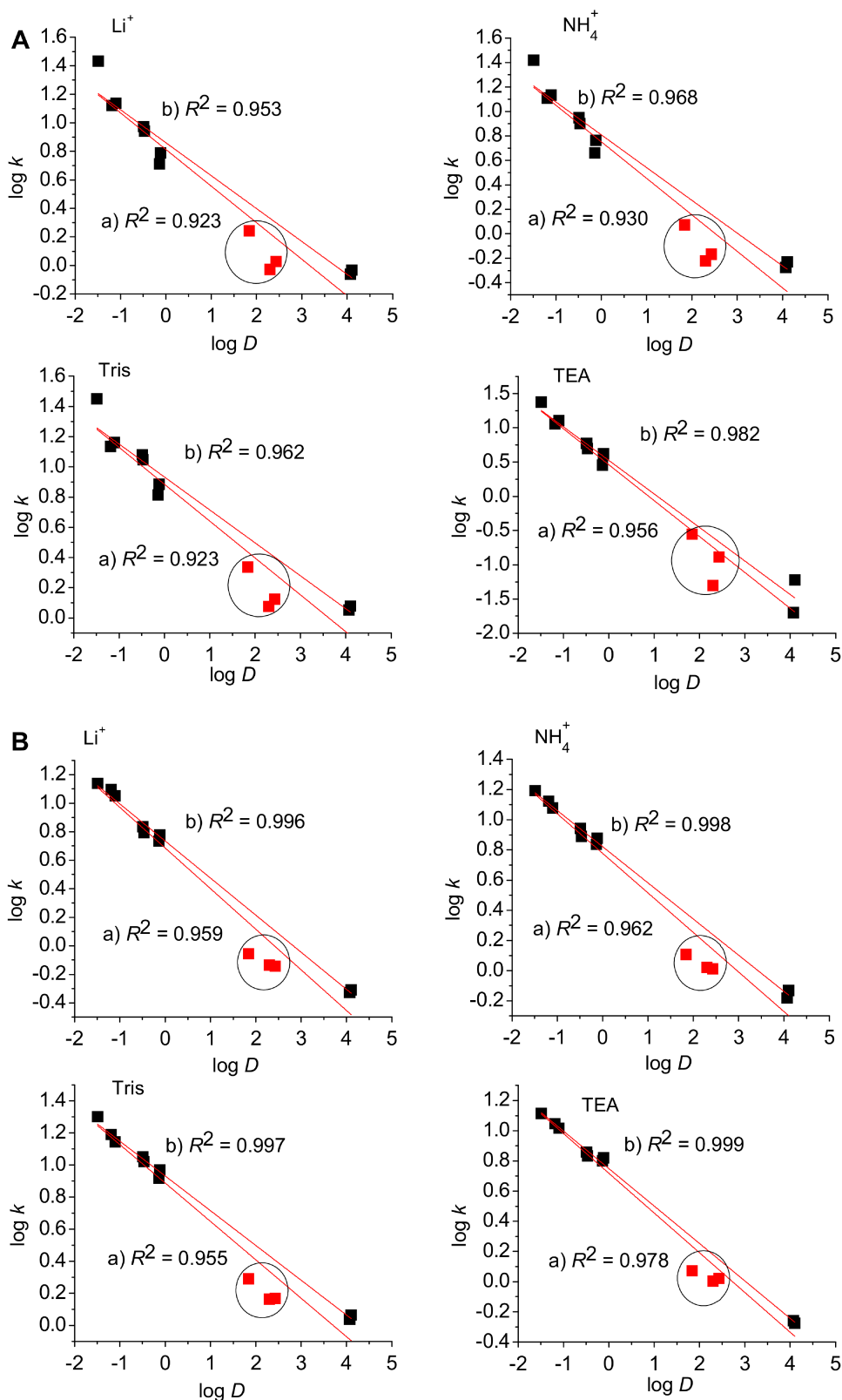
columns in linear fit and show different chromatographic behavior than the other analytes. It means that the retention of the analytes is not strictly driven only by the polarity. It can be seen that higher coefficients of determination were obtained for silica column regardless of all data or data without *t-BOC*-AAs being included. It can be explained as

the polarity of analytes plays more significant role in the retention mechanism on bare silica column than on amide column. The chemistry of the amide column offers more interaction possibilities and is more complex than bare silica column. Thus, the retention of tested analytes is more complex on the amide column.

For statistical evaluation of the differences between the columns the *t*-test was performed. The differences of slopes and intercepts of dependencies of log *k* versus log *c* were tested. The *t*-tests were performed for all tested analytes and cation types. The difference between columns in retention can be described by testing similarity of intercepts while the difference in retention change with increasing buffer concentration by testing similarity of slopes. The null hypothesis: the slopes and intercepts are equal was tested against alternative hypothesis: the slopes and intercepts are different. Obtained *p*-values as well as *F*-values and coefficients of determination are summarized in Table S5 in Supporting Information. No generalization can be made. The differences/similarities in the column's behavior are caused by the analyte and also cation types in the buffer. Closer inspection of AAs reveals that null hypothesis is accepted for all AAs only in buffers containing Tris. Using buffers containing NH_4^+ the nonlinear dependencies ($R^2 < 0.7$) of log *k* versus log *c* were observed for all AAs on the amide column. This is caused by small changes in the retention with changing buffer concentration. For *t-BOC*-AAs, the columns differ in both slope and intercept in buffers with TEA. In other buffers some similarities for slopes and/or intercepts were observed. In the case of dipeptides, the same statistical results were observed only for H-Tyr-Phe and H-Phe-Tyr. No difference between the columns in the behavior of blocked dipeptides was observed only in buffers containing Tris and Li^+.

The work proved the influence of cation type and concentration in the MP buffers on the retention of AAs, dipeptides and their *N*-blocked analogues. Therefore, it is important to carefully combine SP and composition of MP buffers to achieve suitable results. For instance, for aromatic AAs the buffers containing NH_4^+ cations are the most "safe" as they showed the lowest shift of retention. Buffers composed of TEA gave the lowest retention of tested analytes on the amide column. Moreover, the retention of AAs significantly decreased with increasing TEA concentration in the MPs on both columns. The other buffers gave opposite results, i.e., increasing retention of AAs with increasing cation concentration.

Using different types and concentration of buffers forming the mobile phase could be exploited to tuning the retention especially when more complex mixtures are analyzed.

References

Česla P, Vaňková N, Křenková J, Fischer J (2016) Comparison of isocratic retention models for hydrophilic interaction liquid chromatographic separation of native and fluorescently labeled oligosaccharides. J Chromatogr A 1438:179–188. doi:10.1016/j.chroma.2016.02.032

Douša M, Srbek J, Stránský Z, Gibala P, Nováková L (2014) Retention behavior of a homologous series and positional isomers of aliphatic amino acids in hydrophilic interaction chromatography. J Sep Sci 37:739–747. doi:10.1002/jssc.201301348

Guo Y (2015) Recent progress in the fundamental understanding of hydrophilic interaction chromatography (HILIC). Analyst 140:6452–6466. doi:10.1039/c5an00670h

Guo Y, Gaiki S (2005) Retention behavior of small polar compounds on polar stationary phases in hydrophilic interaction chromatography. J Chromatogr A 1074:71–80. doi:10.1016/j.chroma.2005.03.058

Heaton JC, Russell JJ, Underwood T, Boughtflower R, McCalley DV (2014) Comparison of peak shape in hydrophilic interaction chromatography using acidic salt buffers and simple acid solutions. J Chromatogr A 1347:39–48. doi:10.1016/j.chroma.2014.04.026

Hemstrom P, Irgum K (2006) Hydrophilic interaction chromatography. J Sep Sci 29:1784–1821. doi:10.1002/jssc.200600199

Jandera P (2016) Stationary and mobile phases in hydrophilic interaction chromatography: a review. Anal Chim Acta 692:1–25. doi:10.1016/j.aca.2011.02.047

Jandera P, Janás P (2017) Recent advances in stationary phases and understanding of retention in hydrophilic interaction chromatography. A review. Anal Chim Acta 967:12–32. doi:10.1016/j.aca.2017.01.060

Kalíková K, Kozlík P, Gilar M, Tesařová E (2013) Properties of two amide-based hydrophilic interaction liquid chromatography columns. J Sep Sci 36:2421–2429. doi:10.1002/jssc.201300232

Kozlík P, Šímová V, Kalíková K, Bosáková Z, Armstrong DW, Tesařová E (2012) Effect of silica gel modification with cyclofructans on properties of hydrophilic interaction liquid chromatography stationary phases. J Chromatogr A 1257:58–65. doi:10.1016/j.chroma.2012.08.004

Kozlík P, Krajíček J, Kalíková K, Tesařová E, Čabala R, Exnerová A, Štys P, Bosáková Z (2013) Hydrophilic interaction liquid chromatography with tandem mass spectrometric detection applied for analysis of pteridines in two *Graphosoma* species (Insecta: Heteroptera). J Chromatogr B 930:82–89. doi:10.1016/j.jchromb.2013.05.004

Maier V, Kalíková K, Přibylka A, Vozka J, Smuts J, Švidrnoch M, Ševčík J, Armstrong DW, Tesařová E (2014) Isopropyl derivative of cyclofructan 6 as chiral selector in liquid chromatography and capillary electrophoresis. J Chromatogr A 1338:197–200. doi:10.1016/j.chroma.2014.02.061

McCalley DV (2010) Study of the selectivity, retention mechanisms and performance of alternative silica-based stationary phases for separation of ionised solutes in hydrophilic interaction chromatography. J Chromatogr A 1217:3408–3417. doi:10.1016/j.chroma.2010.03.011

McCalley DV (2017) Effect of mobile phase additives on solute retention at low aqueous pH in hydrophilic interaction liquid

chromatography. J Chromatogr A 1483:71–79. doi:10.1016/j.chroma.2016.12.035

McCalley DV, Neue UD (2008) Estimation of the extent of the water-rich layer associated with the silica surface in hydrophilic interaction chromatography. J Chromatogr A 1192:225–229. doi:10.1016/j.chroma.2008.03.049

Noga S, Jandera P, Buszewski B (2013) Retention mechanism studies of selected amino acids and vitamin B6 on HILIC columns with evaporative light scattering detection. Chromatographia 76:929–937. doi:10.1007/s10337-013-2502-y

Qiao L, Shi X, Xu G (2016) Recent advances in development and characterization of stationary phases for hydrophilic interaction chromatography. Trends Anal Chem 81:23–33. doi:10.1016/j.trac.2016.03.021

Schuster G, Lindner W (2013) Comparative characterization of hydrophilic interaction liquid chromatography columns by linear solvation energy relationships. J Chromatogr A 1273:73–94. doi:10.1016/j.chroma.2012.11.075

Soukup J, Jandera P (2014) Adsorption of water from aqueous acetonitrile on silica-based stationary phases in aqueous normal-phase liquid chromatography. J Chromatogr A 1374:102–111. doi:10.1016/j.chroma.2014.11.028

Špačková V, Pazourek J (2013) Identification of carbohydrate isomers in flavonoid glycosides after hydrolysis by hydrophilic interaction chromatography. Chem Pap 67:357–364. doi:10.2478/s11696-012-0302-8

Tircová B, Kozlík P (2017) HILIC-MS/MS method for analysis of ephedrine in internet-available drugs. Chromatographia 80:523–528. doi:10.1007/s10337-016-3170-5

West C, Auroux E (2016) Deconvoluting the effects of buffer salt concentration in hydrophilic interaction chromatography on a zwitterionic stationary phase. J Chromatogr A 1461:92–97. doi:10.1016/j.chroma.2016.07.059

Zhang Q, Yang F-Q, Ge L, Hu Y-J, Xia Z-N (2017) Recent applications of hydrophilic interaction liquid chromatography in pharmaceutical analysis. J Sep Sci 40:49–80. doi:10.1002/jssc.201600843

V

CE determination of the thermodynamic p*K*a values and limiting ionic mobilities of 14 low molecular mass UV absorbing ampholytes for accurate characterization of the pH gradient in carrier ampholytes-based IEF and its numeric simulation

M. Ansorge, B. Gaš, M. Boublík, M. Malý, J. Šteflová, V. Hruška, G. Vigh

Martin Ansorge[1]
Bohuslav Gaš[1] (iD)
Milan Boublík[1]
Michal Malý[1]
Jana Šteflová[1,2]
Vlastimil Hruška[2]
Gyula Vigh[3]

[1]Department of Physical and
  Macromolecular Chemistry,
  Faculty of Science, Charles
  University, Prague, Czech
  Republic
[2]Agilent Technologies
  Deutschland GmbH, Waldbronn,
  Germany
[3]Chemistry Department, Texas
  A&M University, College
  Station, TX, USA

Research Article

CE determination of the thermodynamic pK_a values and limiting ionic mobilities of 14 low molecular mass UV absorbing ampholytes for accurate characterization of the pH gradient in carrier ampholytes-based IEF and its numeric simulation

Fourteen low molecular mass UV absorbing ampholytes containing 1 or 2 weakly acidic and 1 or 2 weakly basic functional groups that best satisfy Rilbe's requirement for being good carrier ampholytes ($\Delta pK_a = pKa_{monoanion} - pKa_{monocation} < 2$) were selected from a large group of commercially readily available ampholytes in a computational study using two software packages (ChemSketch and SPARC). Their electrophoretic mobilities were measured in 10 mM ionic strength BGEs covering the $2 < pH < 12$ range. Using our Debye-Hückel and Onsager-Fuoss laws-based new software, AnglerFish (freeware, https://echmet.natur.cuni.cz/software/download), the effective mobilities were recalculated to zero ionic strength from which the thermodynamic pK_a values and limiting ionic mobilities of the ampholytes were directly calculated by Henderson-Hasselbalch equation-type nonlinear regression. The tabulated thermodynamic pK_a values and limiting ionic mobilities of these ampholytes (pI markers) facilitate both the overall and the narrow-segment characterization of the pH gradients obtained in IEF in order to mitigate the errors of analyte ampholyte pI assignments caused by the usual (but rarely proven) assumption of pH gradient linearity. These thermodynamic pK_a and limiting mobility values also enable the reality-based numeric simulation of the IEF process using, for example, Simul (freeware, https://echmet.natur.cuni.cz/software/download).

1 Introduction

According to a seminal paper of Rilbe [1], for a successful IEF separation in a natural pH gradient, the following conditions have to be met. First, the anode compartment of the electrophoretic device has to be filled with an acidic solution (the anolyte, e.g. 20 mM H_3PO_4). Second, the separation compartment has to be filled with a mixture of carrier ampholytes (ampholytes for which it holds that $\Delta pK_a = pKa_{monoanion} - pKa_{monocation} < 2$). Third, the cathode

compartment has to be filled with a base (the catholyte, e.g. 20 mM NaOH). Fourth, convective disturbances have to be absent or suppressed in the system (either by using an anti-convective medium or a capillary as the separation compartment). Fifth, a sufficiently large DC voltage has to be applied between the anode and the cathode for a sufficiently long period of time to allow any and all of the initially cationic and anionic carrier ampholytes in the mixture to migrate out of sections of the separation compartment in which the local pH value is different from their isoelectric point value. (Since Rilbe considered the isoelectric point value to be very close to the isoprotic point value–which he calculated as $(pKa_{monocation} + pKa_{monoanion})/2$–the symbol p$I$, and the term p$I$ value, became loosely–and interchangeably–used in the literature to designate either "iso" value.)

Once all these conditions are fulfilled, adjacent, individual carrier ampholyte bands form across the separation compartment such that the pH in the successive bands increases

Correspondence: Prof. Bohuslav Gaš, Department of Physical and Macromolecular Chemistry, Faculty of Science, Charles University, Prague, Czech Republic
E-mail: bohuslav.gas@natur.cuni.cz

Abbreviations: 3MHIS, 3-methylhistidine; **DNS-Cl**, dansylchloride; **DNS-IDA**, dansylated iminodiacetic acid; **GLYHIS**, glycyl-histidine; **ICIEF**, Imaging capillary isoelectric focusing; **IDA**, iminodiacetic acid; **LAB**, labetalol; **LBB**, Leucoberbelin blue I dye; **SERO**, serotonin

monotonously from that in the anolyte to that in the catholyte. If the concentration of the carrier ampholyte in its band is sufficiently high, the pH approaches the isoprotic/isoelectric value of the individual carrier ampholyte such that, to quote Rilbe [2], "... my contemplated pH gradients should be stable indefinitely.".

When a number of ampholytic analyte molecules are mixed with the carrier ampholytes prior to the separation, they also participate in the formation of the natural pH gradient and end up in segments of the separation compartment where the pH corresponds to their respective pI value. Since the pI value (however defined) of an ampholytic analyte is considered an important material characteristic, it would be valuable if it could be obtained from the IEF experiment itself. It is possible to take fractions from the focused carrier ampholyte train when IEF is carried out in a conventional density gradient column (even when it is miniaturized, see, e.g. [3]) or in a multicompartmental electrolyzer (see, e.g. [4]), or in a free-flow electrophoretic device (see, e.g. [5]) and measure their pH. One can also measure, post focusing, the pH along the surface of an IEF gel with a specialized glass electrode (see, e.g. [6]). However, there is no convenient direct way to do either of these when the separation compartment is a capillary, even if the focusing position of the analyte band is detectable. The usual solution to this conundrum is an indirect one: two or more additional ampholytes with known pI values (the so-called pI markers) that are readily detectable at the end of the IEF process (by whatever detector is used in the instrument) are added to the carrier ampholyte mixture and their known pI values are plotted against their relative focusing positions between the anode and the cathode. The resulting graph is deemed to represent the shape of the pH profile in the separation compartment and is commonly referred to as the pH gradient. Being an indirect method, the accuracy of this representation is ill-defined and depends on the often assumed–yet rarely proven–local linearity of the pH gradient between the adjacent pI markers. In principle, the use of a larger number of pI markers can lead to a more accurate the description of the shape of the pH gradient.

Historically, both proteins and small ampholytic molecules with consensus pI values have been used as pI markers (for an extensive list of early references and their fair critique, see, e.g. [7]). In CIEF, the use of small ampholytic markers is preferred, because multiple analytical methods can be applied for the determination and cross-validation of their pI values. In addition to finding such pI markers by scouring catalogues of fine chemicals (see, e.g. [8]), many groups have synthesized families of pI markers such as, e.g. substituted nitrophenols [7, 9–11], monoalkylpiperidine amides of fluorescein [12], azo dyes [13], oligopeptides [6, 14], and ampholytic trisulfonamido pyrenes [15].

Most of the time, the pK_a values associated with the monocationic and monoanionic forms of the pI markers are determined experimentally and the pI values are calculated as their arithmetic average according to Rilbe's equation (vide supra), yielding the isoprotic point value. The respective pK_a values can be obtained, among others, from

Table 1. Stock BGE compositions and their corresponding pH ranges, c_{stock} stands for concentration of the stock solution

Buffering constituent	c_{stock} mol/dm^3	Titrant	pH range
Phosphoric acid	0.5	–	2
Phosphoric acid	0.5	LiOH	2.30–3.00
Formic acid	1	LiOH	3.00–4.00
Acetic acid	2	LiOH	4.00–5.15
MES	0.5	LiOH	5.15–6.15
MOPS	0.5	LiOH	6.15–7.30
Tricine	1	LiOH	7.30–8.50
CHES	1	LiOH	8.50–9.50
β-Alanine	1	LiOH	9.50–11.70
Lithium	0.5	–	11.70–12.00

potentiometric titrations (see, e.g. [7]), pH-dependent spectroscopic measurements (see, e.g. [12, 13]) or pH-dependent capillary electrophoretic effective mobility measurements (see, e.g. [16–18]). Alternatively, the pI value can be determined directly from pH-dependent pressure-mediated capillary electrophoretic measurements [19] (which can also provide the respective pK_a and limiting electrophoretic mobility values of the pI markers).

The first objective of the work reported in this paper was to identify a set of low molecular mass pI markers suitable for characterization of the pH gradient in the 3 < pH < 10 range that (i) have well-defined structure and contain no more than two acidic and two basic functional groups, (ii) are commercially available (or are very easy to prepare) with adequate purity, at relatively low cost. The second objective was then to determine their respective thermodynamic pK_a and limiting electrophoretic mobility values to facilitate their use (i) for characterization of the shape of the pH gradient in IEF and, (ii) in reality-based numeric simulation of IEF separations with programs such as Simul [20, 21] (freeware, https://echmet.natur.cuni.cz/software/download).

2 Materials and methods

2.1 Chemicals

2.1.1 BGEs

Water used for the preparation of all solutions was purified by Rowapur and Ultrapur (Watrex, San Francisco, CA, USA). The BGE constituents were chosen to buffer in the 2 < pH < 12 range. BGEs were prepared by mixing appropriate amounts of the stock solutions shown in Table 1 according to PeakMaster 6 [22] (freeware, https://echmet.natur.cuni.cz/software/download), and then diluted with deionized water to 10 mM ionic strength. In all cases, 0.5 M lithium hydroxide was used as the titrant, except at pH 2 where pure phosphoric acid and at pH 12 where
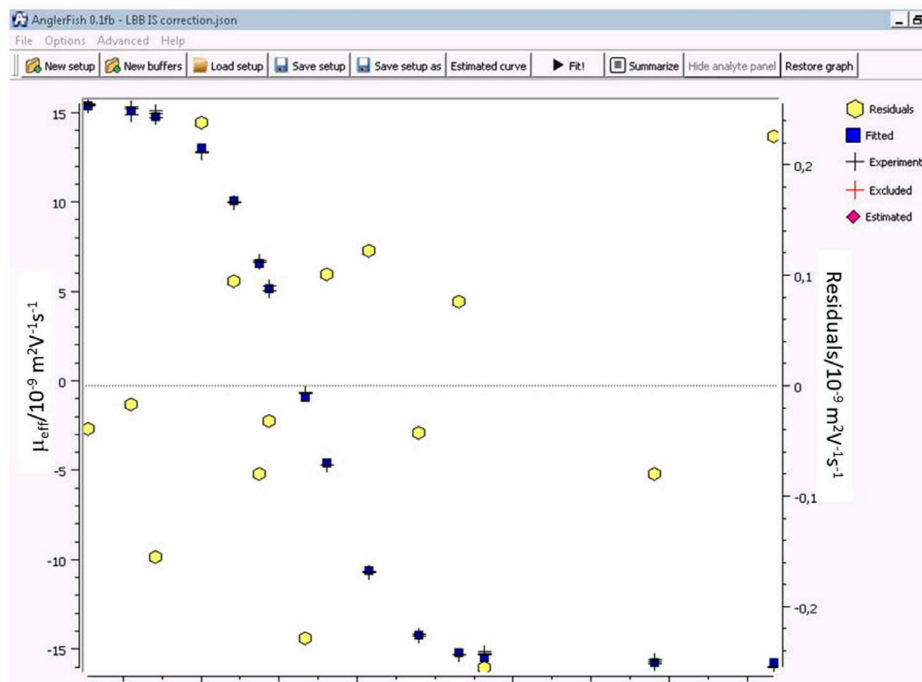
Figure 1. Comparison of the measured effective mobility values (symbol black +) and those calculated by AnglerFish (symbol blue square) using the thermodynamic pK_a and limiting ionic mobility values of Leucoberbelin Blue I, LBB (left vertical axis) as a function of pH (horizontal axis). The yellow hexagon symbols show the residuals, that is, the differences between the average experimental values and the calculated values (right vertical axis, in 10^{-9} m^2/V/s units).

pure lithium hydroxide were used. All BGEs were filtered through 0.45 μm syringe filters (Whatman, GE Healthcare, Chicago, IL, USA). All chemicals used for the stock solutions were of analytical grade purity. Phosphoric acid was purchased from Lachema (Brno, Czech Republic), formic acid, acetic acid (AcOH), MES, MOPS, *N*-(2-hydroxy-1,1-bis(hydroxymethyl)ethyl)glycine (Tricine), CHES, β-alanine and lithium hydroxide were supplied by Sigma-Aldrich (Prague, Czech Republic). The pH of every BGE was measured by a PHM 240 pH/ION Meter (Radiometer Analytical, HACH, Loveland, CO, USA), calibrated with IUPAC buffers of pH 1.679, 4.005, 7.000, 10.012, and 12.450 (Radiometer, Copenhagen, Denmark).

2.1.2 Commercially available low molecular mass ampholytes used as p*I* markers

These ampholytes were purchased from Sigma-Aldrich (Prague, Czech Republic). Their names and abbreviations (in parentheses) are as follows: 3-methylhistidine (3MHIS), 4-(4-aminophenyl)butyric acid, epinephrine (EPI), glycyl-histidine (GLYHIS), labetalol (LAB), leucoberbelin blue I dye (LBB), metanephrine (MEPI), norepinephrine (NEPI), serotonin (SERO), and tyramine (TYRA) (purchased as chloride salt).

2.1.3 p*I* markers prepared by dansylation of amino acids

Aspartic acid (ASP), γ-aminobutyric acid, glutamic acid, and iminodiacetic acid (IDA), were dansylated by dansylchloride

(DNS-Cl) (all from Sigma-Aldrich, Prague, Czech Republic) according to the procedure in [23] yielding dansylated ASP, dansylated GABA, dansylated GLU, and dansylated IDA (DNS-IDA). Briefly, a 1 mM stock solution of the selected amino acid was prepared in 40 mM aqueous lithium carbonate and its pH was adjusted to 9.2 with hydrochloric acid. A 5.5 mM DNS-Cl solution was prepared in acetonitrile (Sigma-Aldrich, Prague, Czech Republic) and 1 mL of it was added rapidly to 2 mL of the amino acid stock solution, mixed for 2 min, then kept in a dark place at room temperature for 60 min. Subsequently, the reaction mixture was applied onto a silica gel column, hydrolysed DNS-Cl was removed from it with a 1:4 methanol:chloroform eluent, followed by the elution of the dansylated amino acid by a 1:1 methanol:chloroform eluent, while the inorganic compounds stayed on the silica gel.

2.2 Capillary electrophoretic experiments

The effective electrophoretic mobilities of the p*I* markers in different pH BGEs were measured by CE using an Agilent CE 7100 system equipped with a diode array detector and operated via ChemStation software (Agilent Technologies, Waldbronn, Germany). In order to minimize analyte-capillary wall interactions, multiple capillaries with different inner surface coatings were used including (i) bare fused silica capillaries (50 μm i.d., 56 and 71.5 cm effective lengths), (ii) fluorocarbon-coated μSil capillaries (75 μm i.d., 56 cm effective length) and PVA-coated capillaries (50 μm i.d., 56 cm effective length, all from Agilent Technologies, Waldbronn, Germany), and (iii) dynamically-coated triple layer Polybrene

Table 2. Thermodynamic pK_a data and their respective standard deviations for the pI markers calculated by AnglerFish from the experimentally measured pH-dependent effective mobilities. Values marked with asterisk (*) are values estimated with insufficient accuracy due to too few data points at high pH. pK_{CC}, pK_C, pK_A, and pK_{AA} denote the pK_a of the +2, +1, −1, and −2 charged species, respectively. Values in the last three columns were calculated as $\Delta pK_a = pK_A - pK_C$ [1], $-dz/dpH = \ln(10)/(1 + 0.5(10^{(pK_A - pK_C)/2}))$ [7] and p$I = (pK_A + pK_C)/2$ [1], respectively

Name	pK_{CC}	σ	pK_C	σ	pK_A	σ	pK_{AA}	σ	ΔpK_a	$-dz/dpH$	pI
DNS-IDA	–	–	2.30	0.07	3.68	0.09	4.84	0.09	1.38	0.67	2.99
DNS–ASP	–	–	2.75	0.01	3.93	0.02	5.13	0.02	1.18	0.78	3.34
DNS–GLU	–	–	2.96	0.02	4.02	0.03	5.29	0.04	1.06	0.85	3.49
DNS–GABA	–	–	3.57	0.01	4.83	0.01	12.53*	–	1.26	0.73	4.20
4APBA	–	–	4.26	0.01	5.45	0.01	–	–	1.19	0.78	4.86
LBB	–	–	4.70	0.01	5.83	0.01	–	–	1.13	0.81	5.27
GLYHIS	2.22	0.06	6.77	0.01	8.32	0.01	–	–	1.55	0.58	7.55
3MHIS	2.04	0.4	6.50	0.01	8.91	0.01	–	–	2.41	0.26	7.71
LAB	–	–	7.32	0.01	9.65	0.01	–	–	2.33	0.28	8.49
NEPI	–	–	8.62	0.04	9.80	0.05	–	–	1.18	0.78	9.21
EPI	–	–	8.62	0.03	10.02	0.07	12.88*	–	1.40	0.66	9.32
MEPI	–	–	9.11	0.01	10.33	0.03	–	–	1.22	0.76	9.72
TYRA	–	–	9.50	0.04	10.84	0.05	–	–	1.34	0.69	10.17
SERO	–	–	10.01	0.02	11.15	0.03	–	–	1.14	0.81	10.58

4APBA, 4-(4-aminophenyl)butyric acid; DNS-ASP, dansylated aspartic acid; 3MHIS, 3-methylhistidine; DNS-GABA, dansylated γ-aminobutyric acid; DNS-GLU, dansylated glutamic acid; DNS-IDA, dansylated iminodiacetic acid; EPI, epinephrine; GLYHIS, glycyl-histidine; LAB, labetalol; LBB, Leucoberbelin blue I dye; MEPI, metanephrine; NEPI, norepinephrine; SERO, serotonin; TYRA, tyramine

capillaries (50 μm i.d., 71.5 cm effective length, made in our laboratory according to [24]. Briefly, a bare fused silica capillary was rinsed with 1 M NaOH (Sigma-Aldrich, Prague, Czech Republic) solution for 30 min, then with deionized water for 10 min, then sequentially with aqueous 5%, w/v Polybrene, 3%, w/v dextran sulfate and again with 5%, w/v Polybrene solutions for 20 min each.

All CE experiments were performed at a constant 25°C temperature and +15 kV voltage (except with the Polybrene-coated capillary, where −15 kV was used). All capillaries were preconditioned prior to the CE measurements: the bare fused silica capillaries were rinsed with 0.1 M NaOH solution for 10 min, deionized water for another 10 min and with the respective BGEs for 5 min, whereas the fluorocarbon- and PVA-coated capillaries were rinsed with 10 mM phosphoric acid prior to deionized water, 10 min each. When switching BGEs, the capillaries were flushed with the new BGE for 5 min, then for 1 min before each run. The sample was an aqueous solution of the analyte at a concentration of 0.1 mg/mL and 0.08%, v/v DMSO as an EOF marker. The sample was injected by applying 20 mbar pressure for 5 s. All measurements were performed in triplicates.

2.3 Imaging capillary isoelectric focusing experiments

Imaging capillary isoelectric focusing (ICIEF) experiments were carried out on a CEInfinite instrument equipped with an on-line whole column imaging detector operating at 280 nm wavelength (Advanced Electrophoresis Solutions, Cambridge, ON, Canada). The separation cassette contained a 100 μm i.d. fluorocarbon-coated capillary (50 mm scanned length) between the two electrode reservoirs (containing 0.3 M phosphoric acid and 0.2 M lithium hydroxide, respectively). IDA and arginine (ARG), used as sacrificial ampholytes [25] were purchased from Sigma-Aldrich (Prague, Czech Republic).

The carrier ampholyte stock solution consisted of 5 mL of 0.25%, w/v aqueous methylcellulose (1500 cP / 2%, w/w, aq) solution, 300 μL of 0.2 M IDA (anodic sacrificial ampholyte [25]), 100 μL of 0.5 M ARG (cathodic sacrificial ampholyte [25]), and 150 μL of AES SH 3–10 carrier ampholyte mixture (Advanced Electrophoresis Solutions Ltd., Cambridge, ON, Canada), resulting in nominal 10.8 mM IDA and 9 mM ARG concentrations in the carrier ampholyte stock solution. A pI marker stock solution containing each marker at a concentration of 1 mg/mL was prepared and 1 μL of it was added to 0.5 mL of the carrier ampholyte mixture, resulting in individual pI marker concentrations of 2 μg/mL.

The sample-containing carrier ampholyte solutions were filled into the ICIEF capillary manually by introducing 0.8 mL of air into the headspace of the 2 mL sample vial through its tightly closed septum for 3 min. The length of time has been experimentally verified to be sufficient for complete replacement of the content of the whole capillary with a fresh solution. ICIEF measurements were made at ambient temperature. The applied voltage was set to 1 kV for 1 min, followed by a step change to 3 kV for 4 min. Whole column images were taken in 10 s intervals.

Table 3. Limiting ionic mobility data of the p*I* markers calculated by AnglerFish from the experimentally measured pH-dependent effective mobilities. Values marked with asterisk (*) are values estimated with insufficient accuracy due to too few data points at high pH. u_{CC}, u_C, u_A, and u_{AA} stand for the limiting ionic mobility of the +2, +1, −1, and −2 charged species in 10^{-9} m^2/V/s units. $\triangle u$ is the difference between the absolute values of limiting mobilities of the monocationic and monoanionic species (i.e., $\triangle u = |u_C|-|u_A|$)

Name	u_{CC}	σ	u_C	σ	u_A	σ	u_{AA}	σ	$\triangle u = |u_C|-|u_A|$
DNS-IDA	–	–	21.6	1.2	−18.6	2.1	−39.4	0.2	3.0
DNS–ASP	–	–	20.9	0.1	−18.4	0.4	−40.5	0.1	2.5
DNS–GLU	–	–	20.6	0.2	−19.2	0.8	−40.0	0.1	1.4
DNS–GABA	–	–	22.0	0.1	−21.3	0.1	−46.7*	–	0.7
4APBA	–	–	26.9	0.1	−26.6	0.1	–	–	0.3
LBB	–	–	18.4	0.1	−18.6	0.1	–	–	−0.2
GLYHIS	51.9	1.8	25.3	0.1	−25.0	0.1	–	–	0.3
3MHIS	42.5	6.8	27.4	0.2	−26.6	0.1	–	–	0.8
LAB	–	–	19.3	0.1	−19.1	0.1	–	–	0.2
NEPI	–	–	26.4	0.3	−26.2	0.6	–	–	0.2
EPI	–	–	25.7	0.2	−22.6	1.3	−50*	–	3.1
MEPI	–	–	25.1	0.1	−20.9	1.1	–	–	4.2
TYRA	–	–	30.0	0.3	−27.0	0.7	–	–	3
SERO	–	–	28.1	0.2	−24.0	0.5	–	–	4.1

4APBA, 4-(4-aminophenyl)butyric acid; DNS-ASP, dansylated aspartic acid; 3MHIS, 3-methylhistidine; DNS-GABA, dansylated γ-aminobutyric acid; DNS-GLU, dansylated glutamic acid; DNS-IDA, dansylated iminodiacetic acid; EPI, epinephrine; GLYHIS, glycyl-histidine; LAB, labetalol; LBB, Leucoberbelin blue I dye; MEPI, metanephrine; NEPI, norepinephrine; SERO, serotonin; TYRA, tyramine.

3 Results and discussion

Based on prior experience with low molecular mass ampholytic p*I* markers in one of our laboratories [17, 19, 25, 26], corroborated by structure-based pK_a predictions by SPARC (SPARC 2018, ARChem, Danielsville, GA, USA, www.archemcalc.com) and ChemSketch (ACD/Labs, 2017.2.1, Advanced Chemistry Development, Toronto, ON, Canada, www.acdlabs.com), a series of relatively inexpensive, commercially available or simple-to-synthesize p*I* marker candidates were selected for the CE measurements of their pH-dependent effective mobilities, from which their pK_a and electrophoretic mobility values could be calculated. However, due to the ionic strength dependence of the measured effective mobilities, a direct nonlinear regression fit of the data by the Henderson-Hasselbalch equation [27] yields only the apparent pK_a and apparent ionic mobilities. Our laboratory recently devised a new model and new software, called AnglerFish [28] (freeware, https://echmet.natur.cuni.cz/software/download), for the direct determination of the thermodynamic pK_a and limiting ionic mobility values of weak electrolytes by nonlinear regression of the experimental data. The program uses the Debye-Hückel [29–31] and Onsager-Fuoss [32] laws to calculate thermodynamic pK_a and limiting ionic mobilities. First, using both the experimentally measured pH and the actual buffer compositions of the set of BGEs as input data, the program recalculates the effective mobilities by the correction engine to the corresponding infinite-dilution, limiting mobility values, followed by nonlinear regression using the Henderson-Hasselbalch equation which yields, in one fit, both the thermodynamic pK_a values and the limiting ionic mobilities. This approach is universally valid within

the limitations of the Debye-Hückel and Onsager-Fuoss laws.

As an example, Fig. 1 shows the measured effective mobility values (symbol **+**) and those calculated by AnglerFish (symbol blue square) using the thermodynamic pK_a and limiting ionic mobility values of Leucoberbelin Blue I, LBB (left vertical axis) as a function of pH (horizontal axis). The yellow hexagon symbols show the residuals, that is, the differences between the average experimental values and the calculated values (right vertical axis, in 10^{-9} m^2/V/s units). Similar graphs were obtained for the other p*I* markers as well.

The calculated thermodynamic pK_a and limiting ionic mobility data of all of the p*I* markers obtained by AnglerFish are shown in Tables 2 and 3. The last three columns in Table 2 list the ΔpK_a and −dz/dpH values of the markers (characterizing their focusing ability), along with their p*I* values. Eleven out of the 14 p*I* markers have Δp$K_a < 1.5$ values (i.e., they are excellent focusers), the remaining three have acceptable focusing speeds, $1.55 < \Delta$p$K_a < 2.41$ (GLYHIS, 3MHIS, and LAB). Table 3 lists the limiting ionic mobility data, where u_{CC}, u_C, u_A, and u_{AA} stand for the limiting ionic mobility of the +2, +1, −1, and −2 charged species in 10^{-9} cm^2/V/s units and Δu is the difference between the absolute values of limiting mobilities of the monocationic and monoanionic species (i.e., $\Delta u = |u_C|-|u_A|$). The limiting mobilities of the monocharged ions are in the $18 < |u| < 30$ range (in 10^{-9} m^2/V/s units), in agreement with what is found for similar structures in Hirokawa's database [33] implemented in PeakMaster 6 what is typically used in computer simulations of CIEF, for example, [34]. Interestingly though, and contrary to what is typically used in the numeric simulation of CIEF, the limiting mobilities of the monocations are larger than those of the
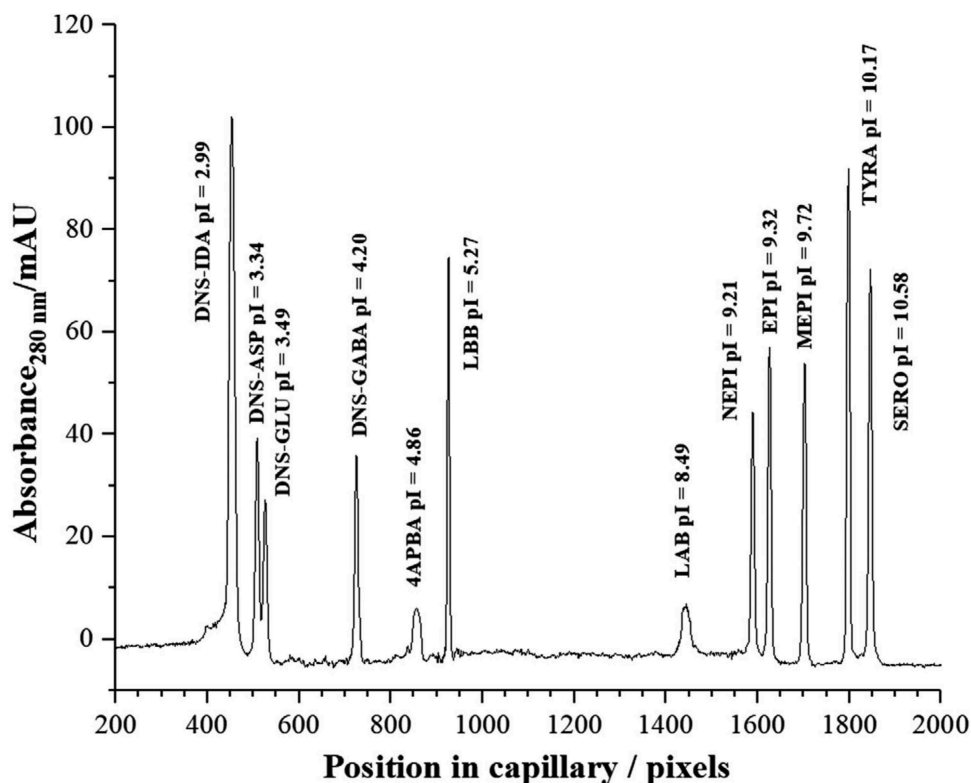
Figure 2. Image of the 12 focused ampholytes detectable at 280 nm and serving as potential p*I* markers, distributed alongside the pH gradient obtained with the SH AES carrier ampholyte mixture. For experimental conditions see Section 2.3.

monoanions (see the last column of Table 3) for 13 out of the 14 p*I* markers studied. For about half of the p*I* markers that mobility difference is as large as 10 to 15%, for the rest it is in the 1 to 2% range.

These p*I* markers were used in CIEF experiments to trace the shape of the pH gradient obtained with the SH AES carrier ampholyte mixture in a CEInfinite instrument. The p*I* markers that are detectable by the full column imaging photometric detector at 280 nm (12 of the 14, since GLYHIS and 3MHIS are not visible at 280 nm, only at 230 nm) were added to the prepared carrier ampholyte solution and focused as described in Section 2.3 The UV absorbance at 280 nm recorded as a function of position in the capillary is shown in Fig. 2. The 50 mm long capillary is imaged across 2050 pixels of the detector. The rise above the steady baseline at 400 pixels indicates that the 0 to 400 pixels portion of the capillary is filled with the focused anodic sacrificial ampholyte, IDA [25]. The initial concentration of IDA in the 2050 pixels long capillary that was 10.8 mM, increased in the 0 to 400 pixels segment to a steady 55.4 mM value (10.8 mM × 2050/400) after focusing. The 190 pixels long section of the capillary between pixels 1860 and 2050 is filled with the cathodic sacrificial ampholyte, ARG, whose 9 mM initial concentration was increased to about 97 mM by the focusing step (9 mM × 2050/190). The p*I* markers are found between 400 and 1860 pixels in the capillary: their names and p*I* values (from Table 2) are listed on the labels next to the respective peaks. Though the concentrations (in mg/mL) of the markers in the feed solution were identical, the peak height values are different due to their dif-

ferent molecular masses, molar absorbances at 280 nm and their slightly different peak widths.

The shape of the pH gradient created from the SH AES carrier ampholyte mixture (Fig. 2) is deduced from the respective p*I* values and peak maximum positions in the capillary of the p*I* markers, as shown in Fig. 3. In the IDA zone (IDA p*I* = 2.33, symbol red ✗) the pH, calculated by PeakMaster 6 is 2.4 (blue solid line), slightly higher than the p*I* value of IDA, and the buffering capacity is high (57 mM), predicting a sharp boundary between the anodic sacrificial ampholyte (anodic blocker [25]) and the focused carrier ampholyte train. The most acidic p*I* marker, DNS-IDA (p*I* = 3.02, symbol red ✚) is only about 30 pixels away from this boundary, indicating a relatively steep change in pH (about 0.7) and confirming the absence of significant amounts of carrier ampholytes with p*I* < 3 in the SH AES 3–10 carrier ampholyte mixture.

At the cathodic side end of the capillary that is filled with ARG (p*I* = 11.36), the pH calculated by PeakMaster for the 97 mM ARG concentration is only 10.9 (blue solid line), and the buffering capacity is only 4.4 mM, due to the relatively large ΔpK_a of ARG (4.88). Thus, the boundary between the focused carrier ampholyte train and ARG is expected to be less sharp than the boundary with IDA. SERO (p*I* = 10.61) is a good marker to indicate the beginning of the ARG zone.

Figure 3 shows that the pH gradient between the most acidic p*I* marker, DNS-IDA (p*I* = 3.02) and the most basic p*I* maker, SERO (p*I* = 10.61) is nonlinear. One of the factors that leads to this nonlinearity is ITP that is contemporaneous
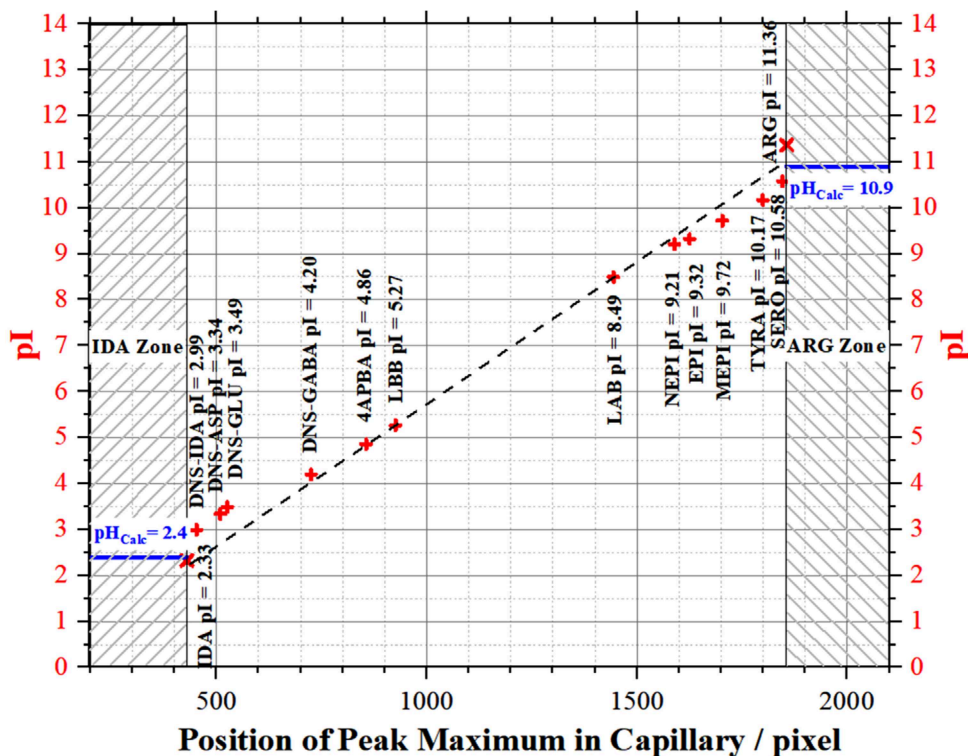
Figure 3. pH profile of the focused SH AES 3–10 carrier ampholyte mixture calculated from the focusing positions of the p*I* markers in Fig. 2 and their p*I* values in Table 2, indicating a nonlinear pH gradient. The rapid increases of pH at the beginning and end of the pH gradient are caused by the boundaries at the IDA- and ARG-filled zones. The pH values in these zones were calculated by PeakMaster using the focused IDA and ARG concentrations (see text) and the pK_a values of IDA from Ref. [35] and of ARG from Ref. [36].

with focusing: it continuously removes the most extreme p*I* components into the respective electrode compartments [34] and over time also alters the width of the focused carrier ampholyte bands. For wide-range carrier ampholytes (3 < p*I* < 10), the extent of change is initially least noticeable in the p*I* range nearest to (and equidistant from) p*I* 7. Thus, by connecting a straight line through the coordinates of the two p*I* markers closest to pH 7 in Fig. 3, LBB (p*I* = 5.26) and LAB (p*I* = 8.49), one can find the approximate slope of the hypothetical linear pH gradient one would find in the absence of ITP, as shown by the black dashed line in Fig. 3. Obviously, the farther away one is from p*I* 7, the shallower the actual slope becomes, until one reaches the boundaries of the anodic and cathodic blockers, wherein there is a rapid change toward the actual pH value of the focused blocker solutions.

The results in Fig. 3 clearly indicate that the common practice of fitting a "best straight line" through the p*I* versus position scatter graph of the focused p*I* makers leads to a systematically incorrect description of the pH profile of the focused carrier ampholyte train.

Since this work provided not only the thermodynamic pK_a values, but also the limiting ionic mobilities, they can be used for reality-based numeric simulation of the IEF process. Therefore, a simulation run was set up using Simul [21]. In the simulation the separation channel had a total length of 72 mm with 1000 grid points and was segmented into three parts in the ratio of 1:6:1. The first and the last parts served as the electrode compartments and contained 0.3 M phosphoric acid and 0.2 M lithium hydroxide, respectively, as anolyte and catholyte. The middle part contained 181 uni-univalent

hypothetical carrier ampholytes with increasing values of pK_a, starting from an anionic pK_a of 3.5 to an anionic pK_a of 10.8 with ΔpK_a = 1 between the anionic and cationic forms, and a pK_a step of 0.0406 for each following ampholyte. The cationic and anionic mobilities of all ampholytes were set to 20×10^{-9} m^2/V/s, their concentrations to 0.1 mM. The p*I* markers occupied the same part of the separation channel as the carrier ampholytes at time zero, but their concentration was set to 0.01 mM. The thermodynamic pK_a and limiting mobility values of the p*I* markers were taken from Tables 2 and 3. The applied voltage was 100 V for 3002 s, which was sufficient for formation of the pH gradient. The results of the simulation are shown in Fig. 4. The tall peaks belong to the carrier ampholytes (only every 10th is shown, starting with the p*I* = 3 one at the IDA zone boundary), the short peaks belong to the 14 p*I* markers, starting with DNS-IDA at the IDA boundary. The pH trace (light purple) shows four plateaus (corresponding to zones of H_3PO_4, IDA, ARG, and LiOH). The horizontal red line shows the maximum possible concentration of any carrier ampholyte that is mostly untouched yet by bidirectional ITP. Notice that the extent of zone expansion–contraction at the low and high p*I* ends of the carrier ampholyte train are different. The pH profile obtained by the simulation and the superimposed p*I* values of the markers from Table 2 and the focusing positions of their peak maxima from Fig. 4 are shown in Fig. 5. Figure 5 closely resembles Fig. 3 indicating that the main source of pH nonlinearity is bidirectional isotachophoresis that accompanies IEF and alters both the concentration and width of the focused carrier ampholyte zones. This effect is more pronounced at the low
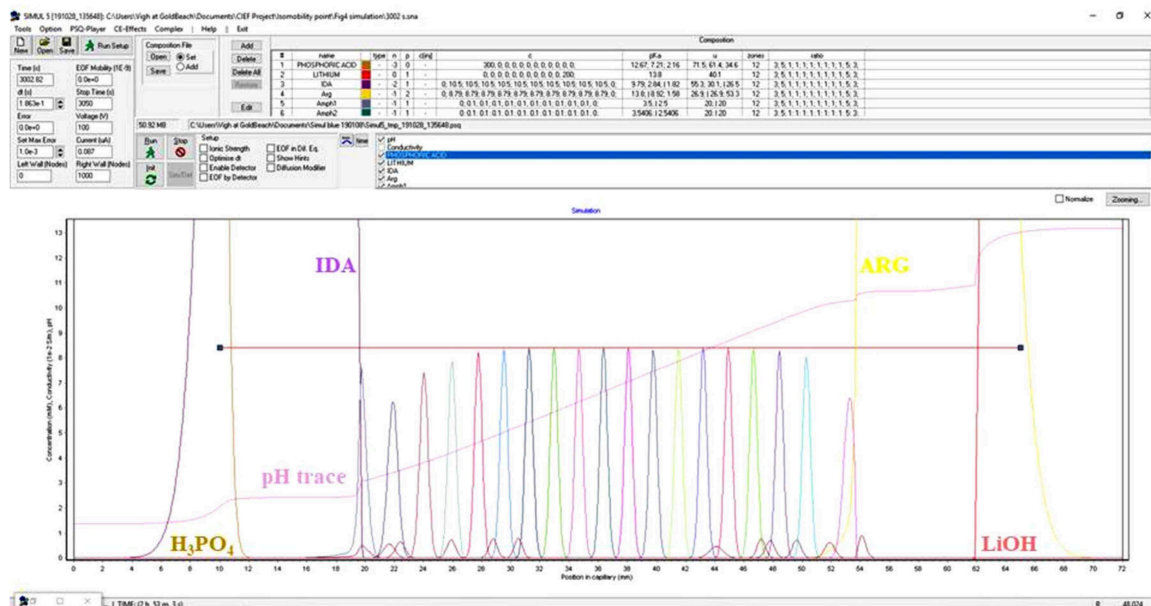
Figure 4. Simulated ICIEF separation of the 14 p*I* markers from Tables 2 and 3. For the simulation conditions, see the text. H₃PO₄ (ochre), IDA (dark purple), ARG (yellow) and LiOH (reddish brown) concentration traces are off-scale, their boundaries pointing toward the middle of the capillary are labeled. pH profile: light purple trace. Tall peaks: carrier ampholytes, every 10th is shown, starting at p*I* 3. Low peaks: 14 p*I* markers of this study starting with DNS-IDA (p*I* = 2.99). For direct compatibility with Fig. 2 (experimental CIEF trace), p*I* markers GLYHIS and MHIS that are not detectable at 280 nm are not shown. Horizontal red line: maximum concentration of carrier ampholyte peaks mostly unaffected yet by ITP.
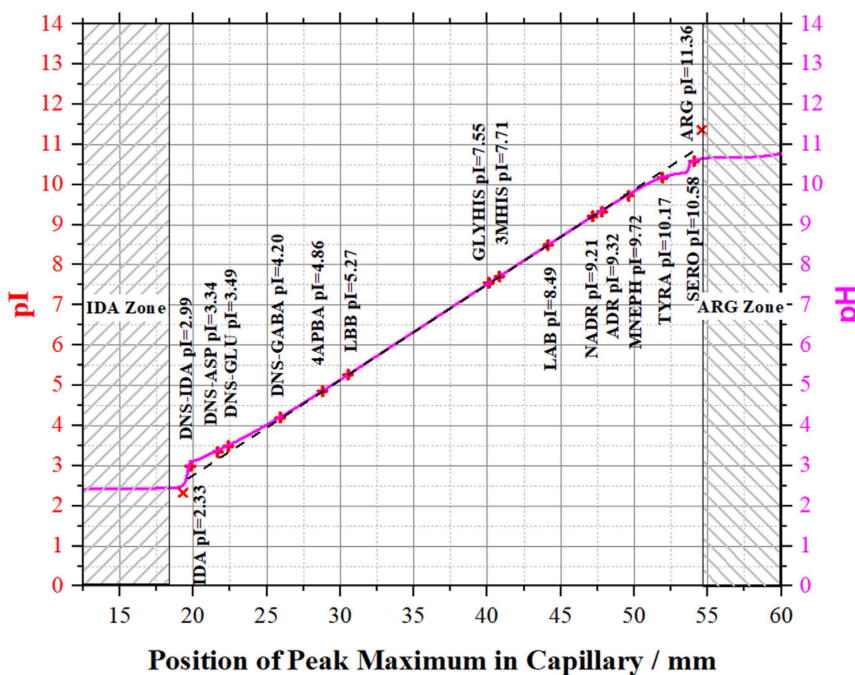

Figure 5. pH profile calculated during simulation of the ICIEF separation of the p*I* markers in Fig. 4 along with the superimposed p*I* values from Table 2.

and high pH extremes of the pH gradient. The agreement between Fig. 3 (obtained with an actual carrier ampholyte mixture SH AES 3–10) and Fig. 5 (obtained with a hypothetical, ideal carrier ampholyte mixture containing only 181 species) is remarkable and reinforces the notion that the practice of using a linear model to describe the shape of the pH gradient is untenable.

4 Concluding remarks

The pH-dependent electrophoretic mobilities of 14 low molecular mass UV absorbing ampholytes containing 1 or 2 weakly acidic and 1 or 2 weakly basic functional groups (p*I* markers) were measured by CE in 10 mM ionic strength background electrolytes in the 2 < pH < 12 range. The measured

effective mobilities were recalculated to zero ionic strength from which the thermodynamic pK_a values and limiting ionic mobilities of the p*I* markers were directly calculated by a Henderson-Hasselbalch equation-type nonlinear regression with the help of our Debye-Hückel and Onsager-Fuoss laws-based new software, AnglerFish. Except for LAB, all of the p*I* markers that can be detected at 280 nm have ΔpK_a < 1.5 and $-dz/d(\mathrm{pH}) > 0.66$, that is, they are rapid focusers. The thermodynamic pK_a values and limiting ionic mobilities of 12 of the 14 markers that are visible at 280 nm were used to characterize the shape of the pH gradients obtained in full column imaging isoelectric focusing experiments. They also enabled the numeric simulation of the IEF process of a hypothetical ideal carrier ampholyte mixture with Simul and revealed that the nonlinearities experimentally observed with an actual carrier ampholyte mixture and in a simulated ICIEF system with a hypothetical ideal carrier ampholyte mixture (identical ΔpK_a, identical initial concentration and identical limiting mobility values) were very similar and were caused by the bidirectional isotachophoretic process that unavoidably accompanies IEF.

The authors have declared no conflict of interest.

5 References

[1] Rilbe, H., *Ann. N. Y. Acad. Sci.* 1973, *209*, 11–22.

[2] Rilbe, H., *Electrophoresis* 1984, *5*, 1–17.

[3] Frederiksson, S., *Anal. Biochem.* 1972, *70*, 575–585.

[4] Righetti, P. G., Wenisch, E., Faupel, M., *J. Chromaotgr.* 1989, *475*, 293–307.

[5] Weber, G., Boček, P., *Electrophoresis* 1996, *17*, 1896–1910.

[6] Shimura, K., Wang, Z., Matsumoto, H., Kasai, K., *Electrophoresis* 2000, *21*, 603–610.

[7] Šlais, K., Friedl, Z., *J. Chromatogr. A* 1994, *661*, 249–256.

[8] Righetti, P. G., Gianazza, E., *J. Chromatogr.* 1977, *137*, 171–181.

[9] Šlais, K., Friedl, Z., *J. Chromatogr. A* 1995, *695*, 113–122.

[10] Caslavska, J., Molteni, S., Chmelik, J., Šlais, K., Matulik, F., Thormann, W., *J. Chromatogr. A* 1995, *680*, 549–559.

[11] Friedl, Z., Šlais, K., *Chem. Listy* 1997, *91*, 679–680.

[12] Šlais, K., Horká, M., Nováčková, J., Friedl, Z., *Electrophoresis* 2002, *23*, 1682–1688.

[13] Šťastná, M., Trávníček, M., Šlais, K., *Electrophoresis* 2005, *26*, 53–59.

[14] Shimura, K., Kamiya, K., Matsumoto, H., Kasai, K., *Electrophoresis* 2002, *74*, 1046–1053.

[15] Vigh, G., Li, M., US Patent 9,689,841, 2017.

[16] Klepárník, K., Šlais, K., Boček, P., *Electrophoresis* 1993, *14*, 475–479.

[17] Lalwani, S., Tutu, E., Vigh, G., *Electrophoresis* 2005, *26*, 2047–2055.

[18] Šolínová, V., Kašička, B., *Electrophoresis* 2013, *34*, 2655–2665.

[19] Glukhovskiy, P. V., Vigh, G., *Electrophoresis* 1998, *19*, 3166–3170.

[20] Hruška, V., Jaroš, M., Gaš, B., *Electrophoresis* 2006, *27*, 984–991.

[21] Hruška, V., Beneš, M., Svobodová, J., Zusková, I., Gaš, B., *Electrophoresis* 2012, *33*, 938–947.

[22] Malý, M., Dovhunová, M., Dvořák, M., Gerlor, G. S., Kler, P. A., Hruška, V., Dubský, P., *Electrophoresis* 2019, *40*, 683–692.

[23] Tahupi, Y., Schmidt, D. E., Lindner, W., Karger, B. L., *Anal. Biochem.* 1981, *115*, 123–129.

[24] Katayama, H., Ishihama, Y., Asakawa, N., *Anal. Chem.* 1998, *70*, 5272–5277.

[25] North, R., Vigh, G., *Electrophoresis* 2008, *29*, 1077–1081.

[26] Lalwani, S., Tutu, E., Vigh, G., *Electrophoresis* 2005, *26*, 2503–2510.

[27] Cai, J., Smith, J. T., *J. High Resolut. Chromatogr.* 1992, *15*, 30–32.

[28] Malý, M., Boublík, M., Pocrnić, M., Ansorge, M., Lorinčíková, K., Svobodová, J., Hruška, V., Dubský, P., Gaš, B., *Electrophoresis* 2020, *41*, https://doi.org/10.1002/elps.201900283.

[29] Debye, P., Hückel, E., *Physik. Z.* 1923, *24*, 185–206.

[30] Debye, P., Hückel, E., *Physik. Z.* 1923, *24*, 305–325.

[31] Davies, C. W., *Ion Association*, Butterworths, London, 1962.

[32] Onsager, L., Fuoss, R. M., *J. Phys. Chem.* 1932, *36*, 2689–2778.

[33] Hirokawa, T., Nishimo, M., Aoki, N., Kiso, Y., Sawamoto, Y., Yagi, T., Akiyama, J., *J. Chromatogr.* 1983, *271*, D1–D106.

[34] Mosher, R. A., Thormann, W., *Electrophoresis* 1990, *11*, 717–723.

[35] Bossi, A., Righetti, P. G, *Electrophoresis* 1997, *18*, 2012–2018.

[36] Fitch, C. A., Platzer, G., Okon, M., Garcia-Moreno, B., McIntosh L. P., *Protein Sci.* 2015, *24*, 752–761.